

AD A099851

ATC Report No. R-92100/9CR-61  
Contract No. N00019-78-C-0599

LEVEL II

1

# THE EFFECT OF ENVIRONMENT ON THE MECHANICAL BEHAVIOR OF AS/3501-6 GRAPHITE/EPOXY MATERIAL PHASE II

T. HO

Vought Corporation Advanced Technology Center  
Dallas, Texas 75266

DTIC  
SELECTED  
JUN 08 1981  
S D  
F

10 January 1980

Final Report for Period I September 1978 to 31 August 1979

Approved for public release; distribution unlimited

Prepared for:

Department of the Navy  
Naval Air Systems Command  
Washington, D.C. 20361

FILE COPY



VOUGHT CORPORATION  
Advanced Technology Center

81 6 08 042

## UNCLASSIFIED

SECURITY CLASSIFICATION OF THIS PAGE (When Data Entered)

REPORT DOCUMENTATION PAGE		READ INSTRUCTIONS BEFORE COMPLETING FORM
1. REPORT NUMBER	2. GOVT ACCESSION NO.	3. RECIPIENT'S CATALOG NUMBER
6) 4. TITLE (and Subtitle) The Effect of Environment on the Mechanical Behavior of AS/3501-6 Graphite/Epoxy Material, Phase II		5. TYPE OF REPORT & PERIOD COVERED Final Report 1 Sept 1978 - 31 Aug 1979
7. AUTHOR(s) 10) T. Ho	6. PERFORMING ORG. REPORT NUMBER R-92100/9CR-61 In Phase	
8. CONTRACT OR GRANT NUMBER(s) N00019-78-C-0599 New		9. PERFORMING ORGANIZATION NAME AND ADDRESS Vought Corporation Advanced Technology Center P. O. Box 226144 Dallas, Texas 75266
11. CONTROLLING OFFICE NAME AND ADDRESS Department of the Navy Naval Air Systems Command Washington, D. C. 20361		10. PROGRAM ELEMENT, PROJECT, TASK AREA & WORK UNIT NUMBERS 12) 192
14. MONITORING AGENCY NAME & ADDRESS (if different from Controlling Office)		12. REPORT DATE 11) 10 January 1980
		13. NUMBER OF PAGES 89
		15. SECURITY CLASS. (of this report) UNCLASSIFIED
		15a. DECLASSIFICATION/DOWNGRADING SCHEDULE
16. DISTRIBUTION STATEMENT (of this Report) Approval for public release; distribution unlimited		
17. DISTRIBUTION STATEMENT (of the abstract entered in Block 20, if different from Report)		
18. SUPPLEMENTARY NOTES		
19. KEY WORDS (Continue on reverse side if necessary and identify by block number) + - 45) 1 2		
Composite, Temperature, Humidity, Fatigue, Creep, Crack Propagation, Viscoelasticity		
20. ABSTRACT (Continue on reverse side if necessary and identify by block number) The effect of temperature and moisture on the fatigue properties of AS/3501-6 composite was explored. This includes the design of a fatigue specimen, its fabrication procedure, displacement and temperature monitoring technique, and analysis/data correlation. The specimens used were of layup [90]20 and [±45]20. The fatigue load ratio was set at 0.1 and the cyclic frequency was set at three hertz. No appreciable heat was generated in the 90° specimen during fatigue. The ±45 specimens experienced appreciable		

**UNCLASSIFIED**

SECURITY CLASSIFICATION OF THIS PAGE(When Data Entered)

temperature increases at various environments. Test data from a fatigue tension test was generated to supplement the analysis of predicting the temperature distribution in the specimen due to continuous heat generation experienced by the ~~+45°~~ specimen. A probabilistic fatigue failure model derived from the concept of crack propagation in viscoelastic material was used for the data analysis. The temperature effect and moisture effect was accounted for by this analysis model.

+ or -45 deg

**UNCLASSIFIED**

SECURITY CLASSIFICATION OF THIS PAGE(When Data Entered)

## FOREWORD

This study for the Phase II program entitled "The Effect of Environment on Mechanical Behavior of AS/3501-6 Graphite/Epoxy Material" was conducted by Vought Corporation Advanced Technology Center and was sponsored by the Naval Air Systems Command under Contract Number N00019-78-C-0599.

Mr. M. Stander was the Navy Project Manager and Dr. W. J. Renton was the Vought Program Manager. Other key personnel are Dr. T. Ho, Principal Investigator, Dr. D. H. Petersen, Technical Coordinator, and Dr. R. A. Schapery, Technical Consultant.

This study was conducted from September 1978 through August 1979.

Accession For	
NTIS GRA&I	<input checked="" type="checkbox"/>
PTIC TAB	<input type="checkbox"/>
Unannounced	<input type="checkbox"/>
Justification	
By _____	
Distribution/	
Availability Class	
Avail and/or	
Dist	Special
A	

## LIST OF FIGURES

<u>FIGURE</u>		
		<u>PAGE NO.</u>
1	Typical Fatigue Specimen	5
2	Fatigue Specimen Fabrication Procedure	6
3	Specimen Edge Surface Finishes Obtained Through Various Kinds of Cutting Techniques	7
4	Fresh GR/EP Surface Obtained From Wafering Cutter Method	9
5	The Porosity Defect and the Carbide Cut Surface Defect In the Specimens	10
6	The Surface Peel Defect in the Specimen	11
7	Cracks in Specimens That Were Conditioned in 200°F/95% R.H. Environment	12
8	Moisture Absorption of 90°-Specimen Under 170°F/95% R.H. Environment	14
9	Calibration of LVDT	17
10	Temperature Sensor Mounted on Specimen In the Environ- mental Test Chamber	18
11	Creep-Recovery Test and Data Aquisition System	20
12	Long Term Creep-Recovery Test of a $\pm 45^\circ$ Specimen Under 176°F/50% R.H. Environment	21
13	Straight Line Analysis for Power Law Equation	22
14	Three Failure Modes of 90° Specimens	26
15	Stress-Strain Curves for 90° Specimens Within Three Environments	27
16	Ultimate Strength of 90° Specimens Within Various Environments	28
17	Ultimate Strain of 90° Specimens Within Various Environments	28
18	Failure Modes of $\pm 45^\circ$ Specimens	29
19	Stress-Strain Curves for $\pm 45^\circ$ Specimens Within Three Environments	30

LIST OF FIGURES  
(Continued)

<u>FIGURE</u>		<u>PAGE NO.</u>
20	Ultimate Strength of $\pm 45^\circ$ Specimens Within Various Environments	32
21	Ultimate Strain of $\pm 45^\circ$ Specimens Within Various Environments	32
22	Extensometer and Temperature Sensors on Fatigue Specimen	33
23	Fatigue Test Arrangement and Data Aquisition System	34
24	Failure and Related Creep of $90^\circ$ Specimen Tested at $170^\circ\text{F}/95\%$ R.H. Environment	35
25	Typical Strip Chart Recording of Load and Displacements for $\pm 45^\circ$ Specimen During Fatigue	36
26	The S-N Curve of $\pm 90^\circ$ Specimen at Various Environments	48
27	The S-N Curve of $\pm 45^\circ$ Specimen at Various Environments	49
28	Strip Chart Recording of Load and Displacement of $\pm 45^\circ$ Specimen During Hysteresis Test at $170^\circ\text{F}/50\%$ R.H. Environment and 60% of Ultimate Strength	51
29	Typical Hysteresis Loops From X-Y Recorder for Fatigue Specimens Tested Under 60% of Ultimate Strength With Load Ratio at 0.1 for 0.1 Hz	53
30	Geometry of Hysteresis Loop For Composite Under Ramp Load	54
31	Sensor Arrangement for Temperature Profile Test	57
32	Temperature Rise on $\pm 45^\circ$ Specimen Surfaces When Fatigue Tested in an $75^\circ\text{F}/50\%$ R.H. Environment	60
33	Temperature Rise on $\pm 45^\circ$ Specimen Surfaces When Fatigue Tested in an $132^\circ\text{F}/50\%$ R.H. Environment	62
34	Temperature Rise on $\pm 45^\circ$ Specimen Surfaces When Fatigue Tested in an $132^\circ\text{F}/95\%$ R.H. Environment	63
35	Temperature Rise on $\pm 45^\circ$ Specimen Surfaces When Fatigue Tested in an $170^\circ\text{F}/50\%$ R.H. Environment	64
36	Temperature Rise on $\pm 45^\circ$ Specimen Surfaces When Fatigue Tested in an $170^\circ\text{F}/95\%$ R.H. Environment.	65

LIST OF FIGURES  
(Continued)

<u>FIGURE</u>		<u>PAGE NO.</u>
37	Fatigue Failure From Quality 90° Specimen	67
38	Porosity That Involved the Fatigue Failure of 90° Specimen	68
39	Machine Defects That Involved the Fatigue Failure of 90° Specimen	69

## LIST OF TABLES

<u>TABLE</u>		<u>PAGE NO.</u>
1	Composite Panels For the Program	4
2	The Layup Procedure and Cure Cycle For AS/3501-6	4
3	Mechanical Properties of Process Control Panel	5
4	Test Matrix For Phase II Program	16
5	Static Properties of 90° Specimens in Various Environments	24
6	Static Properties of $\pm 45^\circ$ Specimens in Various Environments	25
7	Fatigue Test Results For 90° Specimen Within A 75°F/50% R.H. Environment	38
8	Fatigue Test Results For 90° Specimen Within A 132°F/50% R.H. Environment	39
9	Fatigue Test Results For 90° Specimen Within A 132°F/95% R.H. Environment	40
10	Fatigue Test Results For 90° Specimen Within A 170°F/50% R.H. Environment	41
11	Fatigue Test Results For 90° Specimen Within A 170°F/95% R.H. Environment	42
12	Fatigue Test Results For $\pm 45^\circ$ Specimen Within A 75°F/50% R.H. Environment	43
13	Fatigue Test Results For $\pm 45^\circ$ Specimen Within A 132°F/50% R.H. Environment	44
14	Fatigue Test Results For $\pm 45^\circ$ Specimen Within A 132°F/95 % R.H. Environment	45
15	Fatigue Test Results For $\pm 45^\circ$ Specimen Within A 170°F/50% R.H. Environment	46
16	Fatigue Test Results For $\pm 45^\circ$ Specimen Within A 170°F/95% R.H. Environment	47

LIST OF TABLES  
(Continued)

<u>TABLE</u>		<u>PAGE NO.</u>
17	Hysteresis Test Matrix	50
18	Environmental Effect on the Characteristics of Hysteresis Loops at 0.1 Hz Frequency	55
19	Temperature Profile Test of $\pm 45^\circ$ Specimen	58
20	Test/Analysis Correlation Study	73

## TABLE OF CONTENTS

	<u>PAGE NO.</u>
FOREWORD	i
LIST OF FIGURES	ii
LIST OF TABLES	v
1.0 INTRODUCTION	1
2.0 SPECIMEN FABRICATION AND CONDITIONING	3
2.1 SPECIMEN FABRICATION AND QUALITY ANALYSIS	3
2.2 MOISTURE ABSORPTION STUDY AND SPECIMEN CONDITIONING	8
3.0 MECHANICAL TEST	15
3.1 TEST MATRIX AND TEST INSTRUMENTATION	15
3.2 CREEP-RECOVERY TESTS	15
3.3 STATIC TESTS	19
3.4 FATIGUE TESTS	31
3.5 HYSTERESIS TESTS	37
4.0 ANALYSIS OF TEST RESULTS	56
4.1 THERMAL ANALYSIS	56
4.2 FATIGUE ANALYSIS	66
5.0 DISCUSSIONS AND CONCLUSIONS	74
6.0 REFERENCES	76

## 1.0 INTRODUCTION

Wide usage of advanced composite materials in aerospace systems is projected to become a reality over the next ten years. A V/STOL fighter aircraft is one of several Navy articles projected to be increasingly dependent on composite materials for primary and secondary structural components.

Presently, it is known that many realistic service loads and environments have a significant adverse effect on the performance of advanced composite materials. The material's response characterization procedures in severe environments and related fatigue lifetime prediction methods are presently insufficient. This complete research program will assist in resolving this deficiency in the technology base. This in turn will help to ensure that confident usage of advanced composite materials by the stress analyst and designer can be attained in the near future.

The overall objectives of this research program are:

- 0 To ascertain if the mechanical response of AS/3501-6 graphite/epoxy composite material, subject to various time, temperature and moisture effects, can be characterized using traditional viscoelastic shift factors, and to formulate a master curve of material property dependence on time, temperature and humidity.
- 0 To ascertain the feasibility of predicting fatigue failure of a composite material by accounting for the linear viscoelastic behavior of the resin in various temperature and humidity environments.
- 0 To determine if a specific thermal conditioning environment can be directly substituted for a specific moisture conditioning environment over a prescribed temperature vs. humidity range for AS/3501-6 graphite/epoxy material, and obtain an equivalent moisture effect on mechanical and fatigue properties. If this can be shown, a substantial cost and time savings in moisture conditioning of the test specimen can be achieved and possibly extended to other composite specimens.

During the first phase of this program, the basic static properties of AS/3501-6 graphite/epoxy composite material, subjected to various temperature and humidity environments, was characterized through linear viscoelastic theory. The first and third objectives were achieved, at least for the environments investigated. This report covers exploratory research to study the second objective, which calls for the fatigue characterization of composite material in various temperature and humidity environments. Tests of fatigue specimens with basic laminate layups of  $90^\circ$  and  $\pm 45^\circ$  were successfully conducted within several severe environments. Internal damping of the  $\pm 45^\circ$  specimens created a considerable temperature rise in the course of fatigue cycling.

An analytical study of fatigue failure prediction methodology based on the fatigue test results was begun in Phase II and will be pursued during the Phase III segment of this program, and thereby initially determine the extent to which viscoelastic behavior is a necessary factor in predicting the fatigue failure of composite materials.

## 2.0 SPECIMEN FABRICATION AND CONDITIONING

### 2.1 SPECIMEN FABRICATION AND QUALITY ANALYSIS

Hercules AS/3501-6 prepreg tape was used to prepare the specimens for this program. Four composite panels, as shown in Table 1, were fabricated by Vought's Manufacturing Research and Development Division per the fabrication procedure in Table 2 recommended by Hercules. Panels A and B of Table 1 were for  $90^{\circ}$  specimens and panels C and D were for  $\pm 45^{\circ}$  specimens. Each panel was inspected with ultrasonic C-scan by a 5-MHz transducer (40 dB level for  $90^{\circ}$  panels and 45 dB level for  $\pm 45^{\circ}$  panels). Only panel A was shown to possess a defect area. A process control panel was separately made to evaluate the quality of the panels. The mechanical properties of the specimens from the process control panel are summarized in Table 3. The flexural strength, flexural modulus and short beam shear results indicate that our panels yield acceptable properties as compared with vendor published values for AS/3501-6 composite.

A typical fatigue specimen 7.0" long by .75" wide is shown in Figure 1. A specimen fabrication procedure that is capable of minimizing the edge defects was developed as shown in Figure 2. A comparison of the composite's finished cut surfaces as obtained from using different cutting techniques is shown in Figure 3. Upon inspection of the 40X photomicrograph, it becomes apparent that a wafering diamond cutter produces a better surface finish than those produced by a carbide bandsaw, radial diamond saw, or 400 grit fine sandpaper. Most machining defects seem to have disappeared on the wafering cut surface, including the edge area. Approximately 130  $90^{\circ}$ -specimens and 130  $\pm 45^{\circ}$ -specimens were subsequently fabricated according to Figure 2 and used for testing in this program.

The finished thickness of the  $90^{\circ}$ -specimen is approximately 0.10 inches (20 plies) which is considered to be thick enough to avoid normal handling damage of  $90^{\circ}$ -specimens. The thickness of the  $\pm 45^{\circ}$ -specimens is around 0.04 inches (8 plies) which is designed to be thinner than that of the  $90^{\circ}$ -specimens in order to transfer sufficient load through the bonded tab area without inducing a bond tab failure during the fatigue test.

TABLE 1. COMPOSITE PANELS FOR THE PROGRAM

PANEL NO.	LAYUP ORIENTATION	DIMENSION	C-SCAN READING
A	$[90^\circ]_{20}$	48" x 16" x .1"	One Defect Area With Size 5" x 1"
B	$[90^\circ]_{20}$	20" x 16" x .1"	No Defect
C	$[\pm 45^\circ]_{2S}$	48" x 16" x .04"	No Defect
D	$[\pm 45^\circ]_{2S}$	20" x 16" x .04"	No Defect

TABLE 2. THE LAYUP PROCEDURE AND CURE CYCLE FOR AS/3501-6

<p>The layup procedure was:</p> <ul style="list-style-type: none"> <li>o Clean all tooling</li> <li>o Apply a mold release agent to the tooling</li> <li>o Cover both surfaces of the layup with peel ply</li> <li>o Cover both surfaces of the layup with TX-1040</li> <li>o Position the layup on the tool</li> <li>o Apply the cork dam and 6 bleeder plies</li> <li>o Cover the layup with nylon film</li> <li>o Cover the layup with two plies of fiberglass bleeder cloth</li> <li>o Install the layup in a vacuum bag and place in an autoclave</li> </ul>
<p>The cure cycle was:</p> <ul style="list-style-type: none"> <li>o Apply 25" Hg minimum vacuum</li> <li>o Apply 10 psi autoclave pressure</li> <li>o Heat to <math>350 \pm 5^\circ\text{F}</math> (5-10°F/min rate)</li> <li>o Apply <math>90 \pm 5</math> psi autoclave pressure when the panel reaches <math>275 \pm 5^\circ\text{F}</math> (DO NOT VENT)</li> <li>o Maintain the laminate at <math>350 \pm 5^\circ\text{F}</math> for <math>120 \pm 5</math> minutes</li> <li>o Cool slowly to below <math>150^\circ\text{F}</math> (Cool no faster than 5°F per minute - Cool down should take approximately 45 minutes)</li> </ul>

TABLE 3. MECHANICAL PROPERTIES OF PROCESS CONTROL PANEL.

SHORT BEAM SHEAR (PSI)	FLEXURAL STRENGTH (PSI)	FLEXURAL MODULUS ( $10^6$ PSI)
22,018	287,770	21.17
26,181	340,166	21.99
27,143	340,529	24.89
AVE. 25,114(17,500)	322,822(260,000)	22.68(20.6)

NOTE 1: Average Fiber Volume Content is 62.4% For The Panels

2: Vendor Data Are In Parentheses For a 62% Fiber Volume Per AS/3501-6  
Data Sheet

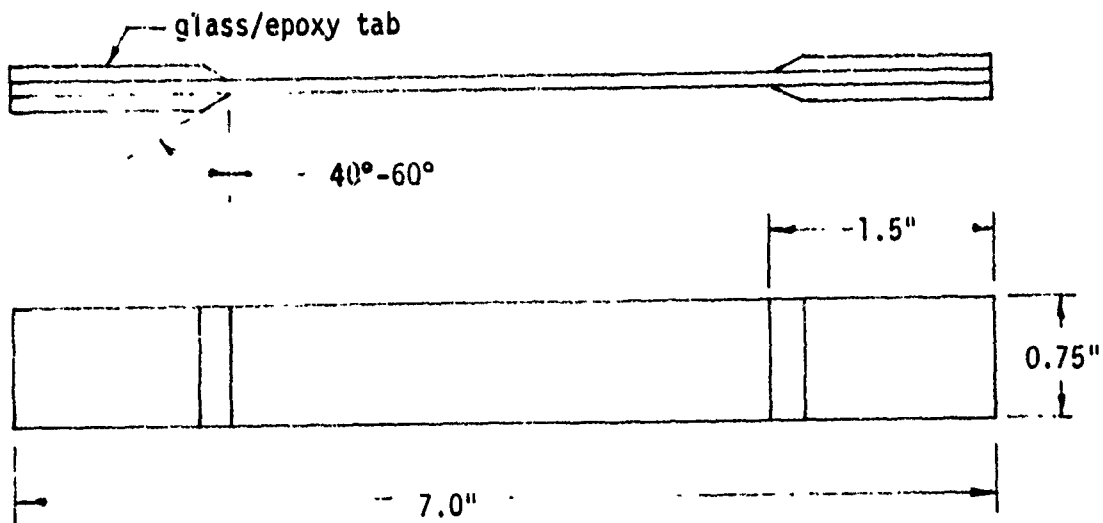


FIGURE 1. TYPICAL FATIGUE SPECIMEN.

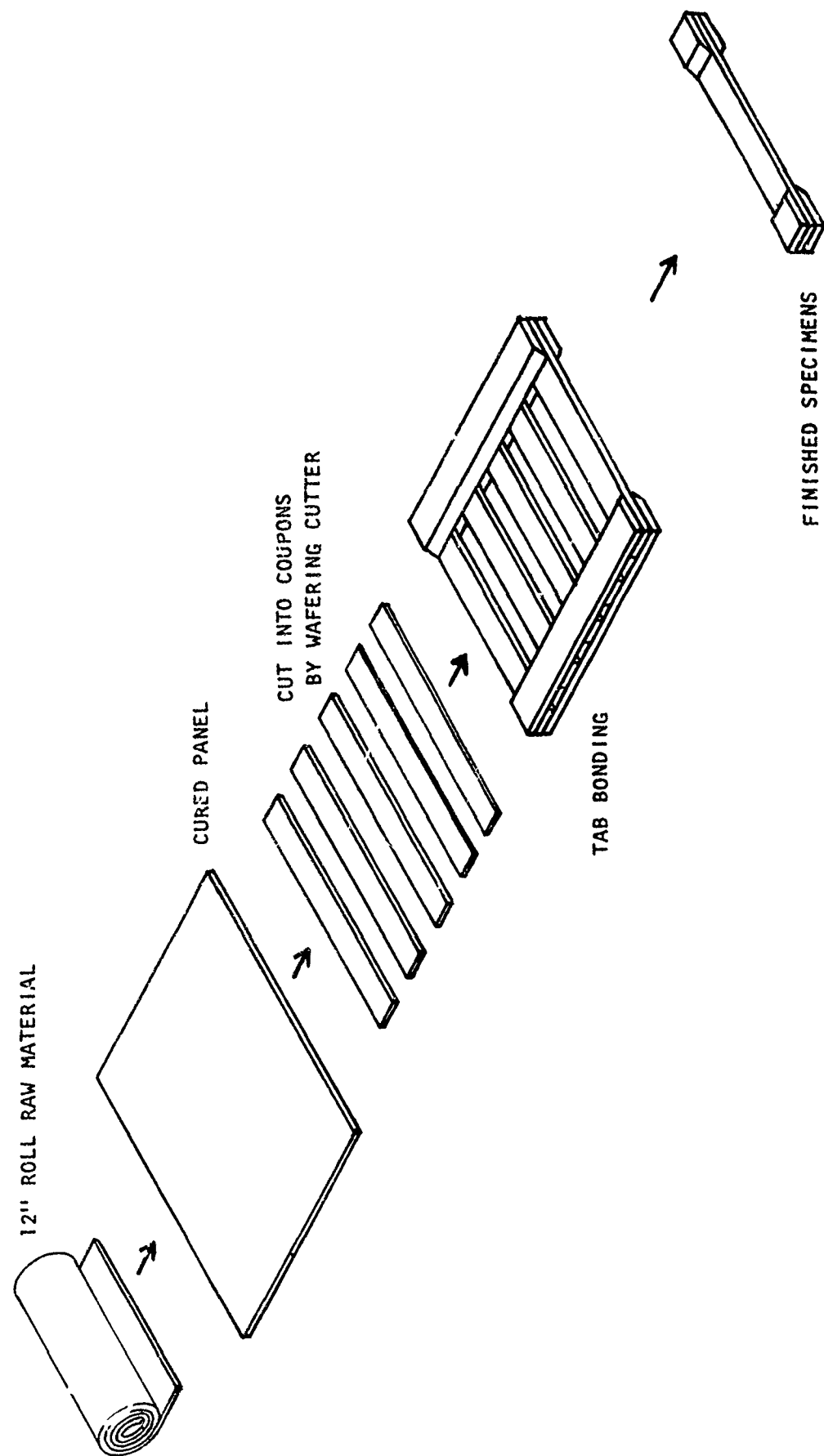
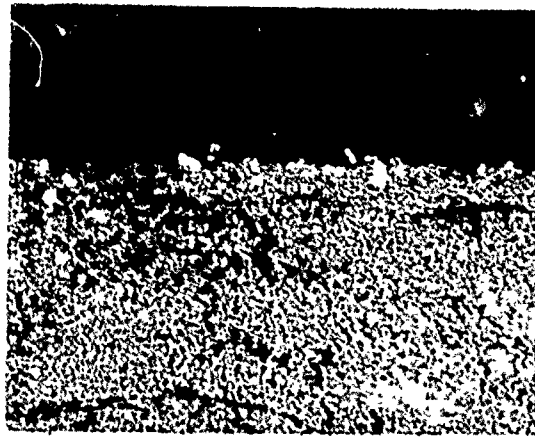
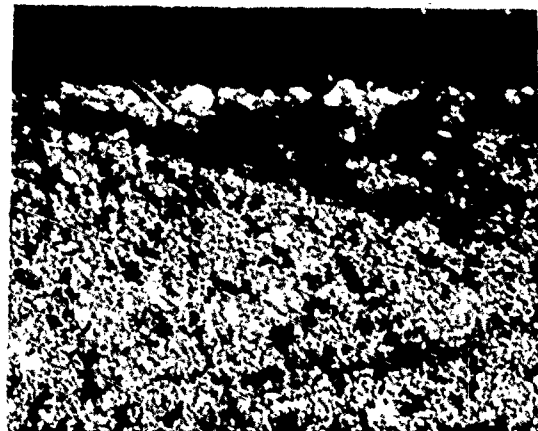


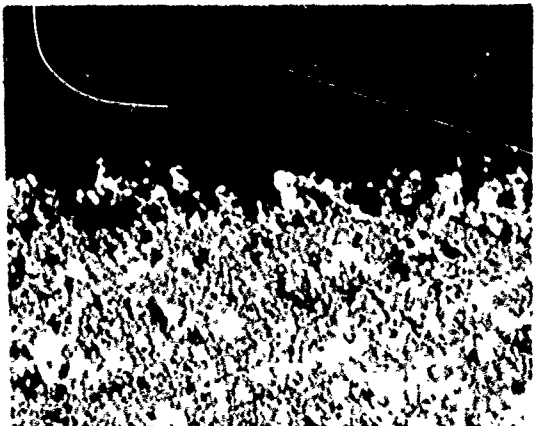
FIGURE 2. FATIGUE SPECIMEN FABRICATION PROCEDURE.



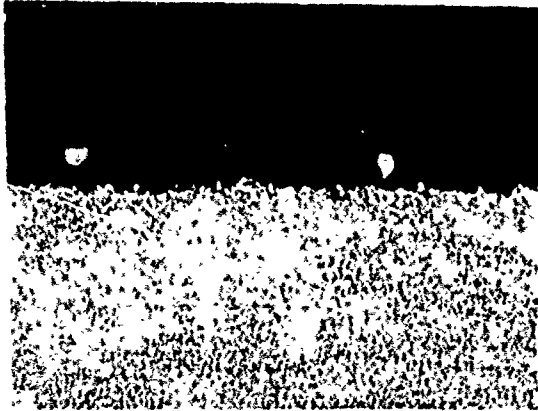
(a) Surface Finish by Wafering  
Diamond Cutter (40X)



(b) Surface Finish by Radial  
Diamond Saw (40X)



(c) Surface Finish by Carbide  
Band Saw (40X)



(d) Surface Finish by 400 Grit  
Sand Paper (40X)

FIGURE 3. SPECIMEN EDGE SURFACE FINISHES OBTAINED THROUGH  
VARIOUS KINDS OF CUTTING TECHNIQUES.

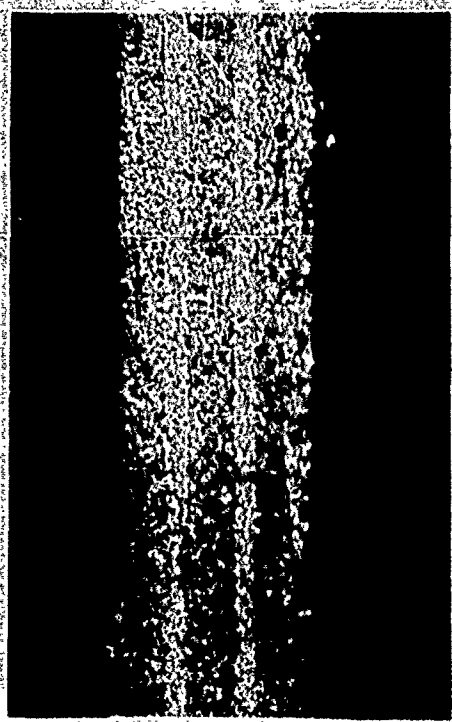
Each individual specimen was examined under a microscope (16X or 25X magnification) to ascertain the presence of porosity and/or possible machining defects. The texture of the edge of a typical specimen is shown in Figure 4. Those surfaces were prepared using a wafering cutter. Most specimens were of high quality. This is a good indication that machining defects have been minimized in the preparation of the current batch of specimens and that the scatter of data would also be more confined.

Although care was taken in specimen preparation, certain defects still existed in some specimens, especially 90°-specimens. Those defects are classified as porosity, carbide cut and surface peel and are shown in Figures 5 and 6 respectively. All three types of defects represent flaws or notches that may have a bearing on the crack propagation in the fatigue specimens. The surface peel defects result from removing the peel ply from the surface of the cured panels. Surface peel defects were found in only two incidents. The average void content in the 90°-specimens was 1.3% based on the photomicrograph pictures. Porosity defects are normally found in only those specimens that have void content in excess of roughly 2.5%. Porosity defects were not found in the  $\pm 45^\circ$  specimens. Carbide cut defects were created by accidentally touching the carbide bandsaw to the edge of the specimen during the cutting of the tabs. Both the carbide cut defect and surface peel defect will be called machine defect in the future quality analysis discussion.

Carbide cut defects on 90°-specimens were removed by sanding the defect surface using 400 grid sandpaper. Porosity defects and surface peel defects were left untreated. The purpose of the above defect observations was to understand the specimen quality and to identify the parameters that might cause a relatively large fatigue data scatter.

## 2.2 MOISTURE ABSORPTION STUDY AND SPECIMEN CONDITIONING

In the process of conditioning the specimens at elevated temperatures and humidities, microcracks may be created in the specimen. Since this program is primarily a fatigue life study, it is important to not introduce any significant damage from conditioning. Several specimens were examined after they had been conditioned to moisture saturation at 200°F. As shown in Figure 7, cracks

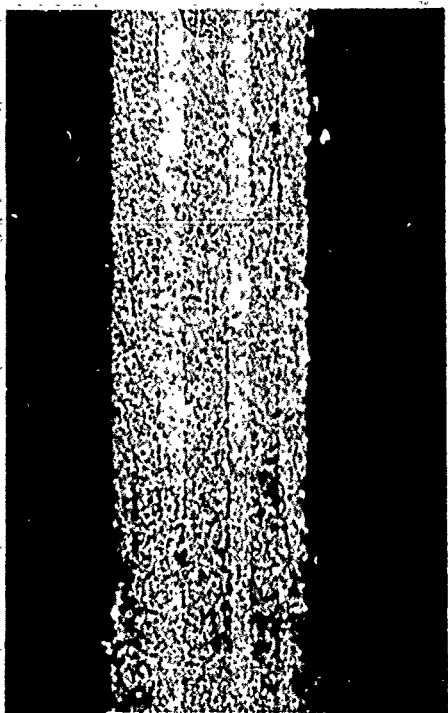


a.  $\pm 45^\circ$  SPECIMEN (25X)

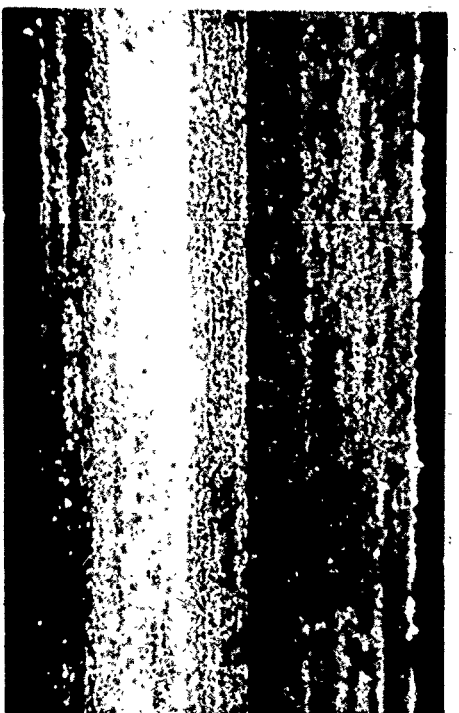


b.  $90^\circ$  SPECIMEN (16X)

FIGURE 4. FRESH GR/EP SURFACE OBTAINED  
FROM WAFERING CUTTER METHOD

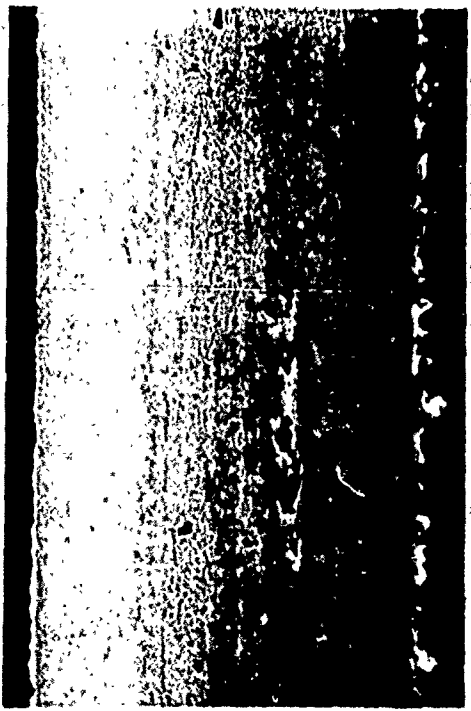


a.  $\pm 45^\circ$  SPECIMEN (25X)

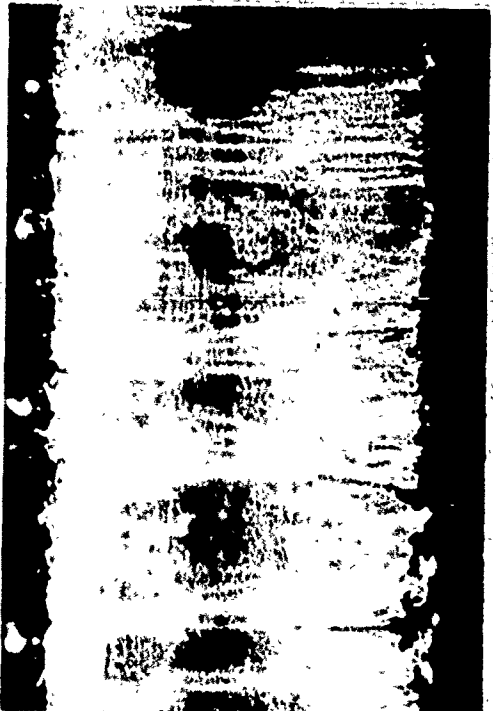


b.  $90^\circ$  SPECIMEN (16X)

FIGURE 4. FRESH GR/EP SURFACE OBTAINED  
FROM WAFERING CUTTER METHOD



a. POROSITY DEFECT (16X)

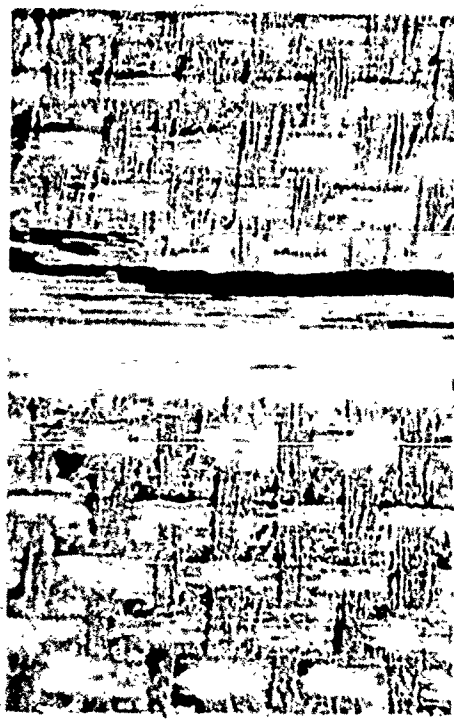


b. CARBIDE CUT SURFACE DEFECT (16X)

FIGURE 5. THE POROSITY DEFECT AND THE CARBIDE CUT SURFACE DEFECT IN THE SPECIMENS

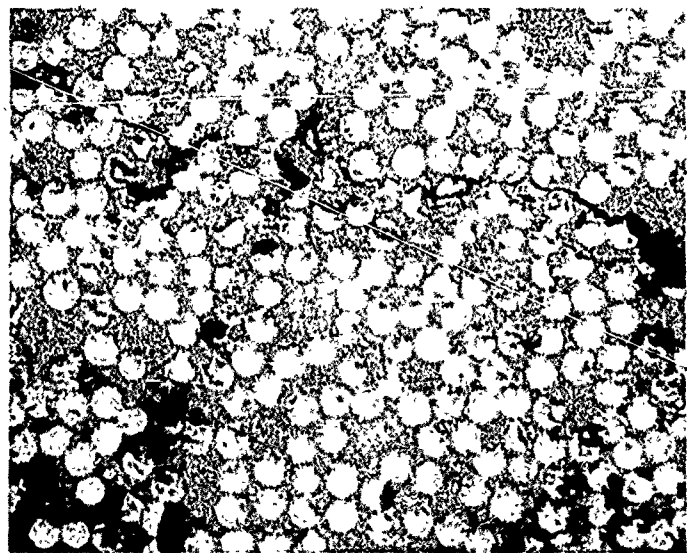


a. SIDE VIEW (16X)

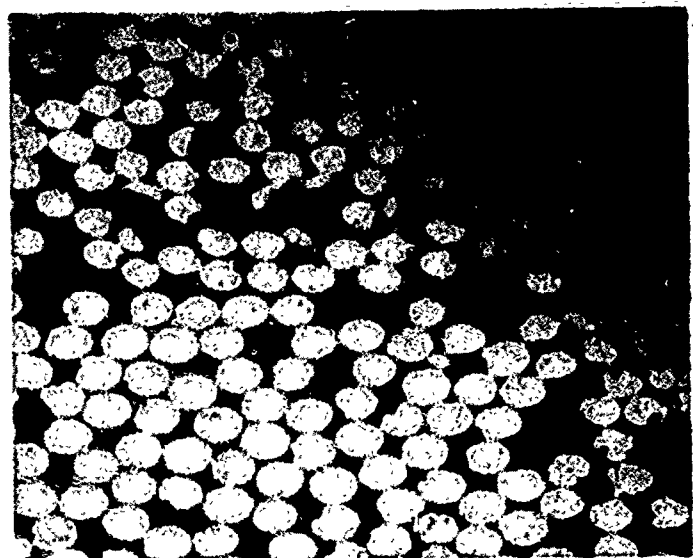


b. TOP VIEW (16X)

FIGURE 6. THE SURFACE PEEL DEFECT IN THE SPECIMEN



(a) Cracks in 90° Specimen (590X)



(b) Cracks in  $\pm 45^\circ$  Specimen (590X)

FIGURE 7. CRACKS IN SPECIMENS THAT WERE CONDITIONED  
IN 200°F/95% R.H. ENVIRONMENT.

were observed in both the  $\pm 45^\circ$  and  $90^\circ$  specimens conditioned in the  $200^\circ\text{F}/95\%$  R.H. environment. Cracks were not observed in specimens from Phase I program that were conditioned in the  $200^\circ\text{F}/71\%$  R.H. environment or room temperature environment. Thus, specimens designated for testing at various temperatures in a 50% and 95% R.H. environments were conditioned for moisture absorption in a  $170^\circ\text{F}$ .

An enclosed glass chamber and a forced air oven were used to environmentally condition the specimens to the desired moisture level. A saturated aqueous solution of Sodium Bromide (NaBr) in contact with a solid phase of the salt at  $170^\circ\text{F}$  temperature was used to generate the 50% relative humidity level and that of Sodium Fluoride (NaF) was used to generate the 95% relative humidity level. The length of time required to attain 95% saturation was determined by moisture absorption tests. Two square samples with dimensions  $0.75'' \times 0.75'' \times 0.1''$  were placed in the  $170^\circ\text{F}/95\%$  R.H. environment for conditioning. The moisture absorption result is shown in Figure 8. It is apparent that 85 days of conditioning is necessary to insure that the specimens with a  $0.10''$  thickness attain at least 95% saturation at the  $170^\circ\text{F}$  temperature environment. Based on results from Shen and Springer<sup>2</sup>, eighty-five days of conditioning for a specimen with a  $0.10''$  thickness will translate to fifteen days of conditioning for  $\pm 45^\circ$  specimens which have a  $0.04''$  thickness. Thus the  $90^\circ$ -specimens were conditioned for at least 85 days and the  $\pm 45^\circ$  specimens for a minimum of 15 days in the  $170^\circ\text{F}$  environments (either 95% R.H. or 50% R.H.) before initiating the physical tests.

During the environmental conditioning, fatigue specimens were positioned in three-level steel racks in the glass chamber. The three-level steel racks can house up to forty-eight specimens and were designed for ease of specimen tracking and handling. Before conditioning, tab areas of all the specimens were coated with Ecco-coat VE on top of the scotch tape to prevent adhesive degradation by moisture ingress so that the bonding strength of the adhesive in the tab area could be maintained at the desired level (around 5000 psi for the bonding adhesive) during the fatigue test.

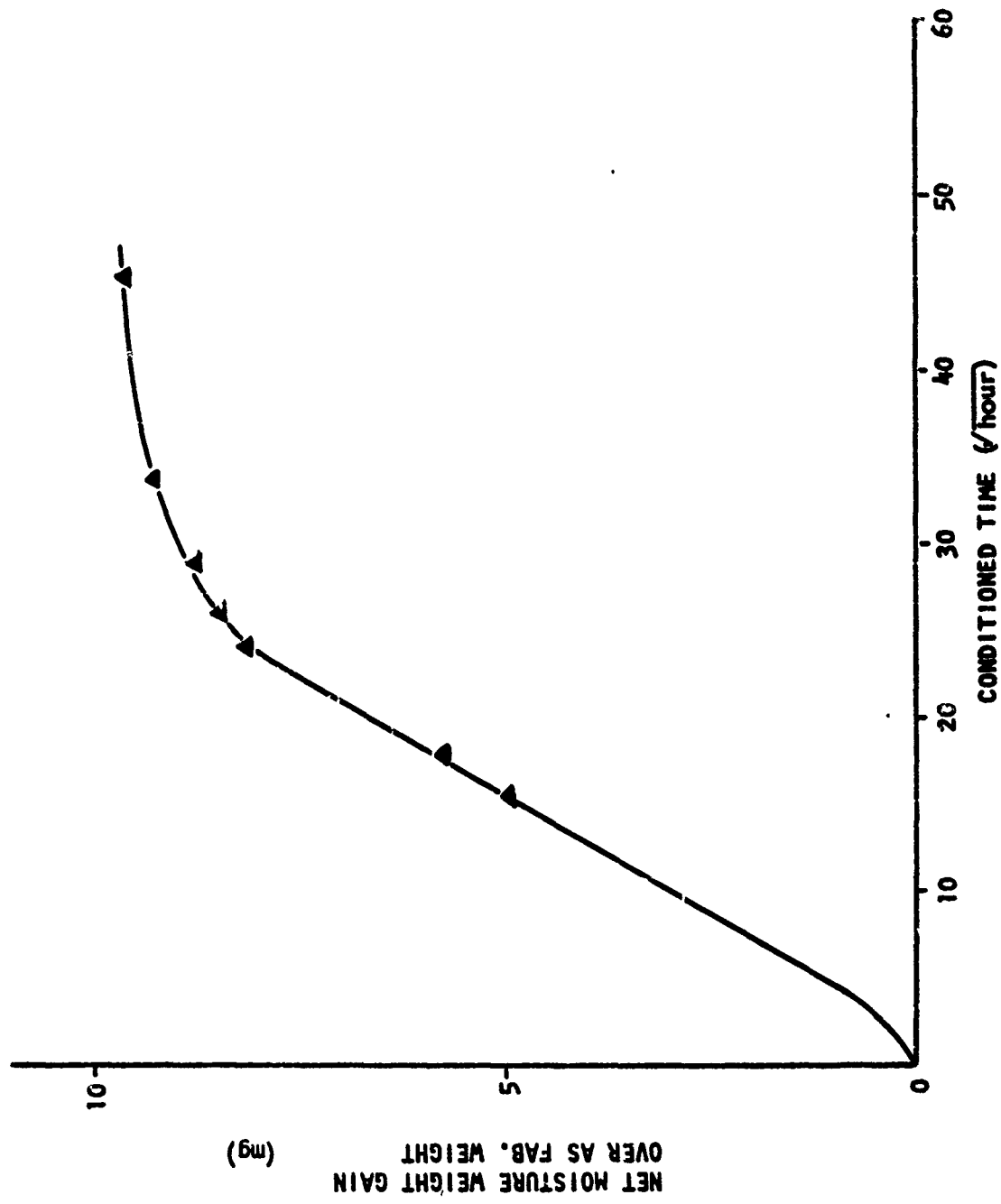


FIGURE 8. MOISTURE ABSORPTION OF 90°-SPECIMEN UNDER 170°F/95% R.H. ENVIRONMENT

### 3.0 MECHANICAL TESTS

#### 3.1 TEST MATRIX AND TEST INSTRUMENTATION

Specific tests that were conducted in this program are shown in the test matrix, Table 4. Baseline data on the fatigue load levels employed in test Item C, were determined by static strength tests from ITEM A of the test matrix. Hysteresis tests (Item B) were conducted at various stress levels and frequencies within various environments to evaluate the temperature rise due to heat generation. Fatigue tests (Item C) were conducted at various environments by keeping the mean stress level and environment unchanged during the cycling. Creep-recovery tests (Item D) were conducted to verify that the long term creep-recovery results are predictable from previous obtained short-term data.

Half of the fatigue specimens had their displacement monitored continuously during testing with the environmental extensometer which Vought developed for the Phase I program. Each extensometer was conditioned in a 180°F dry environment for two weeks to study the long term exposure effect on its data gathering accuracy. As shown in Figure 9, the calibration of the LVDT after the conditioning duplicates its calibration before the conditioning. Thus, extensometer readings were assumed to remain stable throughout the test program. Two sets of extensometers were used alternately. All the  $\pm 45^\circ$ -specimens and selected  $90^\circ$ -specimens had one resistor type temperature sensor (ETG-50B from Micro-Measurements) to monitor the continuous temperature reading of the specimen during fatigue cycling. The temperature sensor was encapsulated between two pieces of 0.5" x 0.5" x 0.004" stainless steel plates, as shown in Figure 10, and is attached to one side of the specimen by using a small U-shape steel spring clamp.

#### 3.2 CREEP-RECOVERY TESTS

Numerous creep-recovery tests were conducted in the Phase I program to study the effect of environment on the mechanical behavior of AS/3501-6 composite material. Those creep-recovery tests were all one hour in duration - 15 minutes loading and 45 minutes unloading. In order to validate the applicability of the test results from a one-hour test to the accurate prediction of long term composite material properties, creep-recovery tests with a one-day loaded and three days unloaded profile, were conducted at the 176°F/50% R.H. environment which is one of the environments used in the Phase I program. The specimen used was a  $\pm 45^\circ$

TABLE 4. TEST MATRIX FOR PHASE II PROGRAM

TEST	TYPE OF TEST	TEST ENVIRONMENT (°F/% R.H.)	REPLICAS PER TEST	NO. OF 90° SPECIMENS	NO. OF 45° SPECIMENS	REMARKS
A	Static Test	AS FAB	2	2	2	To Establish Baseline Data For Fatigue Load Level
		75/50		2	2	
		132/50		2	2	
		132/95		2	2	
		170/50		2	2	
B	Hysteresis Test	170/95	3 Stress x 3 Frequency x 1	1	1	To Correlate Temperature rise to fatigue loading
		170/50		1	1	
		132/95		1	1	
		132/50		1	1	
		70/50		1	1	
C	Fatigue at Single Load and Single Temperature	AS FAB	3 Stress x 6	18	18	To Investigate Basic Fatigue Behavior
		170/95		18	18	
		170/50		18	18	
		132/95		18	18	
		132/50		18	18	
D	Creep-Recovery	75/50	2	1	1	To Study Long Term Creep-Recovery Behavior
		176/50				

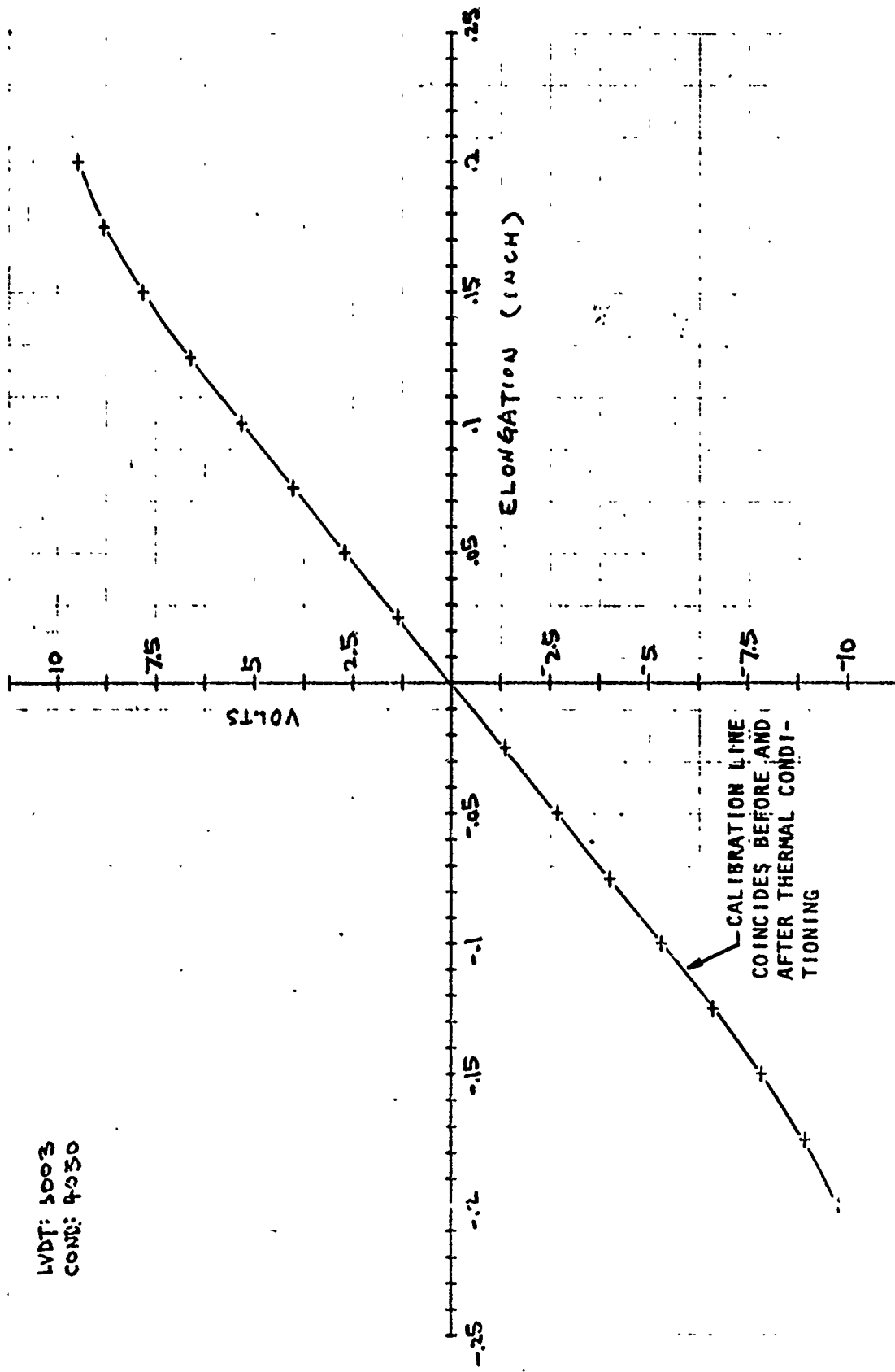


FIGURE 9. CALIBRATION OF LVDT.

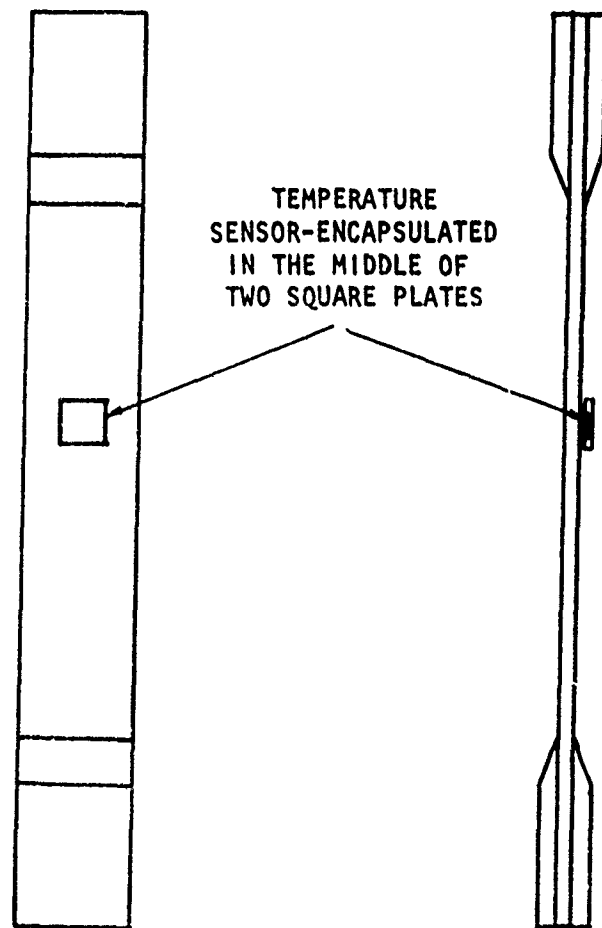


FIGURE 10. TEMPERATURE SENSOR MOUNTED ON SPECIMEN IN THE ENVIRONMENTAL TEST CHAMBER.

specimen which had been cycled in creep-recovery several times in short duration (two cycles per minutes). The creep-recovery test setup is shown in Figure 11. Due to the capability of the test equipment, two creep-recovery cycles were completed. The 8-day creep-recovery test result is shown in Figure 12. The second cycle is used for data analysis. Based on the discussion in the Phase I program, (section 6.0 of Reference 1) the creep compliance,  $\epsilon/\sigma$ , of AS/3501-6 composite material can be represented by the power law equation:

$$D = D(t, T, H) = D_0 + D_1 t^n = D_0 + D_1 \left(\frac{t}{a_T a_H}\right)^n$$

By plotting the creep data vs. various values of  $n$ , we were able to find, from the compliance  $D$  vs.  $t^n$  plots in Figure 13, that  $n = 0.18$  gives the best straight line data fit based on creep-recovery data of the second cycle in Figure 12. That is, 0.18 is the best value for the exponent in the power law equation (1) at 176°F/50% R.H. environment. The exponent value, 0.18 was also the result from short term creep-recovery test data developed in the Phase I program and it is a value that is appropriate for the environments studied (there are small fluctuations of  $n$  value at different environments). By using equation (1) and Figure 13, one can obtain values of initial compliance  $D_0$  and transient compliance  $D_1$ . Together with the data from the Phase I program, the power law constants presently obtained are shown in Figure 13. If the creep-recovery test had been continued into the third or fourth cycle, the values of  $D_0$  and  $D_1$  may have been closer to those found previously. But, as noted below, there is a difference in conditioning environments for the earlier and current tests, which could account for at least some of the difference in the values of  $D_0$  and  $D_1$ .

### 3.3 STATIC TESTS

Since a new procedure was used to fabricate the Phase II specimens and the specimens were conditioned in the 170°F wet environment instead of the 200°F wet environment used in Phase I, new static tests in tension were conducted. The load rate for the static tests was set at 250 lb/min and the displacement in the gage section of the specimen was monitored by using the extensometer system that was developed in Phase I. Before testing, specimens were moisture saturated to their

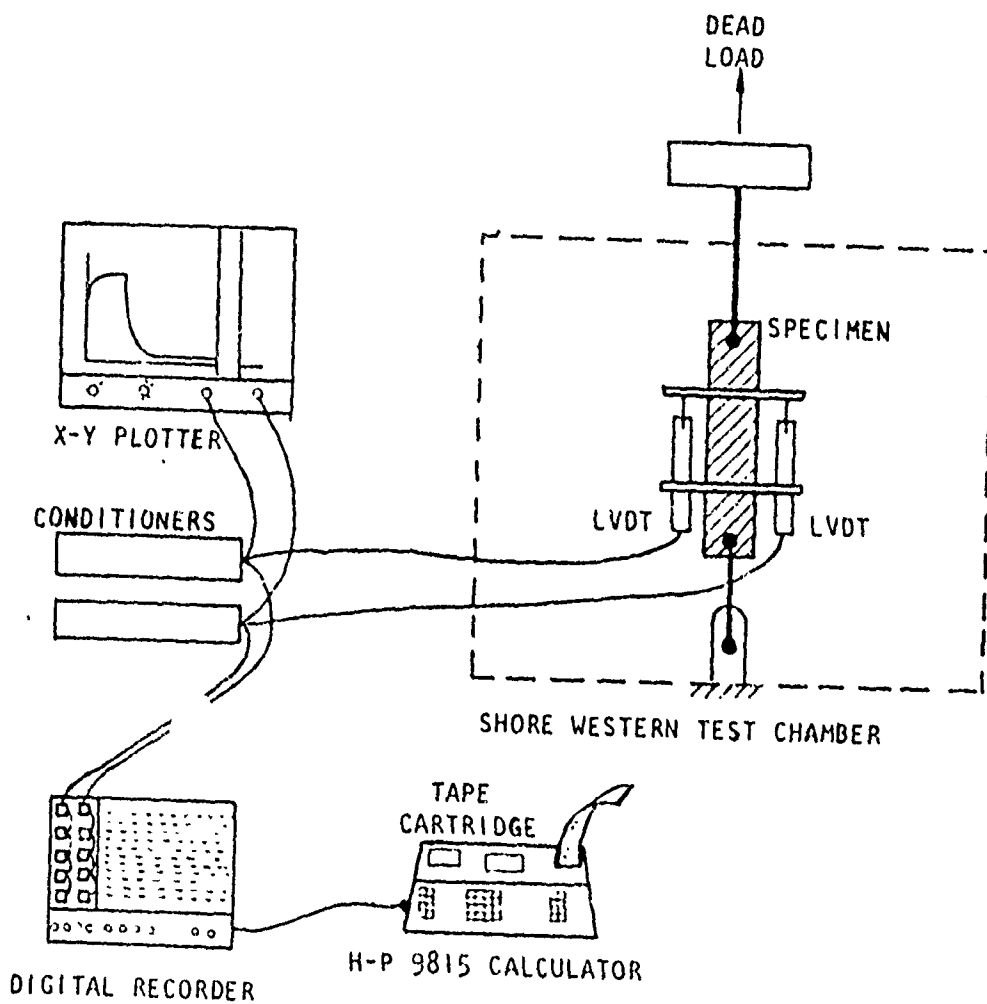


FIGURE 11. CREEP RECOVERY TEST AND DATA ACQUISITION SYSTEM.

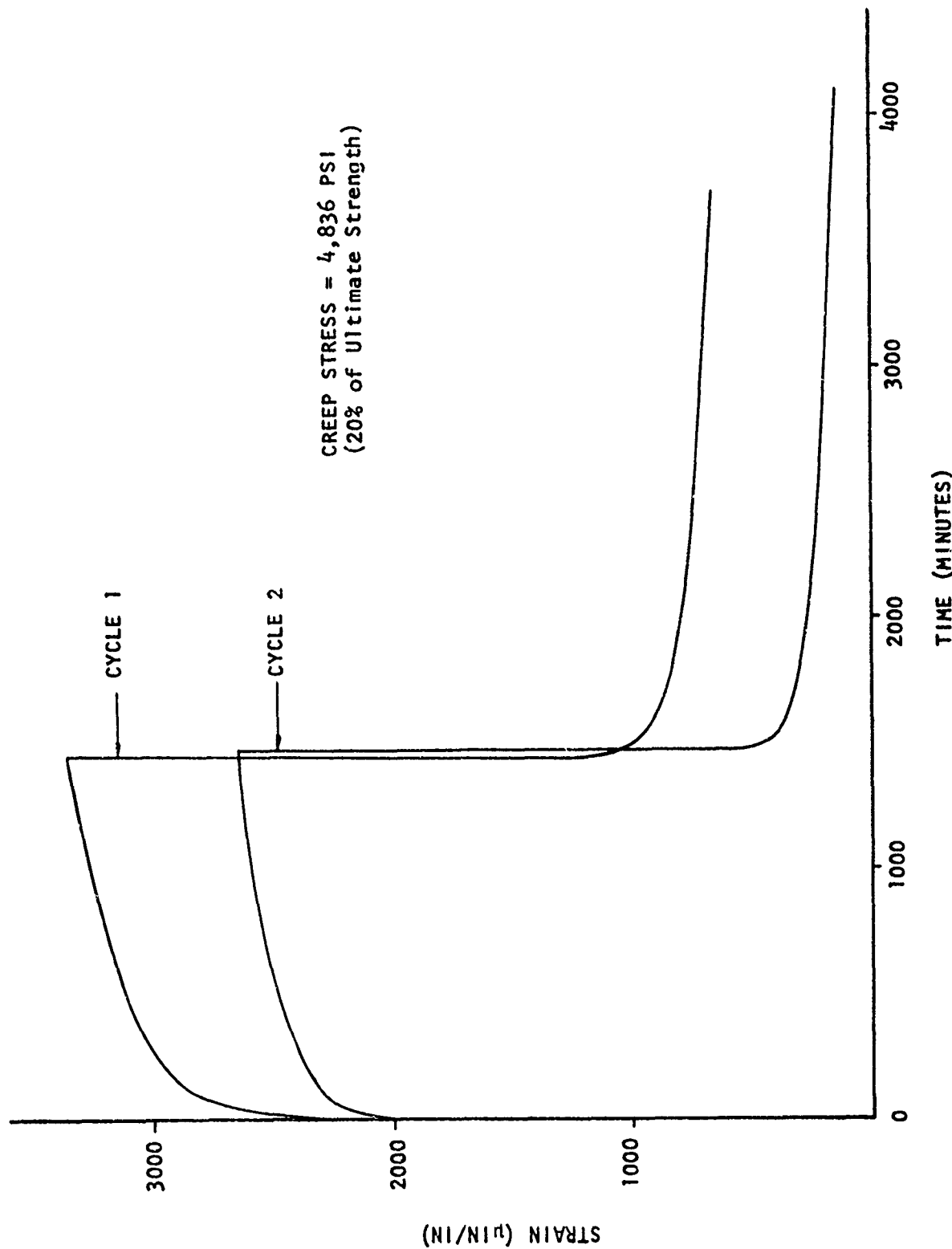


FIGURE 12. LONG TERM CREEP-RECOVERY TEST OF A  $\pm 45^\circ$  SPECIMEN UNDER 176°F/50% R.H. ENVIRONMENT.

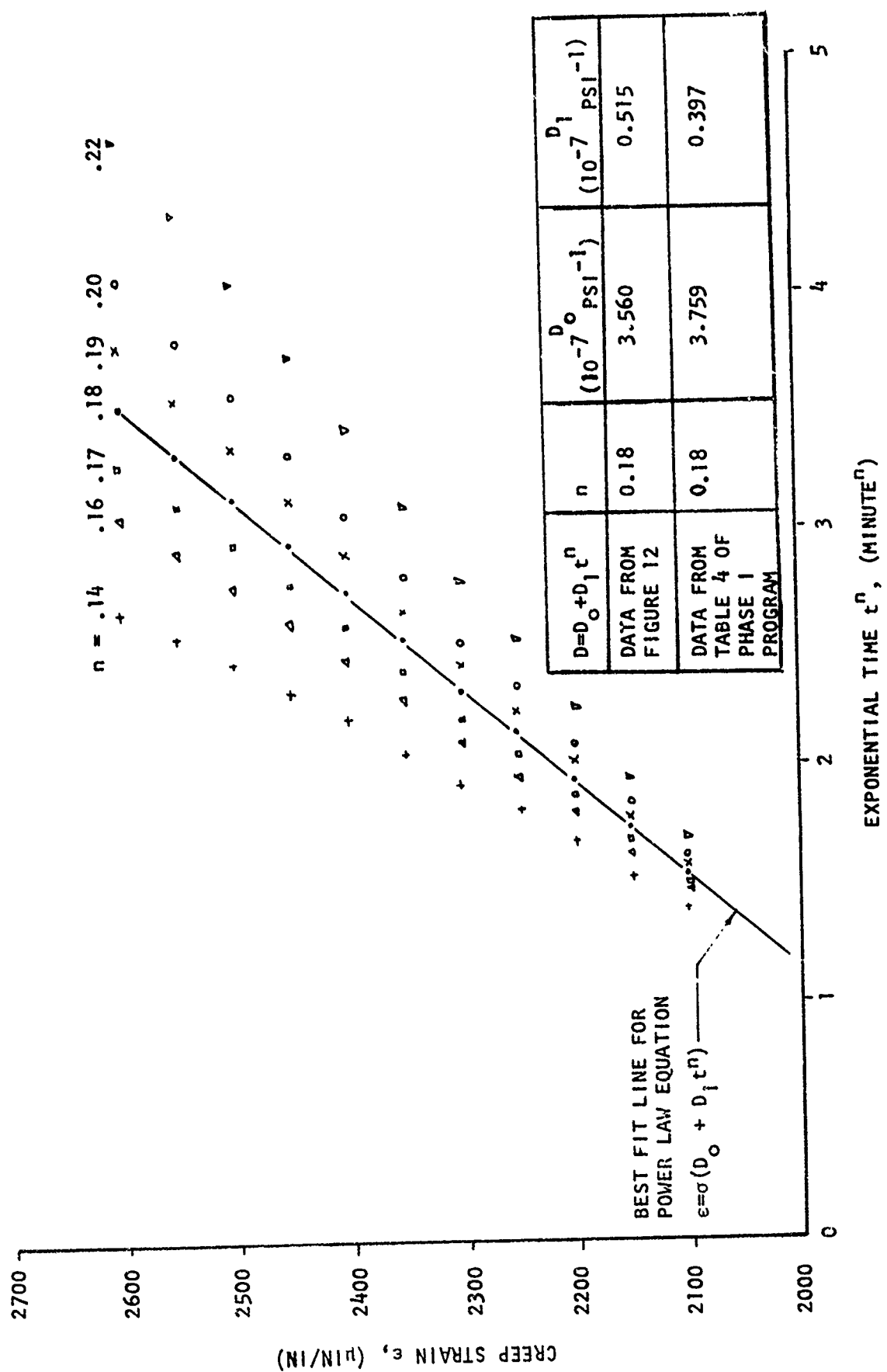


FIGURE 13. STRAIGHT LINE ANALYSIS FOR POWER LAW EQUATION.

respective moisture level in the 170°F wet environment for at least eighty-five days for 90°-specimens and at least fifteen days for  $\pm 45^\circ$ -specimens to attain at least a 95% moisture saturation level. The test results for the 90°-specimens and  $\pm 45^\circ$ -specimens are listed in Tables 5 and 6. The static results from reference 1 are also listed for comparison. The specimens which were tested in the "AS FAB" condition were specimens that were kept and tested within the test laboratory environment within one month after fabrication.

Three distinct types of failure modes, namely edge, gage and hole, were used to describe the failure location within the 90°-specimen. They are described by the pictures in Figure 14. The strength of the 90°-specimens was improved roughly 4% through use of the new fabrication procedure. Its typical stress-strain curves are shown in Figure 15. The material response gradually becomes non-linear when it approaches the failure point. From Table 5, the secant stiffness of the 90°-specimen (secant modulus at 2000  $\mu\text{in/in}$ ) decreases as the temperature and relative humidity becomes more severe. Ultimate strength and ultimate strain of the material in Figures 16 and 17 reflect an effect of residual stress (inherited from 350°F curing).

Failure modes of gage type and edge type were observed on  $\pm 45^\circ$ -specimens under static load (Figure 18). A gage type failure mode is one where the failure area is confined between two end tabs. An edge type of failure means that the tab end of the specimen is adjacent to the failure location. Edge delamination was observed to start forming around 65% of the ultimate load level for "AS FAB" specimens. The failure location and the worst delamination area do not necessarily coincide.

Typical stress-strain curves for  $\pm 45^\circ$  specimens within three environments are shown in Figure 19. Material behavior is highly nonlinear after approximately a 7500 psi stress level is attained. The sample can sometimes be stretched to 90,000  $\mu\text{in/in}$  before failure and creates a necked-down shape over the gage section of the specimen. Secant moduli at various environments are calculated at a 5000  $\mu\text{in/in}$  strain level and are also shown in Table 6. The strain level, 5000  $\mu\text{in/in}$ , is an upper strain region for comfortable design application. Based on the results of Table 6, static failure of  $\pm 45^\circ$  specimens tended to be gage failures. This phenomenon is probably due to the tab constraining the surface from peeling in the tab area and the necking of the gage section. The static results indicate that specimens made by using a wafering cutter technique did not improve properties significantly over those specimens that were made by using

TABLE 5. STATIC PROPERTIES OF 90°-SPECIMENS IN VARIOUS ENVIRONMENTS

SPECIMEN ID	TEST ENVIRONMENT			CONDITIONING ENVIRONMENT		ULTIMATE STRENGTH (KSI)	ULTIMATE STRAIN (μin/in)	YOUNG'S MODULUS (MSI)	FAILURE MODE		
	TEMP. (°F)	HUMIDITY (% R.H.)	TEMP. (°F)	HUMIDITY (% R.H.)	EDGE				GAGE	HOLE	
90-B4-1	75	AS FAB.	-	-	7.41	4862	1.61	X			
90-B8-8	75	AS FAB.	-	-	6.52	4373	1.54	X			
90-B1-4	75	50	170	50	4.58	3142	1.47	X			
90-A4-1	75	95	170	95	4.16	3060	1.43	X			
90-A4-2	75	95	170	95	3.76	2852	1.37	X			
90-B3-6	132	50	170	50	4.83	3450	1.39	X			
90-B3-7	132	50	170	50	4.73	3470	1.36	X			
90-A17-3	132	95	170	95	2.64	2030	1.29	X			
90-A17-4	132	95	170	95	3.46	2640	1.31	X			
90-A4-3	132	95	170	95	3.89	3042	1.27	X			
90-B3-4	170	50	170	50	5.00	3820	1.31	X			
90-B3-5	170	50	170	50	5.65	4200	1.35	X			
90-A17-1	170	95	170	95	3.08	2630	1.28	X			
90-A17-2	170	95	170	95	3.86	3160	1.30	X			

## TEST RESULT FROM PHASE I PROGRAM (REFERENCE 1)

90-1	75	AS FAB.	-	-	6.96	-	-	X			
90-2	75	AS FAB.	-	-	6.41	-	-	X			
90-12	132	95	200	95	2.67	2750	-	X			
90-17	132	95	200	95	3.30	3110	-	X			
90-19	200	95	200	95	3.02	2890	-	X			
90-20	200	95	200	95	3.09	2980	-	X			

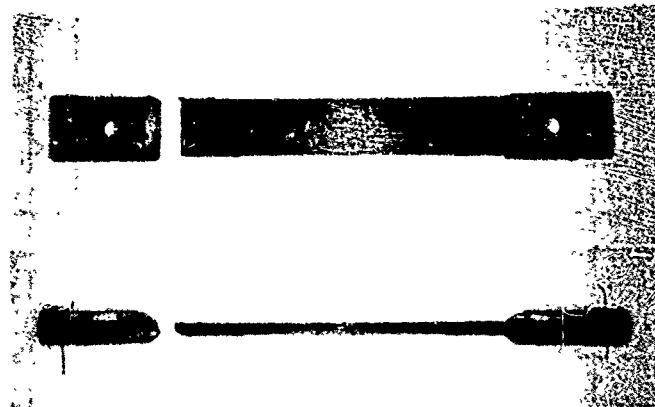
TABLE 6. STATIC PROPERTIES OF  $\pm 45^\circ$ -SPECIMENS IN VARIOUS ENVIRONMENTS.

SPECIMEN ID	TEST ENVIRONMENT		CONDITIONING ENVIRONMENT		ULTIMATE STRENGTH (KSI)	SECANT YOUNG'S MODULUS (PSI)*	FAILURE MODE	
	TEMP. (°F)	HUMIDITY (% R.H.)	TEMP. (°F)	HUMIDITY (% R.H.)			EDGE	GAGE
45-B8-3	75	AS FAB	-	-	29.8	95400	2.80	X
45-A6-1	75	50	170	50	27.1	62990	2.70	X
45-A3-2	75	50	170	50	29.5	76600	2.66	X
45-A1-1	75	95	170	95	31.9	89300	2.44	X
45-A1-2	75	95	170	95	28.3	87300	2.44	X
45-A3-5	132	50	170	50	28.0	88900	2.56	X
45-A3-3	132	50	170	50	30.5	90700	2.44	X
45-A1-3	132	95	170	95	28.3	72000	2.38	X
45-A1-4	132	95	170	95	23.6	74700	2.18	X
45-A2-4	170	50	170	50	25.1	88400	1.90	X
45-A2-1	170	50	170	50	28.2	93600	2.10	X
45-A2-3	170	95	170	95	26.1	90700	2.08	X
45-A2-2	170	95	170	95	25.6	82900	2.04	X

TEST RESULT FROM PHASE I PROGRAM (REFERENCE 1)

45-12	75	55	200	55	27.7	-	-	X
45-13	75	55	200	55	27.8	-	-	X
45-16	132	95	200	95	26.1	-	-	X
45-17	132	95	200	95	24.5	-	-	X
45-14	200	95	200	95	18.2	-	-	X
45-15	200	95	200	95	23.0	-	-	X

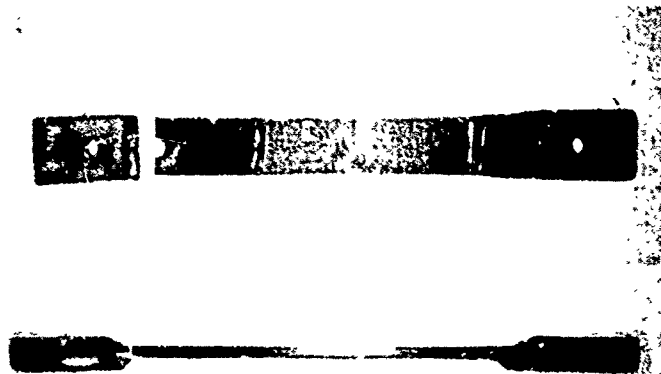
\* Modulus is Calculated at 5000  $\mu$  Strain



a. EDGE MODE



b. GAGE MODE



c. HOLE MODE

FIGURE 14. THREE FAILURE MODES OF 90° SPECIMENS

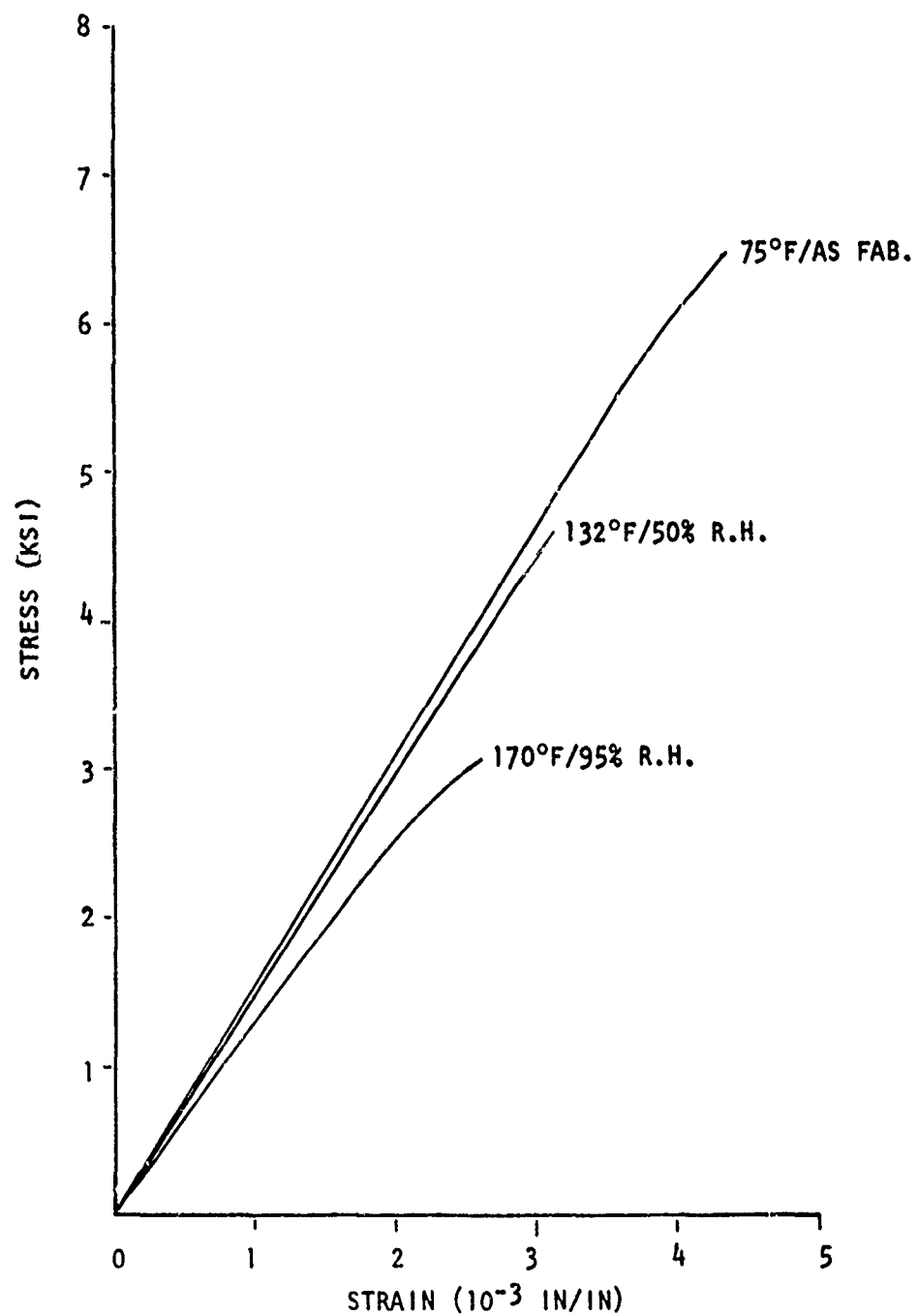


FIGURE 15. STRESS-STRAIN CURVES FOR 90°-SPECIMENS  
WITHIN THREE ENVIRONMENTS.

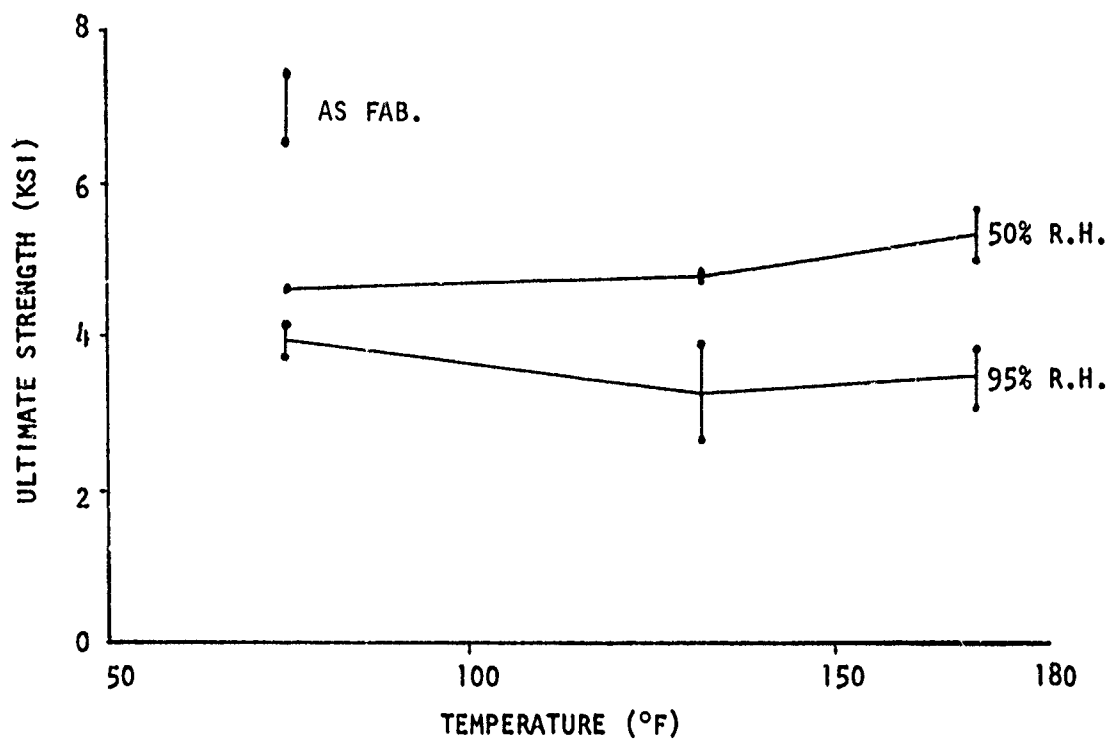


FIGURE 16. ULTIMATE STRENGTH OF 90°-SPECIMENS WITHIN VARIOUS ENVIRONMENTS.

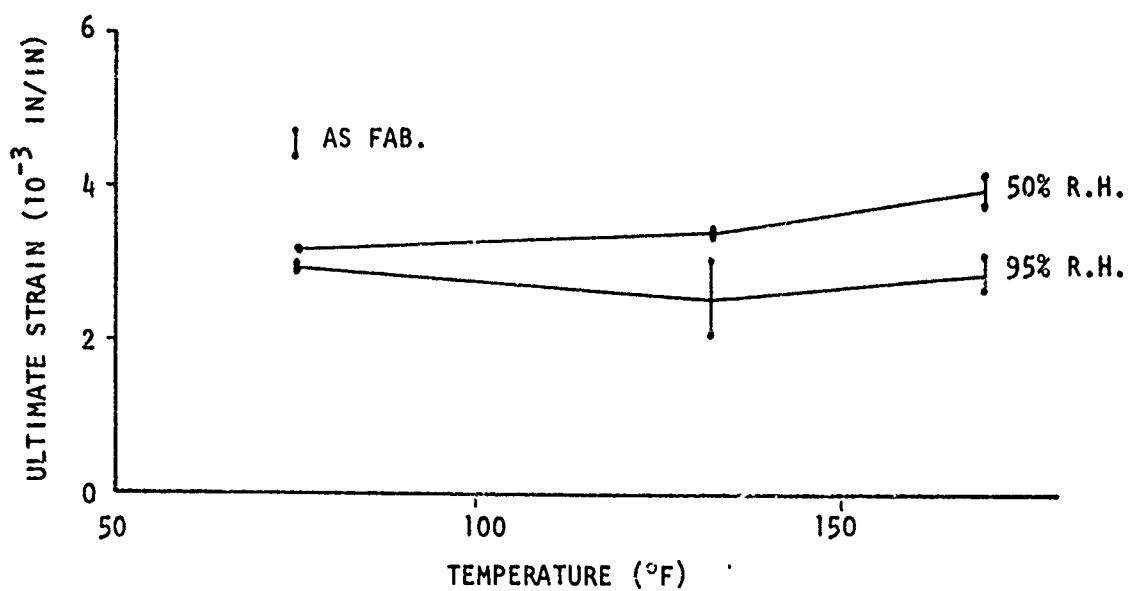


FIGURE 17. ULTIMATE STRAIN OF 90°- SPECIMENS WITHIN VARIOUS ENVIRONMENTS.



a. Gage Failure



b. Edge Failure

FIGURE 18. FAILURE MODES OF  $\pm 45^\circ$ -SPECIMEN.

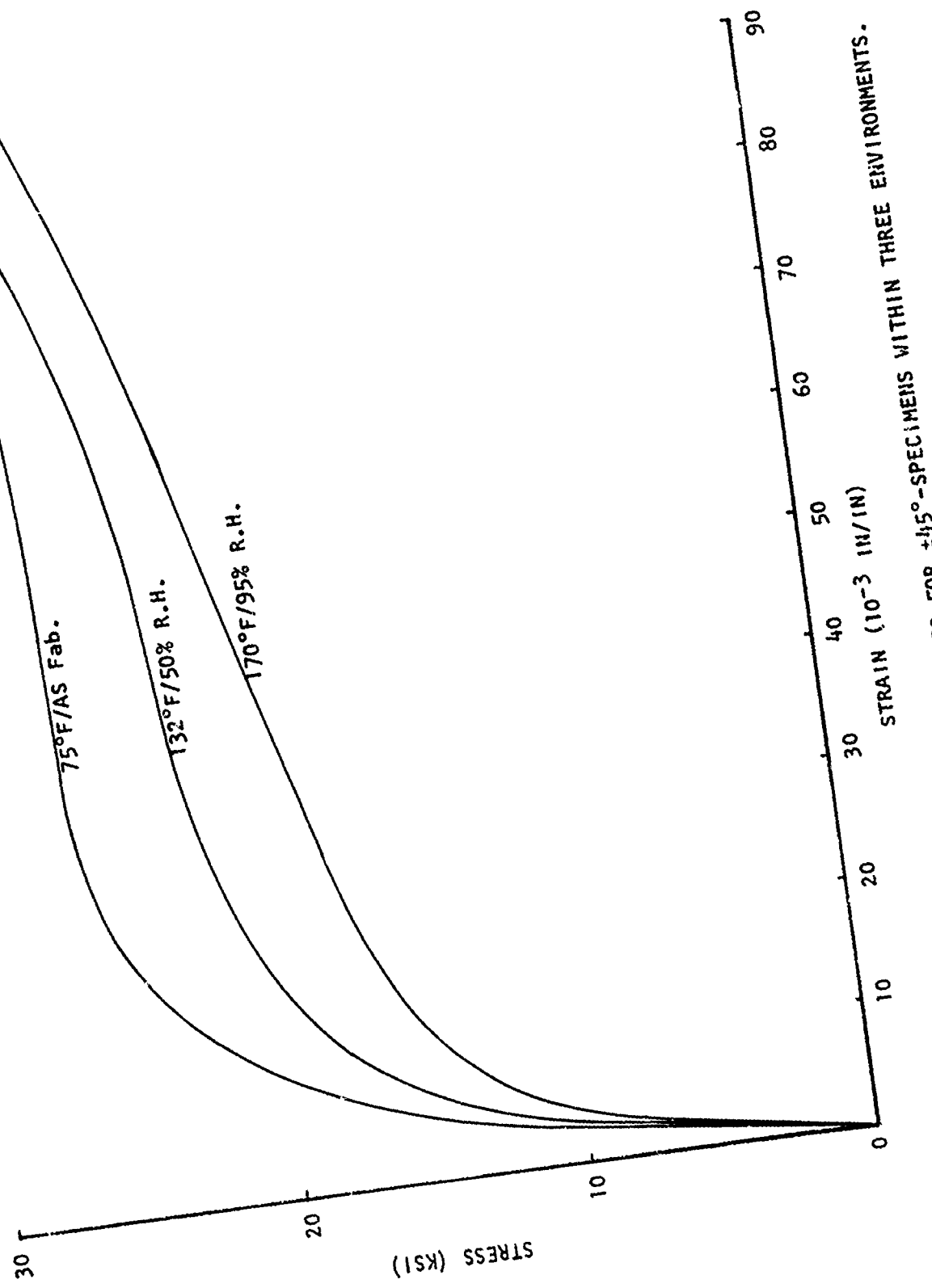


FIGURE 19.

STRESS-STRAIN CURVES FOR  $\pm 15^\circ$ -SPECIMENS WITHIN THREE ENVIRONMENTS.

a carbide bandsaw technique. This is because the machine defects or cracks as caused by higher temperature conditioning of the specimen will effect the crack propagation mechanism most in fatigue loading mode. The effect of environment on the ultimate strength and ultimate strain are shown in Figures 20 and 21 respectively.

### 3.4 FATIGUE TESTS

All the fatigue specimens were tested using a pin-load type loading fixture within the Shore Western Environmental Test Machine. They had 0.25" holes drilled through the two end tabs before they were put into the controlled environments for moisture absorption.

The fatigue test frequency was set at 3 Hertz with the load ratio being 1. Two specimens were tested at the same time. Specimens tested at one hydraulic station had a temperature sensor attached to it. The specimen tested at the other hydraulic station had both a temperature sensor and an extensometer attached to it. Diagrams depicting the fatigue test set-up are shown in Figures 22 and 23. The displacement in each specimen is measured by the extensometer. The LVDT signals in the extensometer are recorded on the strip chart recorder. The temperature in the specimen is monitored by the temperature sensor (ETG-508 from Micro-Measurements) and is recorded on the strip chart through the Vishay 2120 amplifier. Maximum fatigue stress levels were 70%, 60%, and 45% of the ultimate tensile strength and the environments were 75°F/50% R.H., 132°F/50% R.H., 132°F/95% R.H., 170°F/50% R.H. and 170°F/95% R.H.. The selected stress levels produced fatigue tests of adequate duration.

A typical displacement history for a 90° specimen during fatigue testing is shown in Figure 24 (reproduced from Reference 1). The two black lines are LVDT traces and their average is the displacement of the two inch gage section of the specimen. Typical load and displacement curves for a  $\pm 45^\circ$  specimen are shown in Figure 25. The creep of displacement under combined mean and oscillating load is obvious for the  $\pm 45^\circ$  specimen. It demonstrates essentially the viscoelastic shear response of the composite under axial tensile load.

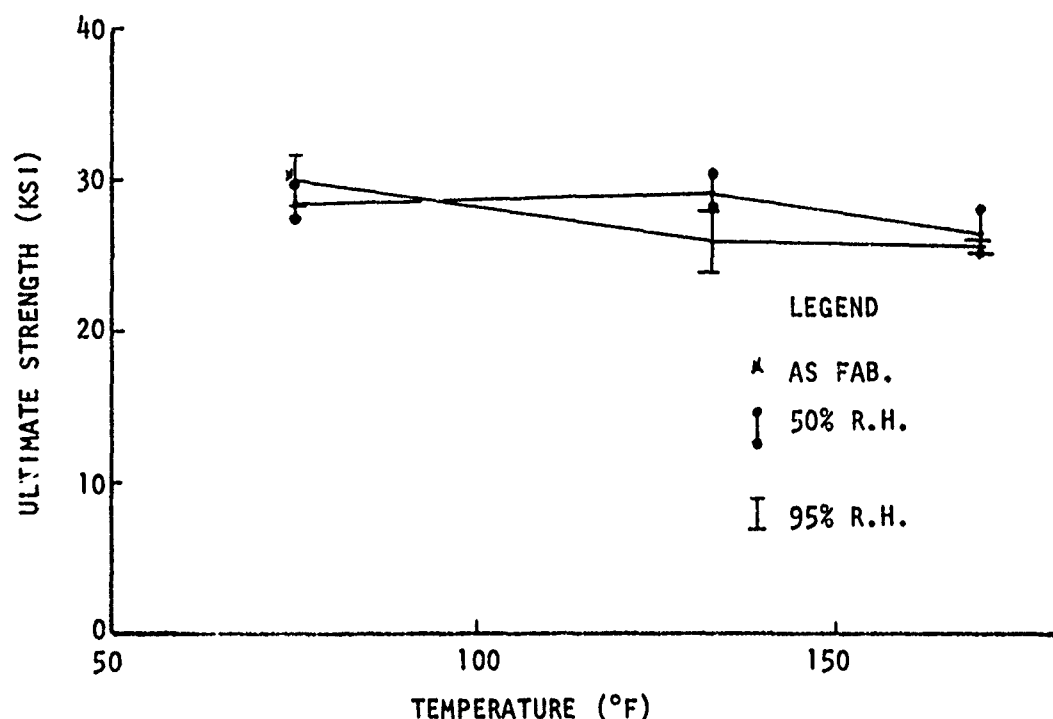


FIGURE 20. ULTIMATE STRENGTH OF  $\pm 45^\circ$ -SPECIMENS WITHIN VARIOUS ENVIRONMENTS.

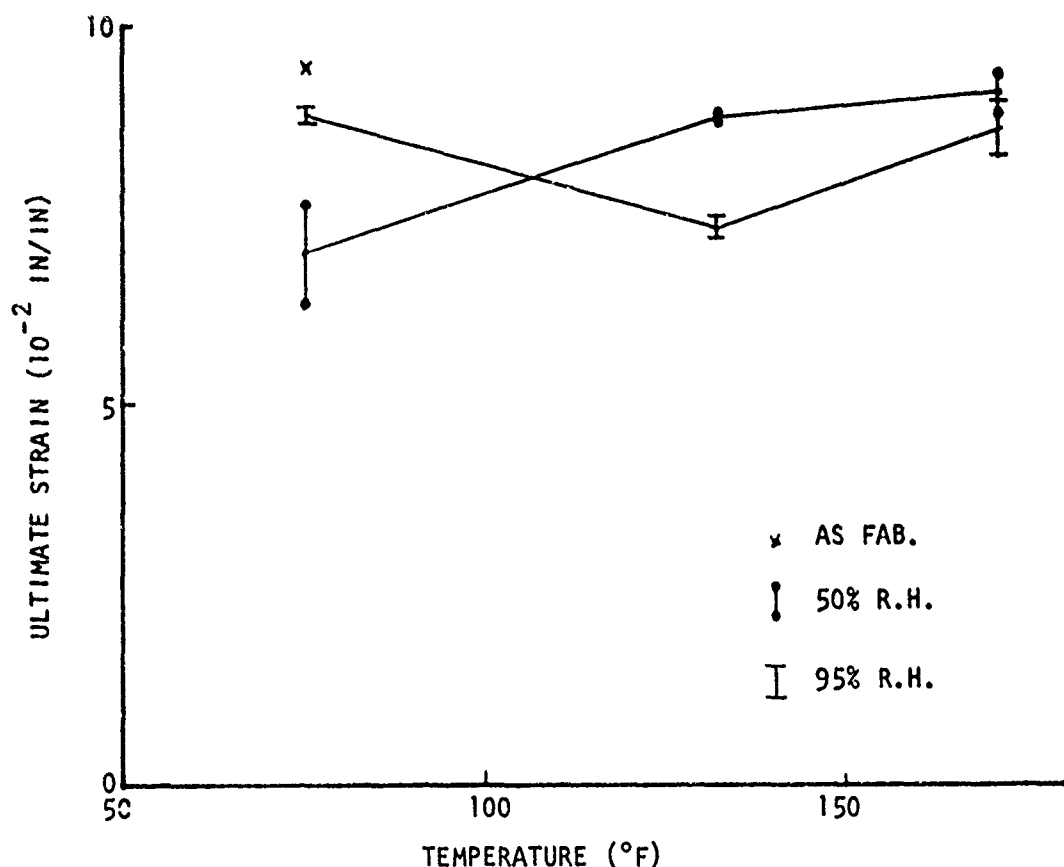


FIGURE 21. ULTIMATE STRAIN OF  $\pm 45^\circ$ - SPECIMENS WITHIN VARIOUS ENVIRONMENTS.

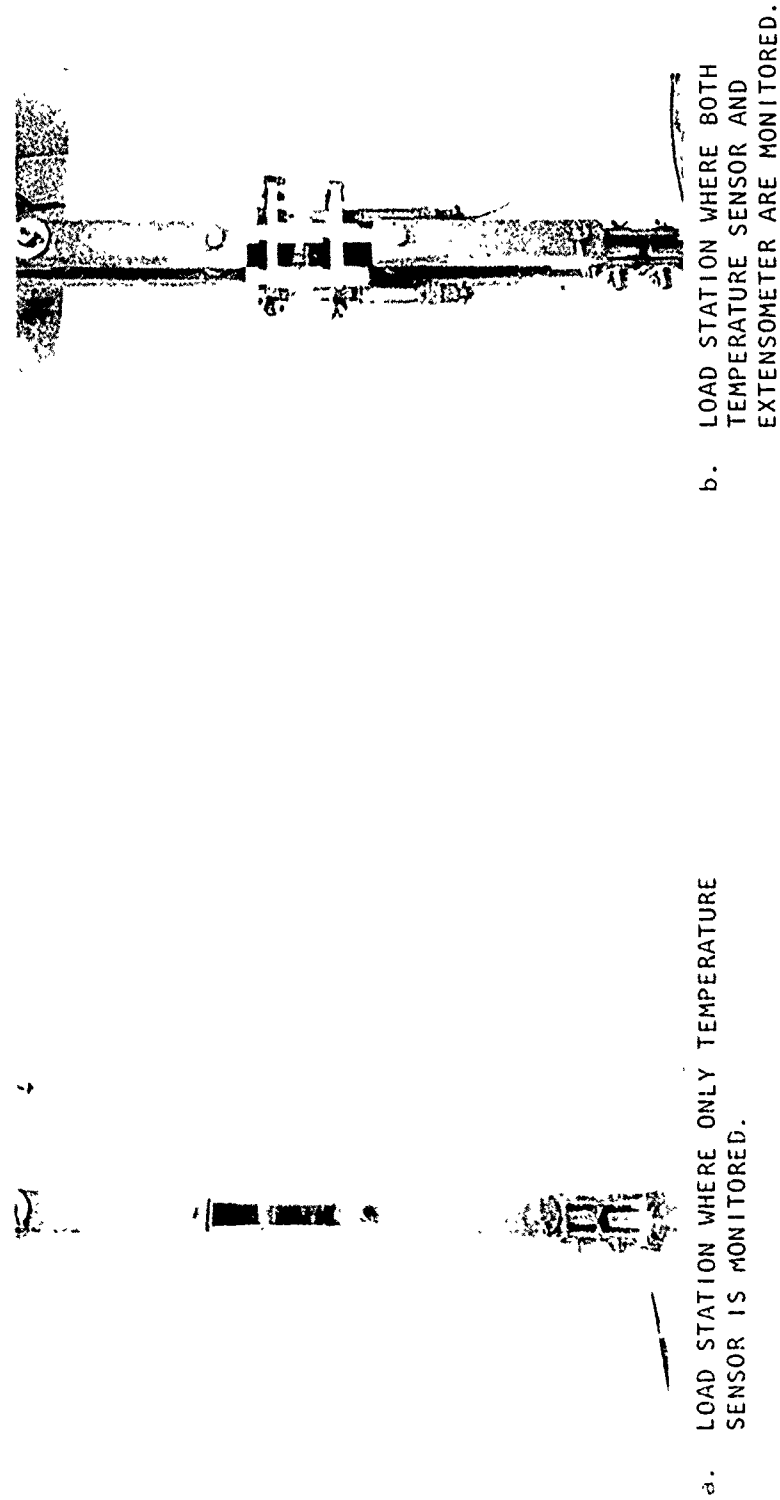


FIGURE 22. EXTENSOMETER AND TEMPERATURE SENSORS ON FATIGUE SPECIMENS

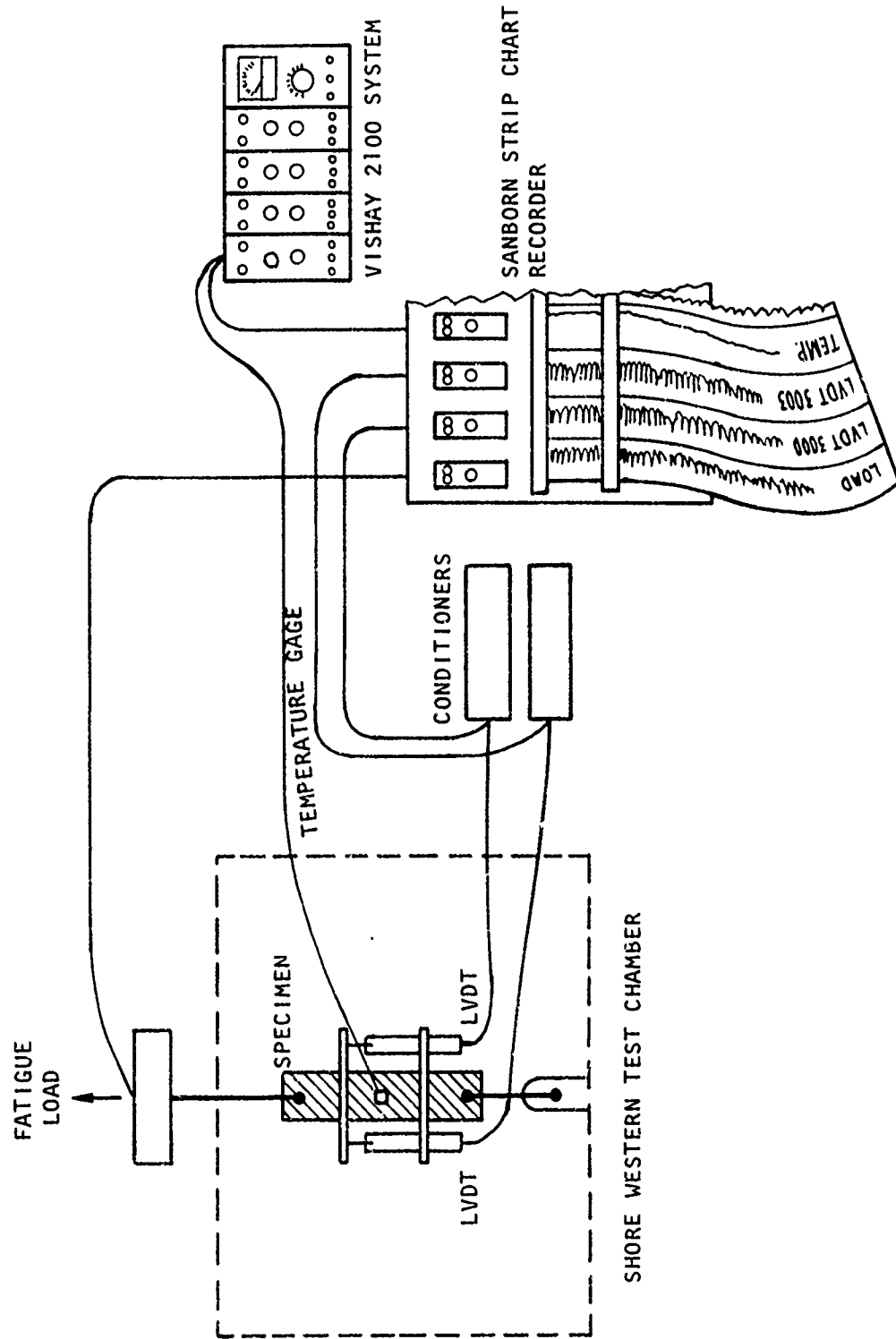


FIGURE 23. FATIGUE TEST ARRANGEMENT AND DATA ACQUISITION SYSTEM

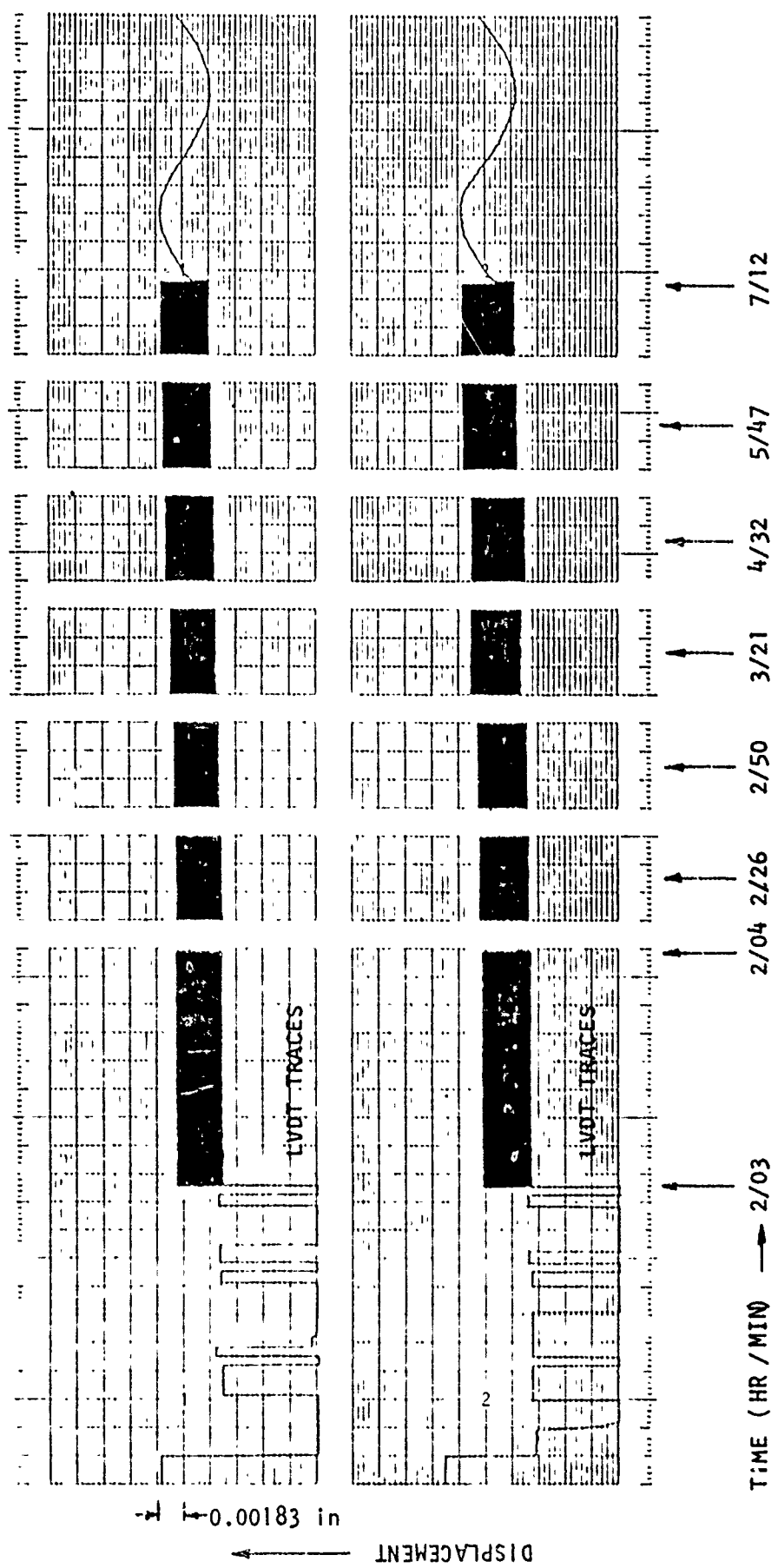


FIGURE 24. FATIGUE AND RELATED CREEP OF 90° SPECIMEN TESTED AT 176°F/95%  
R.H. ENVIRONMENT.

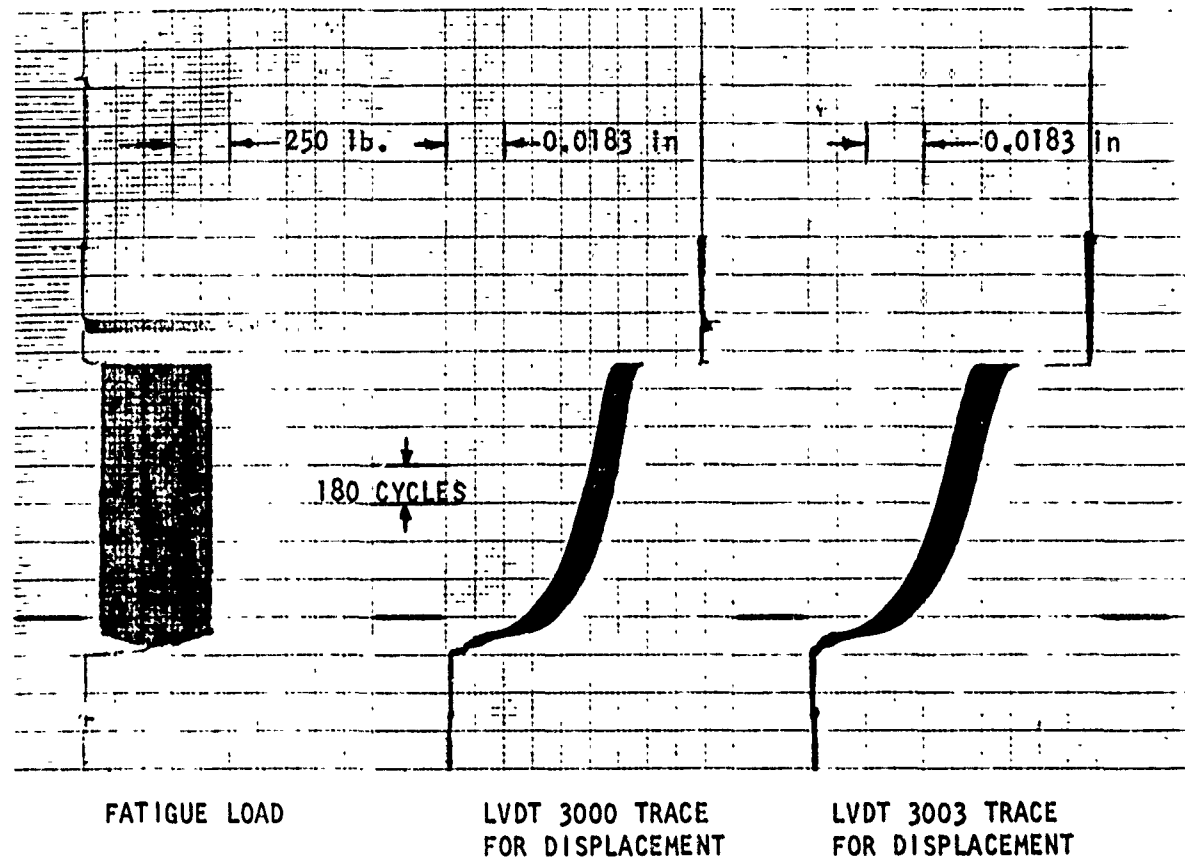


FIGURE 25. TYPICAL STRIP CHART RECORDING OF LOAD AND DISPLACEMENTS  
FOR  $\pm 45^\circ$ -SPECIMEN DURING FATIGUE.

A summary of the fatigue test results is tabulated in Tables 7 to 16. The failure mode definition for fatigue is identical to that for the static specimens shown in Figures 14 and 18. Residual strength tests of unfailed fatigue specimens were conducted only if unusual circumstances happened in the test laboratory (such as equipment malfunction or electric power disruption). Most fatigue failed specimens were compared for defects vs. those defects observed while they were in their as-fabricated state as discussed in Section 2.1

The defect analysis of the as-fabricated specimens, such as high porosity obtained from C-scan results or photomicrographs and machining defects observed in microscope examination, is described in Tables 7 to 16 in the specimen quality column. By excluding the data obtained from the defective specimens, specimens that failed in the hole area and specimens that failed by laboratory incidences, the conventional S-N curves based on data in Tables 7 to 16 is shown in Figures 26 and 27.

### 3.5 HYSTERESIS TESTS

Under a cyclic driving force, the internal damping of a viscoelastic material will cause a hysteresis loop in the stress-strain curve. This hysteresis is associated with a heat buildup in the test specimen. The  $+45^{\circ}$ -specimen fatigue test results indicated that a significant heat buildup had been generated in the form of a temperature rise at the various test environments. To study this thermal behavior of the composite, hysteresis tests were conducted using the Shorewestern Test Machine at various environments and stress levels as shown in the hysteresis test matrix, Table 17. Frequencies were set at 0.1Hz, 0.5 Hz and 1.0 Hz at various environments and stress levels. The effect of a one-hour fatigue test at a 60% ultimate strength level at 3 Hz was also investigated. The Hewlett-Packard 3300A function generator was used to generate the sine wave load. The instrumentation for load and displacement in hysteresis tests was the same as that for fatigue test (see Figure 23). Additionally, two X-Y plotters, one for each LVDT, were used to record the actual hysteresis loop for the load-displacement relation. A typical wave generated by the H-P function generator is of the trapezoidal shape shown in Figure 28 along with the corresponding displacement curves from the two LVDT's.

TABLE 7. FATIGUE TEST RESULTS FOR 90°-SPECIMEN WITHIN A 75°F/50% R.H. ENVIRONMENT.

SPECIMEN ID	FATIGUE STRESS		CYCLES		FAILURE MODE		RESIDUAL STRENGTH (PSI)	SURFACE TEMPERATURE RISE (°F)	SPECIMEN QUALITY
	MAX. STRESS (PSI)	% of F <sub>tu</sub>	EDGE	GAGE	HOLE				
90-A10-2	3275	71.5	60	X			-	-	c, f(168)
90-A10-3	3228	70.5	234	X			-	-	c, f(168)
90-NA5-2	3173	69.3	285	X			-	-	c
90-NA6-1	3183	69.5	604	X			-	-	c
90-NA6-2	3156	68.9	1097	X			-	-	c
90-NA6-4	3183	69.5	15	X			-	-	d
90-NA7-1	2721	59.4	1050	X			-	-	c
90-NA7-2	2712	59.2	3850	X			-	-	c
90-NA8-1	2715	59.3	8110	X			-	-	c
90-NA8-2	2728	59.6	370	X			-	-	d
90-A16-1	2619	57.3	1836	X			-	-	c, f(168)
90-A16-4	2577	56.3	26158	X			-	-	c, f(169)
90-A16-2	2573	56.2	805	X			-	-	d, f(169)
90-B2-2	2576	56.3	3373	X			-	-	c
90-A3-9	2596	56.7	17910	X			-	-	c
90-A16-5	2290	50.	53604	X			-	-	c, f(190)
90-A16-6	2290	50.	4657	X			-	-	c, f(190)
90-NA3-2	2290	50.	1127	X			-	-	d, f(118)
90-NA5-3	2290	50.	6238	X			-	-	d, f(118)
90-NA7-3	2290	50.	536	X			-	-	d, f(118)

a: Specimen Did Not Fall in Fatigue  
 b: Temperature Sensor Was on The Fatigue Failure Location

c: No Machine Defects  
 d: With Machine Defects  
 e: With High Priority

f: Specimen that has been conditioned for (X) days

TABLE 8. FATIGUE TEST RESULTS FOR 90°-SPECIMEN WITHIN A 132°F/50% R.H. ENVIRONMENT.

SPECIMEN ID	FATIGUE STRESS		CYCLES		FAILURE MODE		RESIDUAL STRENGTH (PSI)	SURFACE TEMPERATURE RISE (°F)	SPECIMEN QUALITY
	MAX. STRESS (PSI)	% of $F_{tu}$	EDGE	GAGE	HOLE				
90-A18-2	3115	65.2	2222	X			-	-	C
90-A18-3	3142	65.8	75	X			-	-	e
90-A18-4	3115	65.9	882	X			-	-	C
90-A18-5	3088	64.6	1011	X			-	-	C
90-B1-5	3293	68.9	5245	X			-	-	C
90-A18-6	3088	64.6	940	X			-	-	C
90-A1-2	2702	56.5	13409	X			-	-	C
90-A1-1	2652	55.5	10921	X			-	-	C
90-A1-3	2777	58.1	9468	X			-	-	C
90-A1-4	2670	55.9	4630	X			-	-	C
90-A1-5	2698	56.4	2404	X			-	-	C
90-A1-6	2674	55.9	10411	X			-	-	C
90-A2-4	2391	50.0	18790	X			-	-	C
90-A2-5	2387	49.9	9840	X			-	-	C
90-A2-6	2387	49.9	8400	X			-	-	C
90-B1-1	2406	50.3	90000 <sup>a</sup>	X			5088	-	C
90-B1-3	2387	49.9	37170	X			-	-	C

- a: Specimen Did Not Fail in Fatigue
- b: Temperature Sensor Was on The Failure Location

- c: No Machine Defects
- d: With Machine Defects
- e: With High Porosity

TABLE 9. FATIGUE TEST RESULTS FOR 90°-SPECIMEN WITHIN A 132°F/95% R.H. ENVIRONMENT.

SPECIMEN ID	FATIGUE STRESS		CYCLES		FAILURE MODE		RESIDUAL STRENGTH (PSI)	SURFACE TEMPERATURE RISE (°F)	SPECIMEN QUALITY
	MAX. STRESS (PSI)	% of $F_{tu}$	EDGE	GAGE	HOLE				
90-A12-1	2546	76.5	12940	X			-	-	c
90-A12-2	2614	78.5	210	X			-	-	c
90-A12-3	2568	77.1	30	X			-	-	d
90-A12-4	2539	76.2	2620	X			-	-	c
90-A12-5	2539	75.2	934	X			-	-	c
90-A12-6	2601	78.1	35	X			-	-	d
90-A17-5	2183	65.6	45000 <sup>a</sup>	X			5689	-	c
90-A17-6	2180	65.5	10550	X			-	-	c
90-A11-2	2264	68.0	15000	X			-	-	c
90-A11-1	2324	69.8	2710	X			-	-	c
90-A11-3	2321	69.7	13243	X			-	-	c
90-A11-4	2258	67.8	300	X			-	-	e
90-A6-5	2180	65.5	61519	X			-	-	c
90-B2-1	1865	56.0	29950	X			-	-	c
90-B2-3	1914	57.5	64800	X			-	-	c
90-B5-1	1987	59.7	45000 <sup>a</sup>	X			4973	-	c
90-B5-2	1917	57.5	45000 <sup>a</sup>	X			3656	-	c
90-A6-2	1857	55.8	20670	X			-	-	c
90-A6-3	1857	55.8	25722	X			-	-	c
90-A6-4	1815	54.5	94757 <sup>a</sup>	X			-	-	c

a: Specimen Did Not Fail in Fatigue  
 b: Temperature Sensor Was on The Fatigue Failure Location

c: No Machine Defects  
 d: With Machine Defects  
 e: With High Porosity

TABLE 10. FATIGUE TEST RESULTS FOR 90°-SPECIMEN WITHIN A 170°F/50% R.H. ENVIRONMENT.

SPECIMEN ID	FATIGUE STRESS		CYCLES		FAILURE MODE		RESIDUAL STRENGTH (PSI)	SURFACE TEMPERATURE RISE (°F)	SPECIMEN QUALITY
	MAX. STRESS (PSI)	% of $F_{tu}$	EDGE	GAGE	HOLE				
90-A15-2	3775	70.8	1445	X		-	-	-	c
90-A7-6	3606	67.7	2050	X		-	-	-	c
90-A9-1	3606	67.7	25	X		-	-	-	e
90-A9-3	3853	72.3	255	X		-	-	-	e
90-A9-4	3606	67.7	40	X		-	-	-	e
90-B3-1	3144	59.0	7435	X		-	-	-	c
90-A9-5	3123	58.6	195	X		-	-	-	e
90-A15-4	3157	59.2	30	X		-	-	-	d
90-A15-5	3155	59.2	45	X		-	-	-	d
90-A8-1	3324	62.4	4535	X		-	-	-	c
90-A15-3	3241	60.8	2442	X		-	-	-	c
90-A8-2	2635	49.4	6183	X		-	-	-	c
90-A8-3	2612	49.0	14350	X		-	-	-	c
90-A8-4	2612	49.0	1735	X		-	-	-	c
90-A8-5	2612	49.0	15632	X		-	-	-	c
90-A8-6	2612	49.0	6900	X		-	-	-	c

8: Specimen Did Not Fail in Fatigue

c: No Machine Defects

d: With Machine Defects

g.: Temperature Sensor Was on The Fatigue Specimen, the Test Result Was 100% Wrong

TABLE 11. FATIGUE TEST RESULTS FOR 90°-SPECIMEN WITHIN A 170°F/95% R.H. ENVIRONMENT.

SPECIMEN ID	FATIGUE STRESS		CYCLES		FAILURE MODE		RESIDUAL STRENGTH (PSI)	SURFACE TEMPERATURE RISE (°F)	SPECIMEN QUALITY
	MAX. STRESS (PSI)	% of $F_{tu}$	EDGE	GAGE	HOLE				
90-A14-2	2443	70.4	400		X	-	-	-	C
90-A11-5	2376	68.5	420		X	-	-	-	C
90-A11-6	2376	68.5	150		X	-	-	-	C
90-A13-2	2380	68.6	540	X	-	-	-	-	C
90-A13-1	2383	68.7	1500	X	-	-	-	-	C
90-NA1-1	2174	62.7	23677	X	-	-	-	-	C
90-NA1-3	2108	60.7	10585	X	-	-	-	-	C
90-NA2-1	2058	59.3	275	X	-	-	-	-	d
90-NA3-3	2068	59.6	15441	X	-	-	-	-	C
90-NA3-4	2068	59.6	14653	X	-	-	-	-	C
90-B5-4	1914	55.2	1500	X	-	-	-	-	C
90-B5-3	1912	55.1	1875	X	-	-	-	-	C
90-NA2-2	1704	49.1	671120	X	-	-	-	-	C
90-NA3-5	1721	49.6	435408	X	-	-	-	-	C
90-NA4-1	1746	50.3	236447 <sup>a</sup>	X	-	-	-	-	C
90-NA2-5	1714	49.4	345767	X	-	-	-	-	C
90-NA2-4	1727	49.8	416178	X	-	-	-	-	C

Specimen Did Not Fail in Fatigue Temperature Sensor Was on The Fatigue Failure Location

- c: No Machine Defects
- d: With Machine Defects
- e: With High Porosity

Specimen that has been conditioned for (X) days

TABLE 12. FATIGUE TEST RESULTS FOR  $\pm 45^\circ$ -SPECIMEN WITHIN A 75°F/50% R.H. ENVIRONMENT.

SPECIMEN ID	FATIGUE STRESS		CYCLES		FAILURE MODE		RESIDUAL STRENGTH (PSI)	SURFACE TEMPERATURE RISE (°F)	SPECIMEN QUALITY
	MAX. STRESS (PSI)	% OF F <sub>tu</sub>	EDGE	GAGE	HOLE				
45-B4-1	19641	69.4	396	X			-	14	d
45-B4-2	19641	69.4	1080	X			-	19	c
45-B3-4	19641	69.4	2241	X			-	46b	c
45-B3-5	19577	69.2	2960	X			-	34	c
45-B3-2	20100	71.0	1177	X			-	49 <sup>b</sup>	c
45-B3-3	20100	71.0	2098	X			-	26	c
45-AA7-3	19092	67.5	697	X			-	18	c
45-B3-1	17233	60.9	8280	X			-	29	c
45-B2-4	16840	59.5	15605	X			-	73b	c
45-B2-1	16768	59.3	5546	X			-	45	c
45-B2-2	16768	59.3	12277	X			-	42	c
45-B1-6	16371	57.8	3517	X			-	50b	c
45-A5-2	17675	52.5	4498	X			-	40	c
45-B6-2	13979	49.4	35280	X			-	16b	c
45-B6-3	13979	49.4	36326	X			-	13b	c
45-DD-1	12848	45.4	73605	X			-	5	c
45-DD-2	12848	45.4	128569	X			-	16b	c
45-EE-1	12848	45.4	74823	X			-	--	c
45-EE-2	12848	45.4	189274	X			-	22b	c
45-CC-4	12848	45.4	92276	X			-	10	c
45-CC-5	12848	45.4	168426	X			-	26b	c

a. Specimen Did Not Fail in Fatigue  
 b. Temperature Sensor Was on The Fatigue Failure Location

c. No Machine Defects  
 d. With Machine Defects  
 e. With High Porosity

TABLE 13. FATIGUE TEST RESULTS FOR  $\pm 45^\circ$ -SPECIMEN WITHIN A  $132^\circ\text{F}/50\%$  R.H. ENVIRONMENT.

SPECIMEN ID	FATIGUE STRESS		CYCLES		FAILURE MODE		RESIDUAL STRENGTH (PSI)	SURFACE TEMPERATURE RISE (°F)	SPECIMEN QUALITY
	MAX. STRESS (PSI)	% OF F <sub>tu</sub>	EDGE	GAGE	HOLE				
45-A4-1	20098	68.6	1108	X			-	28	C
45-A4-2	20032	68.4	1410	X			-	29	C
45-B8-4	20032	63.4	1758	X			-	18	C
45-AA-4	20418	69.7	180	X			-	27 <sup>b</sup>	D
45-AA-5	20391	69.6	2775	X			-	41	C
45-AA-6	19920	68.0	1048	X			-	32	C
45-B6-4	17566	60.0	4048	X			-	25 <sup>b</sup>	C
45-B6-5	17566	60.0	4457	X			-	--	C
45-DD-3	17496	59.7	2248	X			-	33	C
45-DD-4	17496	59.7	4043	X			-	--	C
45-DD-5	17496	59.7	2636	X			-	30	C
45-DD-6	17496	59.7	3270	X			-	37	C
45-CC-2	13114	44.8	49475	X			-	12	C
45-CC-3	13148	44.9	57905 <sup>a</sup>	X			24900	12	C
45-CC-1	13096	44.7	49700	X			-	9	C
45-BB-6	13114	44.8	91813	X			-	7	C
45-BB-4	13114	44.8	155910	X			-	5	C
45-BB-5	13114	44.8	58735	X			-	27 <sup>b</sup>	C

a. Specimen Did Not Fail in Fatigue  
 b. Temperature Sensor Was On The Fatigue Failure Location

- a. No Machine Defects
- b. With Machine Defects
- c. With High Porosity
- d. e.

TABLE 14. FATIGUE TEST RESULTS FOR  $\pm 45^\circ$ -SPECIMEN WITHIN A 132°F/95% R.H. ENVIRONMENT.

SPECIMEN ID	FATIGUE STRESS		CYCLES	FAILURE MODE			RESIDUAL STRENGTH (PSI)	SURFACE TEMPERATURE RISE (°F)	SPECIMEN QUALITY
	MAX. STRESS (PSI)	% OF $F_{tu}$		EDGE	GAGE	HOLE			
45-A2-5	18658	71.8	812	X			-	17 <sup>b</sup>	c.
45-A3-4	18683	71.9	225	X			-	4	c.
45-A4-3	18509	71.2	60	X			-	7	d.
45-A5-1	18633	71.7	700	X			-	20	c.
45-A5-3	19111	73.5	2109	X			-	19 <sup>b</sup>	c.
45-A6-2	18203	70.0	1121	X			-	23	c.
45-AA6-2	18608	71.6	558	X			-	13	c.
45-A6-3	15639	60.2	1253	X			-	13	c.
45-A7-2	15577	59.9	191 <sup>c</sup>	X			-	9	c.
45-A7-1	15618	60.1	3939	X			-	13	c.
45-A7-3	15966	61.4	6100	X			-	12	c.
45-A8-1	15391	59.2	4333	X			-	11	c.
45-A8-2	15766	60.6	11893	X			-	13	c.
45-A8-3	12941	49.8	31374	X			-	16	c.
45-A8-4	13479	51.8	360	X			-	2	d.
45-B2-3	12923	49.9	44261	X			-	9	c.
45-B2-5	12958	49.8	19718	X			-	16	c.
45-B5-1	12941	49.8	18666	X			-	18 <sup>b</sup>	c.
45-B5-2	12941	49.8	10627	X			-	5	c.
45-GG-2	11903	45.8	45645	X			-	3	c.
45-GG-3	11950	46.0	162666	X			-	6	c.

a. Specimen Did Not Fail in Fatigue

b. Temperature Sensor Was on The Fatigue Failure Location

c. No Machine Defects

d. With Machine Defects

e. With High Porosity

TABLE I5. FATIGUE TEST RESULTS FOR  $\pm 45^\circ$ -SPECIMEN WITHIN A  $170^\circ\text{F}/50\%$  R.H. ENVIRONMENT.

SPECIMEN ID	FATIGUE STRESS		CYCLES	FAILURE MODE			RESIDUAL STRENGTH (PSI)	SURFACE TEMPERATURE RISE (°F)	SPECIMEN QUALITY
	MAX. STRESS (PSI)	% OF $F_{tu}$		EDGE	GAGE	HOLE			
45-B6-6	18584	69.6	952	X			-	---	C
45-B7-5	18149	68.0	533	X			-	---	C
45-B7-6	18149	68.0	1673	X			-	35	C
45-FF-2	18559	69.5	180	X			-	27	C
45-AA7-2	18683	70.0	979	X			-	33	C
45-AA7-1	18534	69.4	1251	X			-	26	C
45-EE-3	15903	59.6	7323	X			-	26	C
45-EE-4	15903	59.6	6164	X			-	21	C
45-AA-3	16913	63.3	1756	X			-	28	C
45-EE-5	15903	59.6	7300	X			-	25	C
45-CC-6	15903	59.6	4414	X			-	20	C
45-FF-1	15903	59.6	5564	X			-	20	C
45-B7-4	15990	59.9	2274	X			-	23 <sup>b</sup>	C
45-BB-3	11288	42.3	126875	X			-	10 <sup>b</sup>	C
45-BB-2	11288	42.3	158469	X			-	6	d
45-DD-1	11303	42.3	233967	X			-	8 <sup>b</sup>	C
45-AA-1	11288	42.3	959929	X			-	13	C
45-AA-2	11288	42.3	16943	X			-	5	C
45-AA8-1	11176	41.9	750740	X			-	16	C

a. Specimen Did Not Fail in Fatigue

## Temperature Sensor Was on The Fatigue Failure Location

- c. No Machine Defects
- d. With Machine Defects
- e. With High Porosity

TABLE 16. FATIGUE TEST RESULTS FOR  $\pm 45^\circ$ -SPECIMEN WITHIN A  $170^\circ\text{F}/95\%$  R.H. ENVIRONMENT.

SPECIMEN ID	FATIGUE STRESS		CYCLES		FAILURE MODE		RESIDUAL STRENGTH (PSI)	SURFACE TEMPERATURE RISE ( $^\circ\text{F}$ )	SPECIMEN QUALITY
	MAX. STRESS (PSI)	% OF $F_{tu}$	EDGE	GAGE	HOLE				
45-BB-2	18758	72.4	374	X			-	10	c
45-B1-1	18484	71.4	194	X			-	8	c
45-GG-1	18932	73.1	200		X		-	8	c
45-FF-6	18459	71.3	160		X		-	9	c
45-HH-3	18459	71.3	366	X			-	6	c
45-HH-2	18484	71.4	360	X			-	3	c
45-B1-2	15070	58.2	537	X			-	3	d
45-B1-4	15090	58.3	1300	X			-	2	d
45-B1-3	15070	58.2	422	X			-	6	c
45-B1-5	15070	58.2	332	X			-	5 <sup>b</sup>	d
45-FF-4	15824	61.1	1080	X			-	6	c
45-FF-5	15803	61.0	1095	X			-	9	c
45-B5-3	12795	49.4	14879		X		-	8	c
45-B5-5	12778	49.3	2145	X			-	-	c
45-GG-4	12143	46.9	37029	X			-	5	c
45-HH-1	11868	45.8	130497	X			-	7	c
45-HH-4	11853	45.8	137777	X			-	2	c
45-AA1-1	11915	46.0	25942	X			-	6	c

a. Specimen Did Not Fail in Fatigue

b. Temperature Sensor Was on The Fatigue Failure Location

c. No Machine Defects

d. With Machine Defects

e. With High Porosity

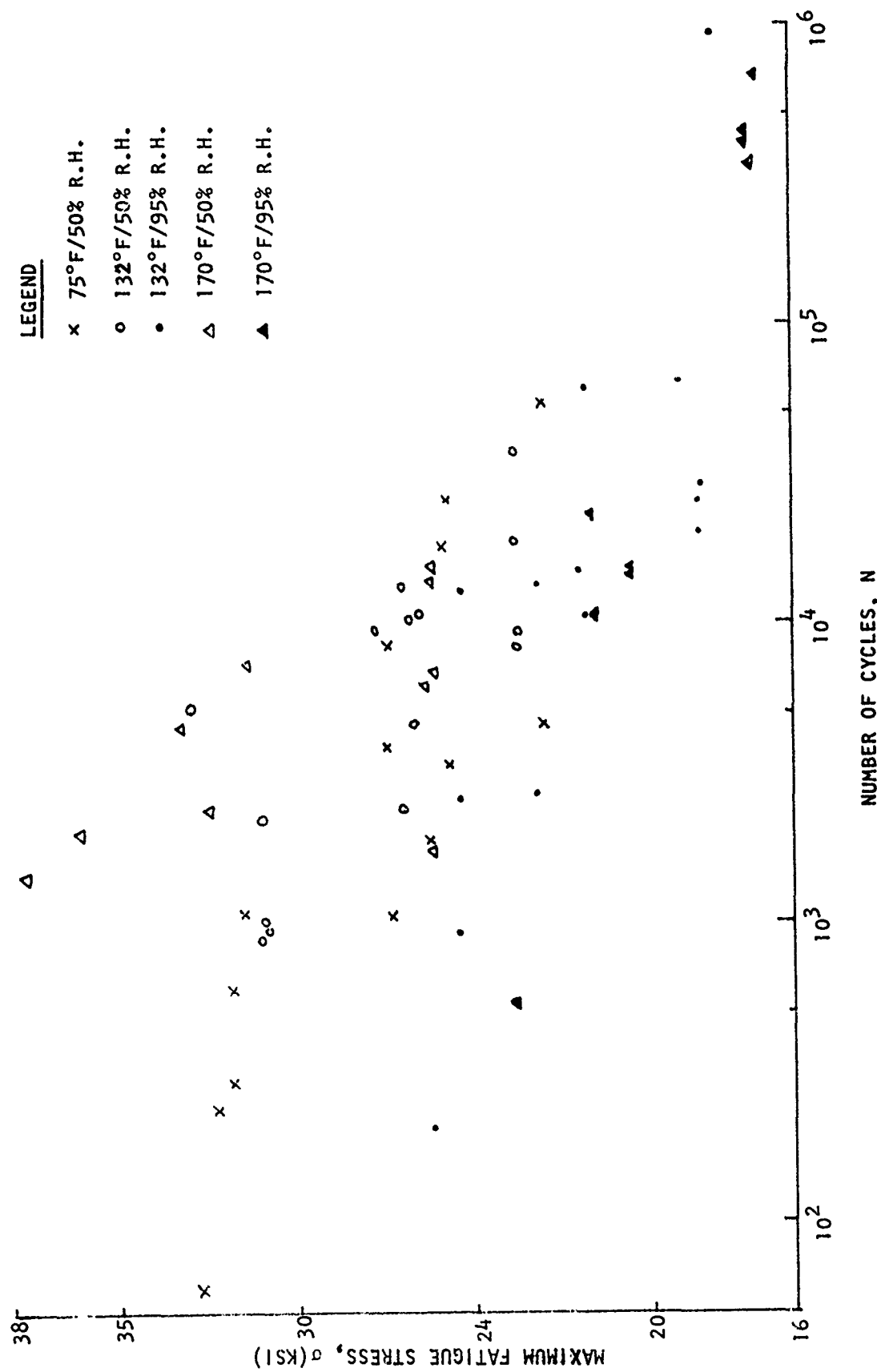


FIGURE 26. THE S-N CURVE OF  $90^{\circ}$ -SPECIMENS AT VARIOUS ENVIRONMENTS.

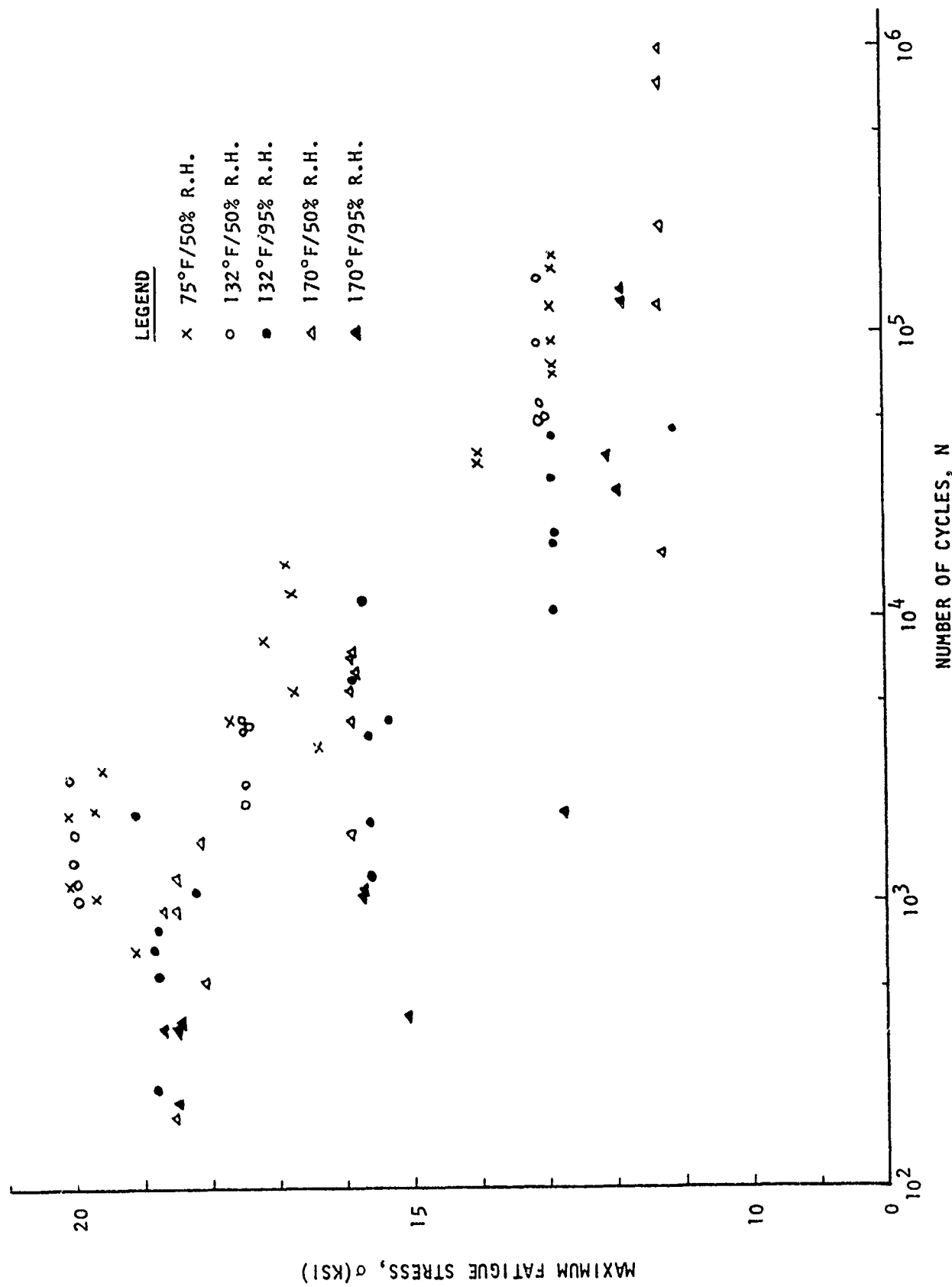


FIGURE 27. THE S-N CURVE OF  $\pm 45^\circ$ -SPECIMENS AT VARIOUS ENVIRONMENTS.

TABLE 17. HYSTERESIS TEST MATRIX.

LOAD FREQUENCY (Hz)	LEVEL	20% $F_{tu}$	45% $F_{tu}$	60% $F_{tu}$
0.1		X	X	X
0.5		X	X	X
1.0		X	X	X
(After One 1.0 Hour Fatigue)		---	---	X

NOTE: a. The environments for the above hysteresis matrix are AS-FAB; 75°F/50% R.H., 132°F/50% R.H., 132°F/95% R.H.  
170°F/50% RH, 170°F/95% RH.  
b. The ultimate tensile strength ( $F_{tu}$ ) of the cyclic load level is based on the following table with units in psi:

ENVIRONMENT SPECIMENS	75/DRY	75/50	132/50	132/95	170/50	170/95
$\pm 45^\circ$	29,800	28,300	29,300	26,000	26,700	25,900
90°	6,970	4,580	4,780	3,330	5,330	3,470

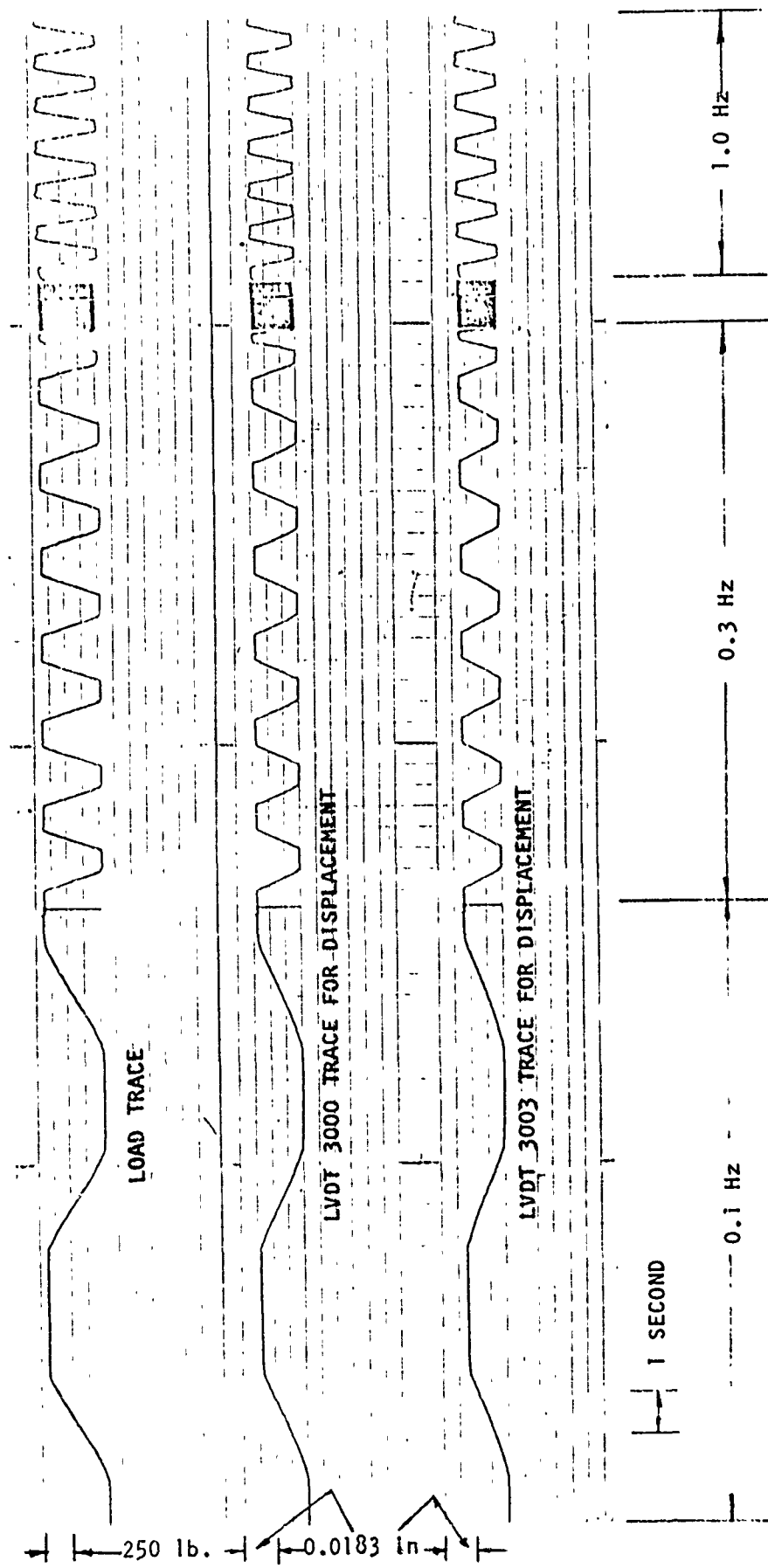
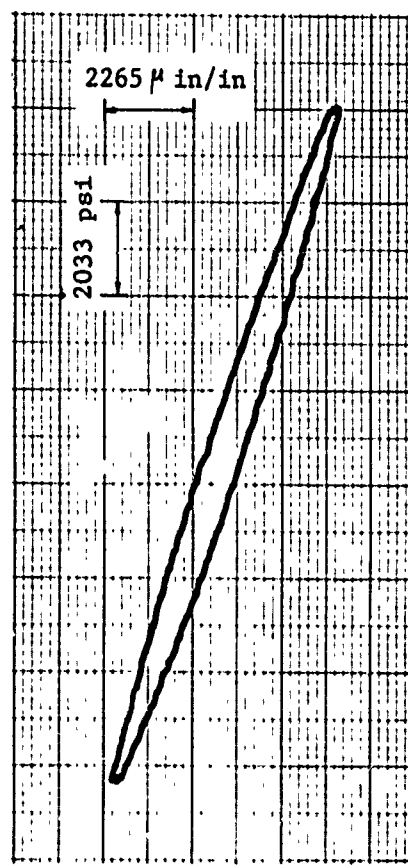
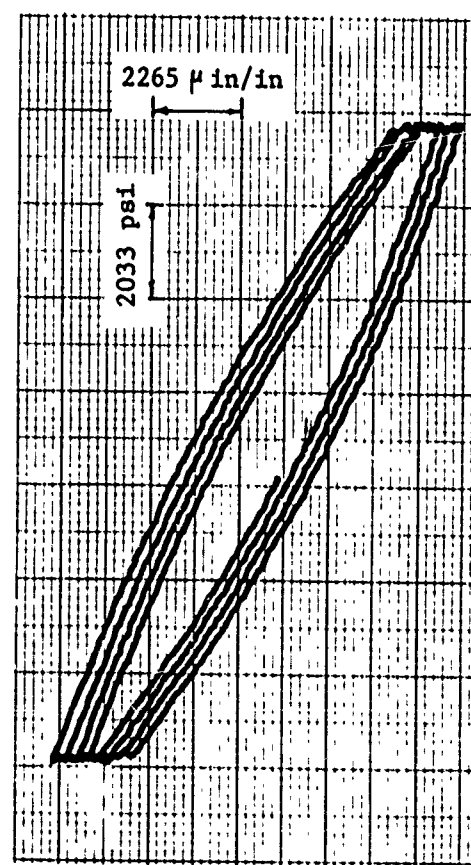


FIGURE 28. STRIP CHART RECORDING OF LOAD AND DISPLACEMENT OF  $\pm 45^\circ$ -SPECIMEN DURING HYSTERESIS TEST AT  $170^\circ\text{F}/50\%$  R.H. ENVIRONMENT AND 60% OF ULTIMATE STRENGTH.

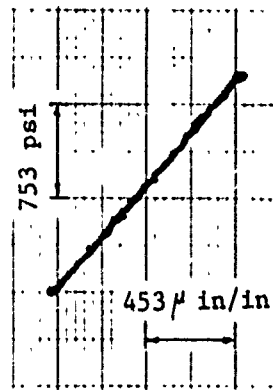
Based on the results in Figure 28, a gradual distortion on the flat section of the trapezoidal wave at 0.5 Hz frequency which became more severe at 1.0 Hz is probably due to the inertia effect of the hydraulic loading system. Hence, subsequent data analysis was confined to 0.1 Hz frequency results. Typical hysteresis curves at 0.1 Hz, recorded by the X-Y plotters, are shown in Figure 29. The creep in displacement under mean cyclic load from cycle to cycle is apparent at the 170°F/95% R.H. environment for a  $\pm 45^\circ$  specimen. For data analysis purposes, those hysteresis curves can be idealized to the shape shown in Figure 30 together with the dimensions that characterize the hysteresis. Table 18 gives a list of dimensions of hysteresis loops at various environments and stress levels. The dynamic modulus is defined in the last cyclic loading. Both  $90^\circ$  and  $\pm 45^\circ$  specimens became stiffer after being fatigue loaded for one hour at 60% Ftu and 3 Hz frequency.



a.  $\pm 45^\circ$  SPECIMEN AT  
75° F/50% RH ENVIRONMENT



b.  $\pm 45^\circ$  SPECIMEN AT 170° F/95% RH  
ENVIRONMENT



c. 90° SPECIMEN AT  
132° F/95% RH  
ENVIRONMENT

FIGURE 29. Typical Hysteresis Loops From X-Y Recorder for Fatigue Specimens  
Tested Under 60% of Ultimate Strength with Load Ratio at 0.1  
For .10 Hz.

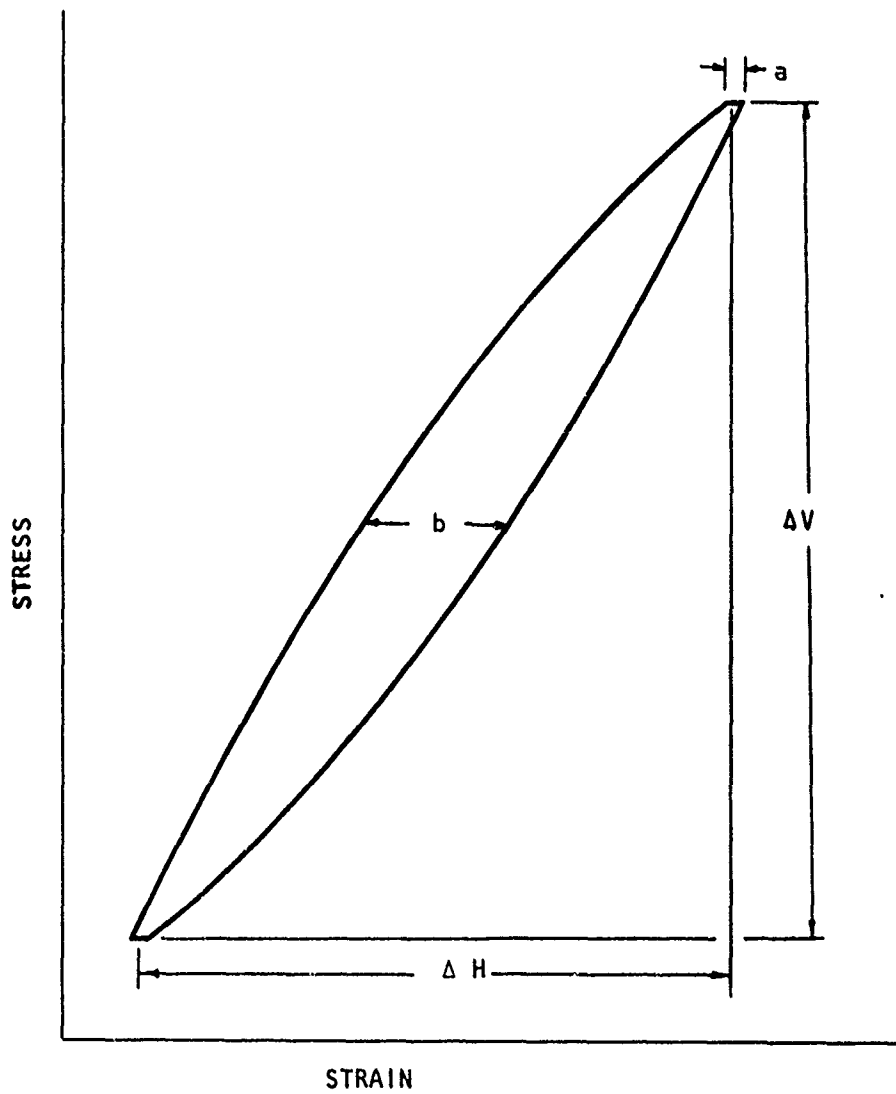


FIGURE 30. Geometry Of Hysteresis Loop for Composite Under Ramp Load

TABLE 18. ENVIRONMENTAL EFFECT ON THE CHARACTERISTICS OF HYSTERESIS LOOPS AT 0.1 Hz FREQUENCY.

TEST ENVIRONMENT (OF/% RH)	CYCLIC STRESS LEVEL KSI	<sup>a</sup> ( $\mu$ IN/IN)	<sup>b</sup> ( $\mu$ IN/IN)	$\Delta V$ (PSI)	$\Delta H$ ( $\mu$ IN/IN)	$E = \Delta V / \Delta H$ (10 <sup>6</sup> PSI)
90° - 132/95	9.01	0	0	810.	623.	1.32
	1.843	34.0	34.0	1,659.	1,395.	1.20
	2.404	40.7	40.7	2,164.	1,795.	1.22
	2.404 (after fatigue)	40.7	40.7	2,164.	1,747.	1.25
$\pm 45^\circ$ - AS-FAB	9.27	85.	85.	8,334.	2,984.	2.83
	18.25	171.	373.	16,420.	6,951.	2.39
	28.20	543.	1,560.	25,376.	10,850.	2.37
	28.20 (after fatigue)	289.	882.	25,376.	10,308.	2.49
$\pm 45^\circ$ - 75/50	6.35	69.	69.	5,722.	2,305.	2.52
	15.20	171.	611.	13,683.	6,443.	2.15
	19.77	340.	1,085.	17,787.	8,985.	2.00
	19.77 (after fatigue)	171.	780.	17,787.	8,478.	2.13
$\pm 45^\circ$ - 132/50	5.80	102.	102.	5,224.	2,136.	2.48
	15.75	238.	678.	14,180.	7,121.	2.02
	20.33	882.	2,171.	18,310.	10,952.	1.69
	20.98 (after fatigue)	611.	1,696.	18,883.	10,647.	1.80
$\pm 45^\circ$ - 132/95	6.92	136.	136.	5,722.	2,442.	2.38
	14.10	289.	645.	12,688.	6,272.	2.05
	18.19	645.	1,814.	17,016.	10,138.	1.70
	18.19 (after fatigue)	576.	1,611.	17,016.	9,698.	1.78
$\pm 45^\circ$ - 170/50	5.81	136.	136.	5,231.	2,374.	2.23
	14.37	475.	1,425.	12,928.	7,799.	1.68
	16.46	1,085.	3,052.	14,820.	11,325.	1.31
$\pm 45^\circ$ - 170/95	6.07	204.	204.	5,464.	2,543.	2.18
	14.04	645.	1,425.	12,639.	7,969.	1.61
	19.29	1,798.	4,171.	17,362.	12,241.	1.43
	--	--	--	--	--	--

## 4.0 ANALYSIS OF TEST RESULTS

## 4.1 THERMAL ANALYSIS

Based on the temperature results in Tables 7 through 16, a significant temperature rise in the  $\pm 45^\circ$ -specimen was recorded during fatigue testing at various environments. The  $90^\circ$  specimens experienced at most a  $2^\circ\text{F}$  temperature increase. This temperature rise is important in data analysis for viscoelastic material where the temperature shift factor is effected. To explore this phenomenon, temperature profile tests for  $\pm 45^\circ$ -specimens were conducted by attaching four temperature sensors to the specimen in the arrangements shown in Figure 31 with three configurations. The temperature profile test results are shown in Table 19. Unless the sensor was close to the failure location of the specimen, temperature variations on the surface of the specimens may be due to free edge effects and the inhomogeneity in the specimen and between specimens. The temperature field on the surface can be considered uniform during fatigue cycling for reasons to be discussed below.

Definition of the exact temperature variation across the thickness of a specimen is difficult. Therefore, the heat conduction equation for a cycle-average temperature field was used (e.g. Schapery<sup>3</sup>):

$$\frac{\partial^2 T}{\partial x^2} = \frac{c}{K} \frac{\partial T}{\partial t} - \frac{\sigma_0^2 \omega D''}{2K} \quad (2)$$

where  $T$  is the temperature at location  $x$  ( $^\circ\text{F}$ )

$c$  is the specific heat ( $\text{In-Lb}/\text{In}^3\text{-}^\circ\text{F}$ )

$K$  is the transverse thermal conductivity ( $\text{In-Lb}/\text{In-Sec}^\circ\text{F}$ )

$\sigma_0$  is the amplitude of the applied cyclic stress (psi)

$\omega$  is the cyclic frequency (radian/sec); stress is assumed sinusoidal

$D''$  is the imaginary part of the dynamic compliance  $D^* = D' + i D''$

$t$  is the time

By assuming steady state thermal conduction, equation (2) can be solved without the time dependent term. Thus, the maximum temperature difference in the specimen with thickness  $2h$  is between the center of the specimen and its surface or

$$\theta_{\max} = T_c - T_s = \frac{\sigma_0^2 \omega h^2 D''}{4K} \quad (3)$$

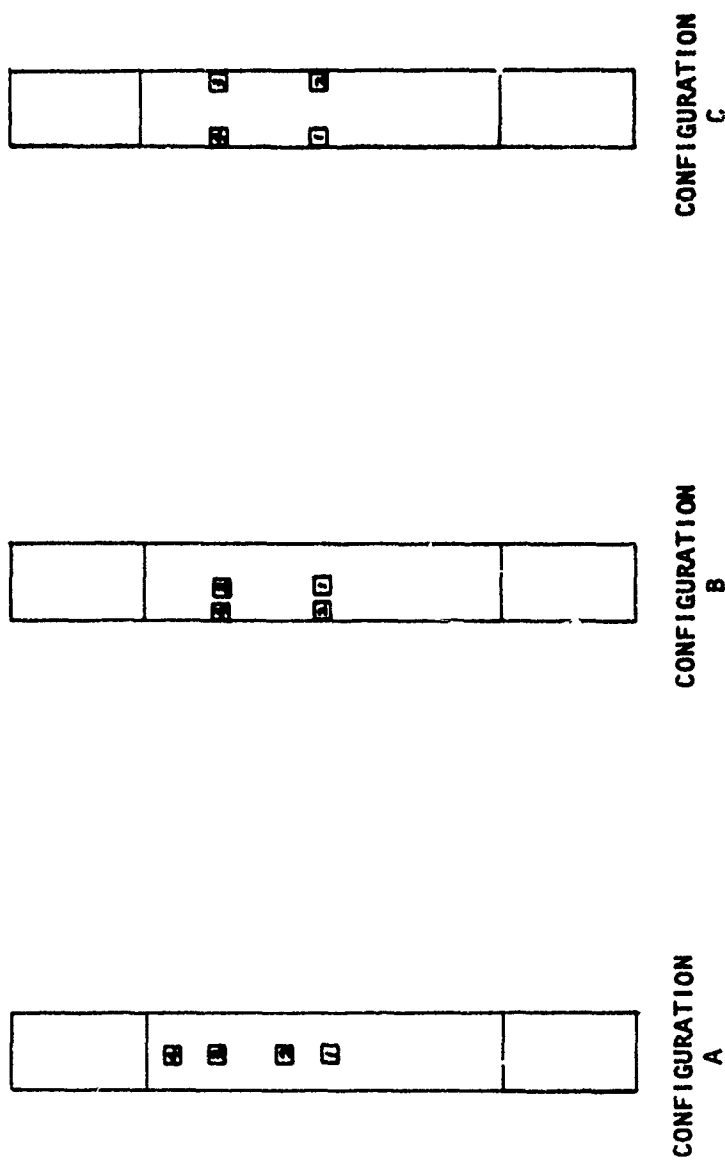


FIGURE 31. SENSOR ARRANGEMENT FOR TEMPERATURE PROFILE TEST.

TABLE 19. TEMPERATURE PROFILE TEST OF  $\pm 45^\circ$  SPECIMEN

TEMPERATURE SENSOR ARRANGEMENT	SPECIMEN ID	TEST ENV. ( $^\circ$ F / % RH)	MAXIMUM FATIGUE STRESS (psi)	TEMPERATURE RISE IN TEMPERATURE SENSORS ( $^\circ$ F)				SENSORS THAT WERE CLOSE TO FAILURE LOCATION
				1	2	3	4	
CONFIGURATION A OF FIGURE 31	AA6-2	132/95	18608	10	13	6	7	2
	AA7-2	170/50	18683	32	33	29	27	3
	AA8-1	170/50	11176	17	16	22	20	-
CONFIGURATION B OF FIGURE 31	B7-4	170/50	15990	19	17	23	22	3,4
CONFIGURATION C OF FIGURE 31	AA7-3	75/50	19092	18	18	16	13	-
	AA7-1	170/50	18534	26	26	31	25	3
	AA1-1	170/95	11915	6	5	6	6	-

where  $D''$  is related to the energy dissipation  $\bar{W}$  (in-lb/in<sup>3</sup>) by

$$D'' = \frac{\bar{W}}{\pi \sigma_0^2} \quad (4)$$

By using Figure 29a, the energy that is converted to heat per cycle is calculated as 12.361 in-lb/in<sup>3</sup>. When values of parameters

$$K = 0.1684 \text{ in-lb/in-Sec}^{-\circ}\text{F}$$

$$c = 2240 \text{ in-lb/lb}^{\circ}\text{F}$$

$$a_T = a_H = 1 \text{ (for } 75^{\circ}\text{F/50% R.H. environment)}$$

$$\sigma_0 = 7278 \text{ Psi}$$

$$\omega = 0.1 \times 2\pi \text{ Rad/Sec}$$

are substituted into equations (4) and (3), the maximum temperature difference in the  $\pm 45^{\circ}$  specimen is approximately  $0.001^{\circ}\text{F}$ . To justify the steady state assumption in the above arguments, we find that the time required to attain 95% of the steady state condition, according to Schneider<sup>5</sup> and Equation (2), is

$$t = \frac{12h^2c}{\pi^2 K} \quad (5)$$

and is 6.47 seconds for the  $\pm 45^{\circ}$  specimen. The short duration to reach a steady state condition and the small difference in temperature between center and surface of the specimen indicates that the temperature field through the thickness of the specimen can be assumed essentially uniform throughout its fatigue life.

The specimen's surface temperature was monitored continuously by temperature sensors and the results for  $\pm 45^{\circ}$  specimens at various environments and approximate stress levels are shown in Figures 32 through 36. Steady state temperature was reached in only a few cases. Temperature data scatter from specimen to specimen at each environment is typical. Several factors contributed to the scatter.

- a. The temperature sensor location during testing was not always in the area where the specimen failed. Usually a  $3^{\circ}\text{F}$  or more temperature jump was observed seconds before failing at the failure location.

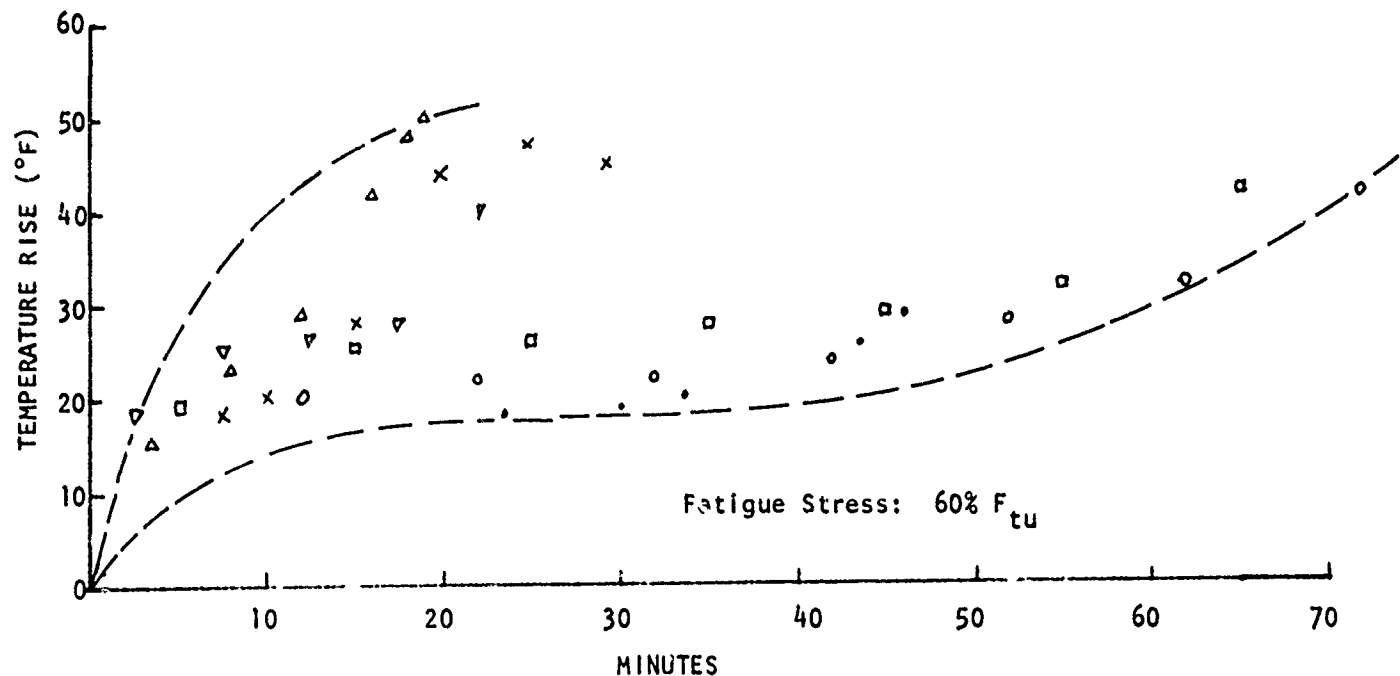
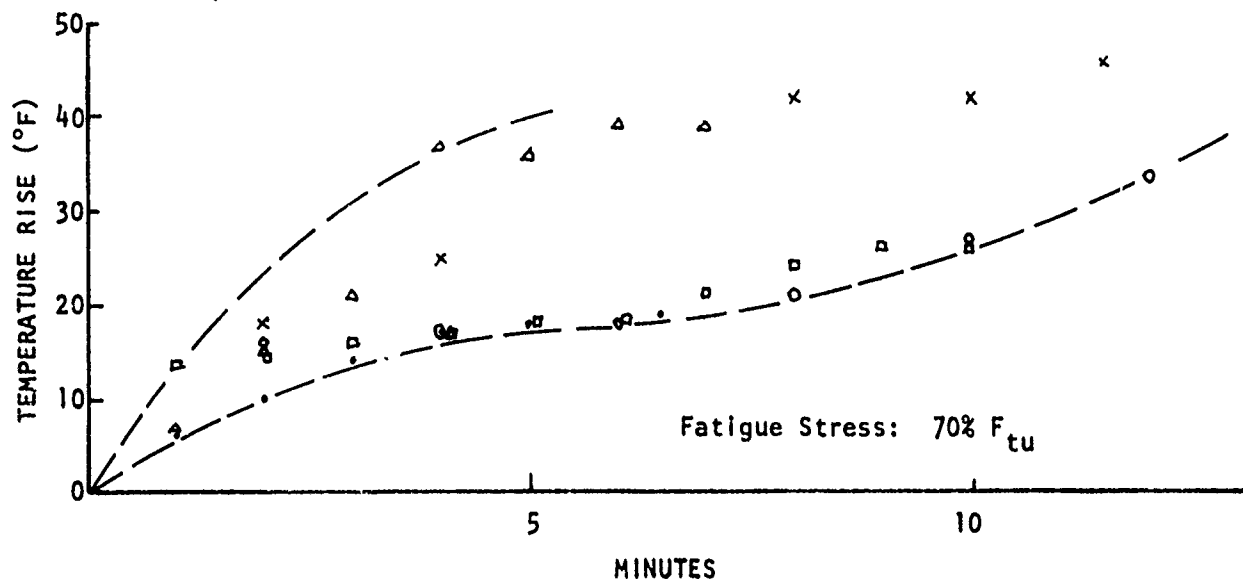


FIGURE 32. TEMPERATURE RISE ON  $\pm 45^{\circ}$ -SPECIMEN SURFACES WHEN FATIGUE TESTED IN AN  $75^{\circ}$ F/50% R.H. ENVIRONMENT.

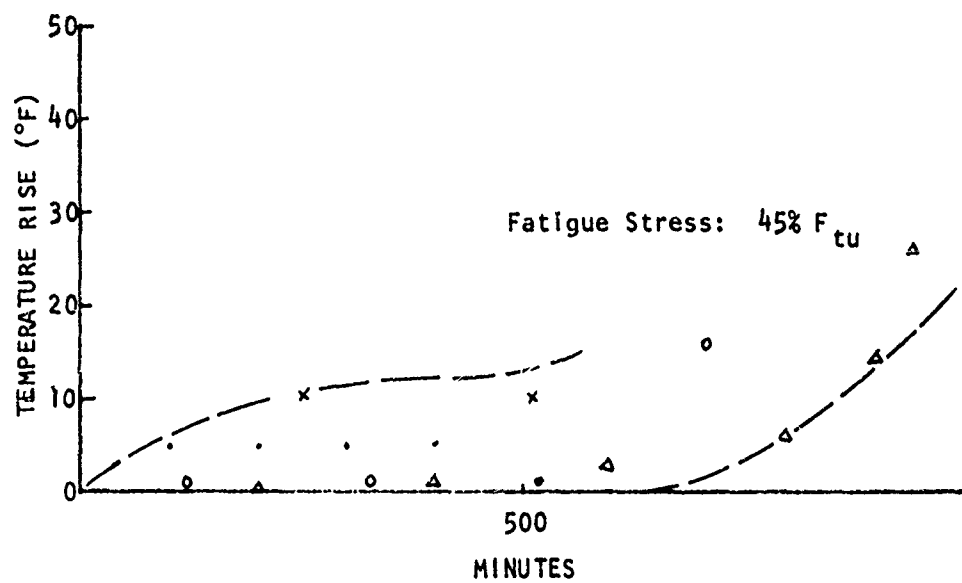
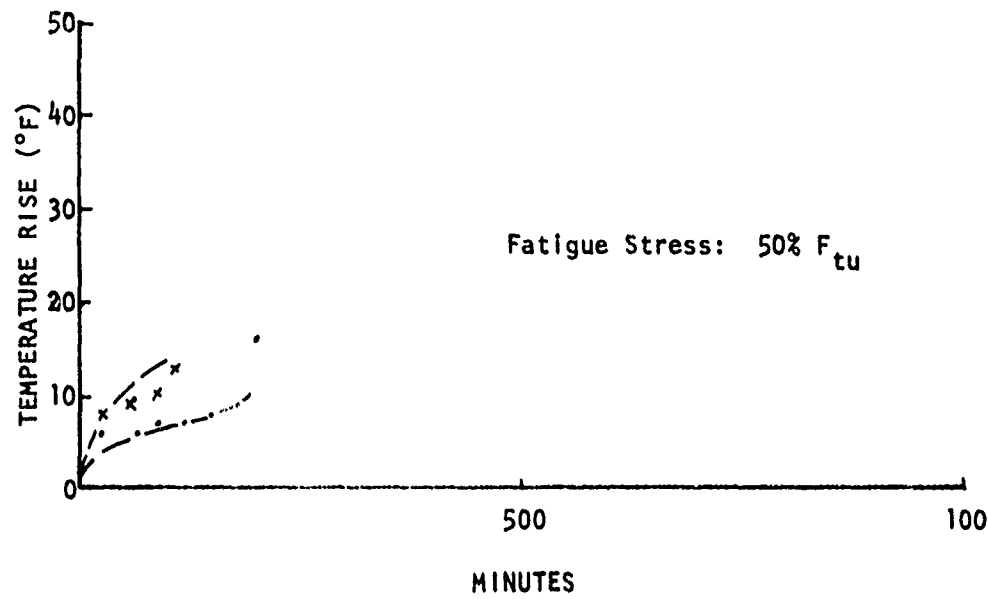


FIGURE 32 (Continued). TEMPERATURE RISE ON  $\pm 45^{\circ}$ -SPECIMEN SURFACES WHEN FATIGUE TESTED IN AN  $75^{\circ}$ F/50% R.H. ENVIRONMENT.

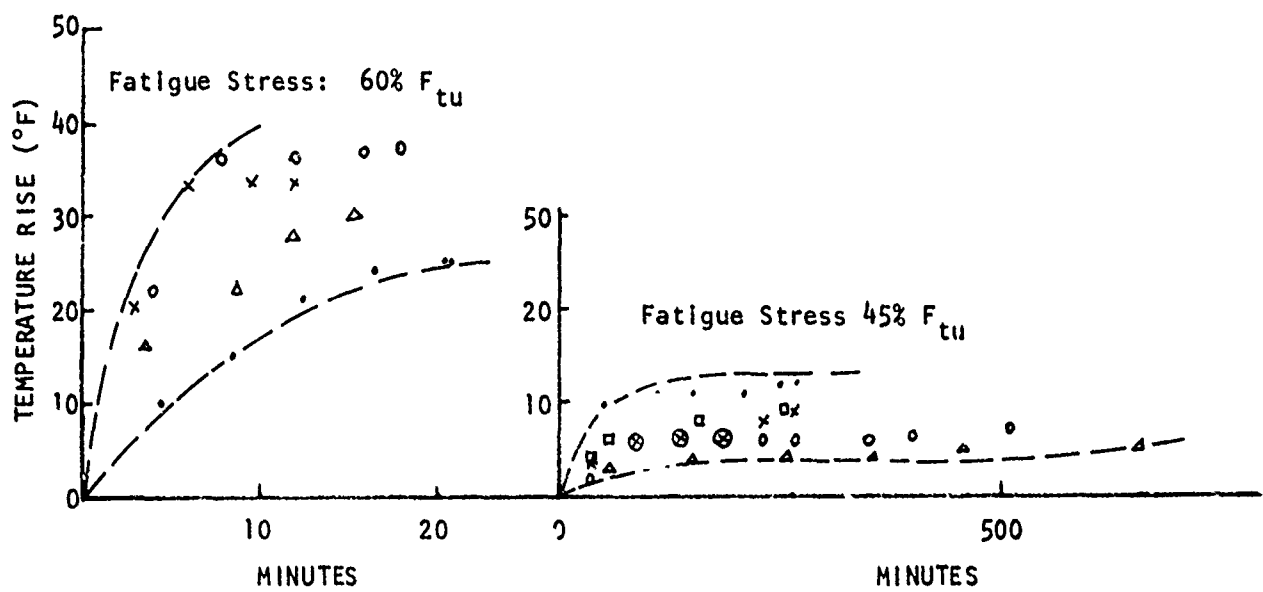
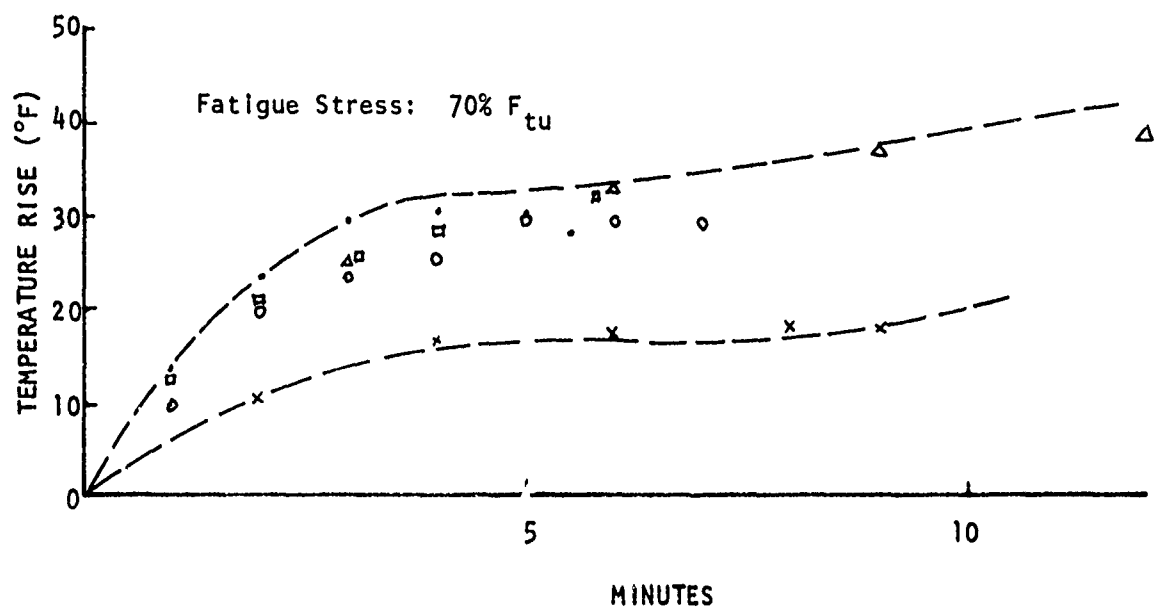


FIGURE 33. TEMPERATURE RISE ON  $\pm 45^\circ$ -SPECIMEN SURFACES WHEN FATIGUE TESTED IN AN  $132^\circ\text{F}/50\%$  R.H. ENVIRONMENT.

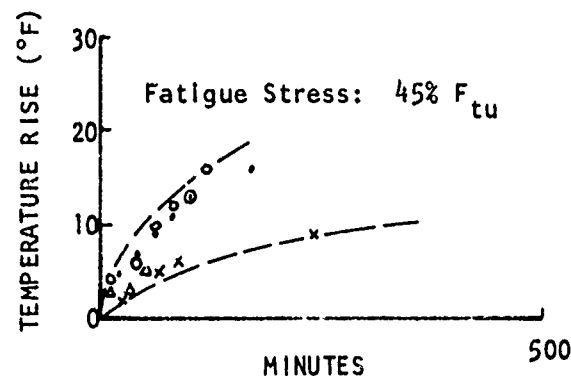
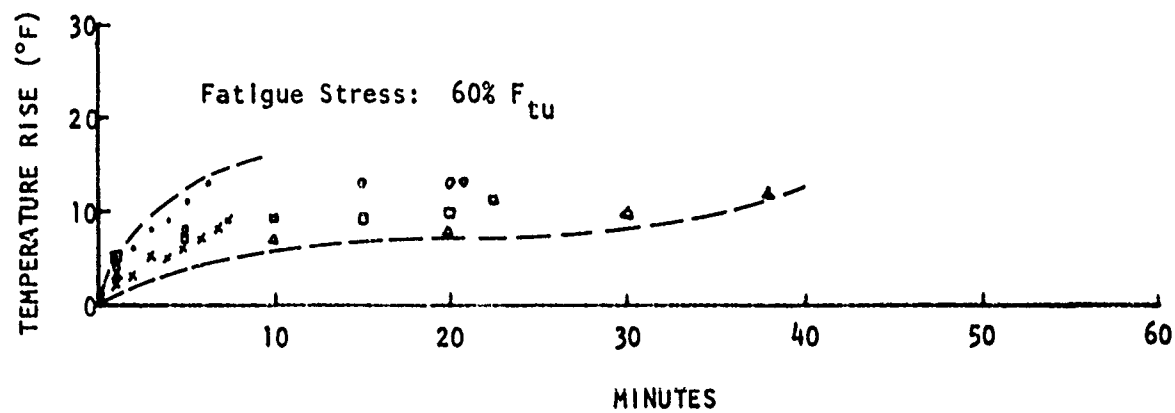
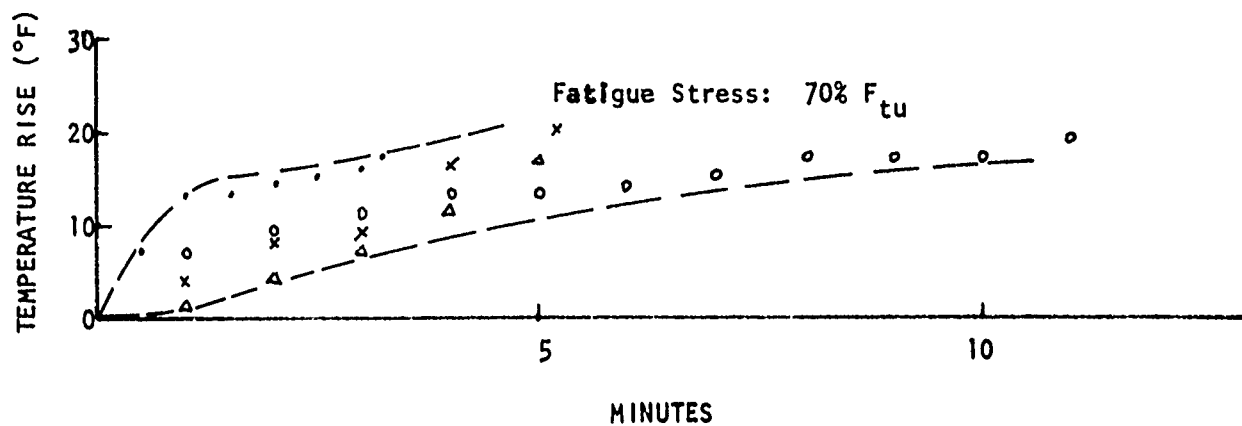


FIGURE 34. TEMPERATURE RISE ON  $\pm 45^{\circ}$ -SPECIMEN SURFACES WHEN FATIGUE TESTED IN AN  $132^{\circ}$ F/95% R.H. ENVIRONMENT.

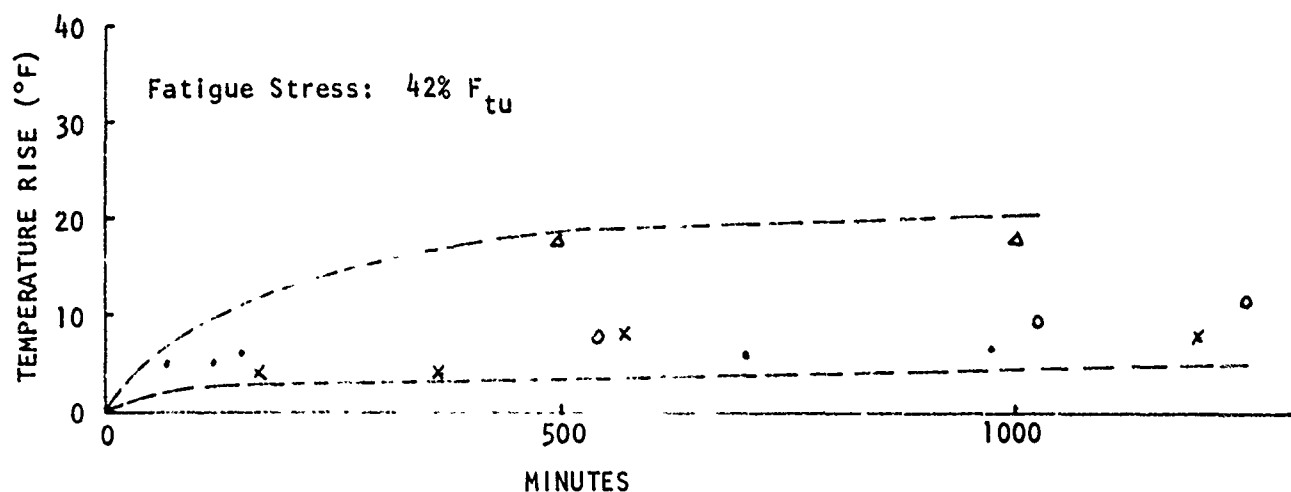
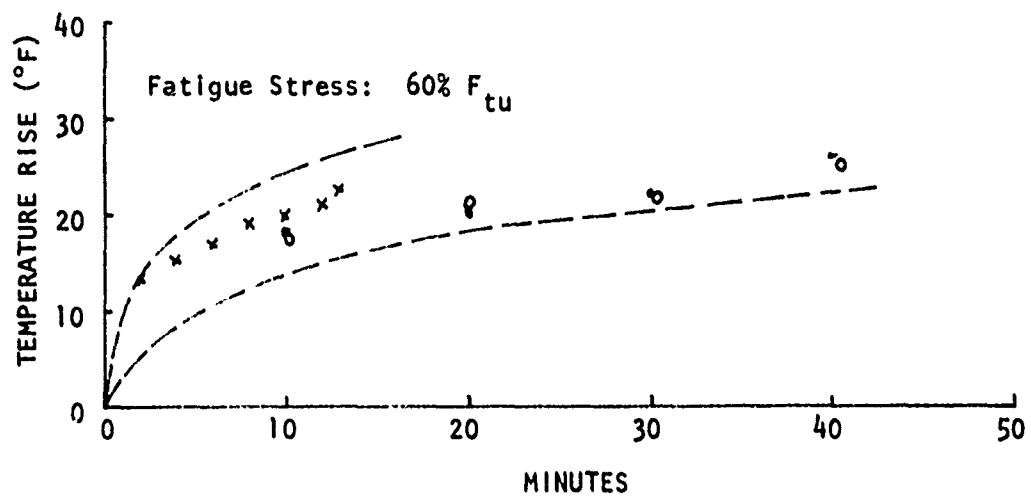
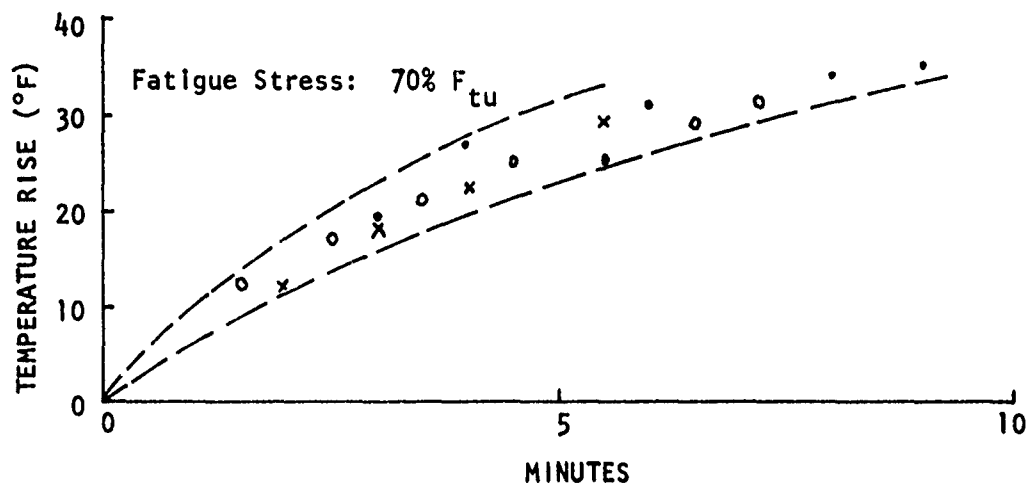


FIGURE 35. TEMPERATURE RISE ON  $\pm 45^{\circ}$  SPECIMEN SURFACES WHEN FATIGUE TESTED IN AN  $170^{\circ}$ F/50% R.R. ENVIRONMENT.

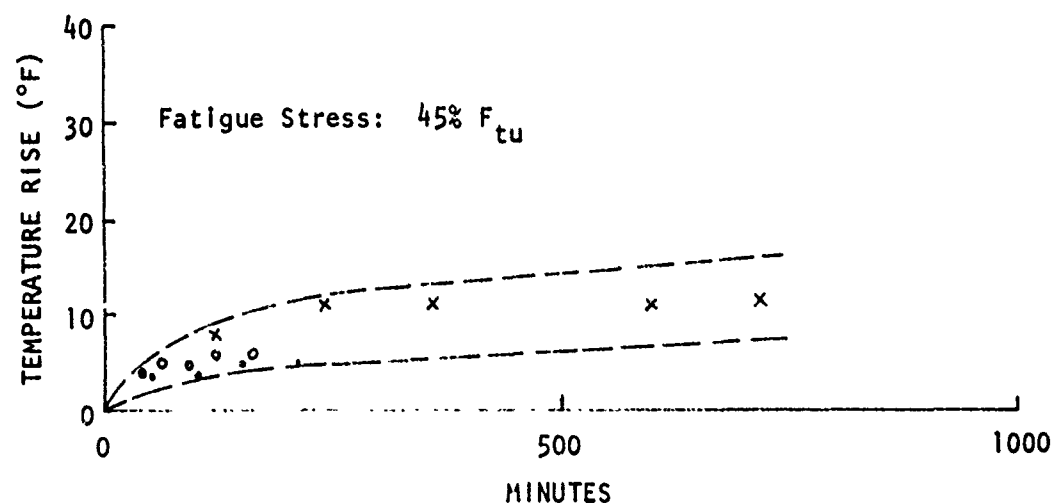
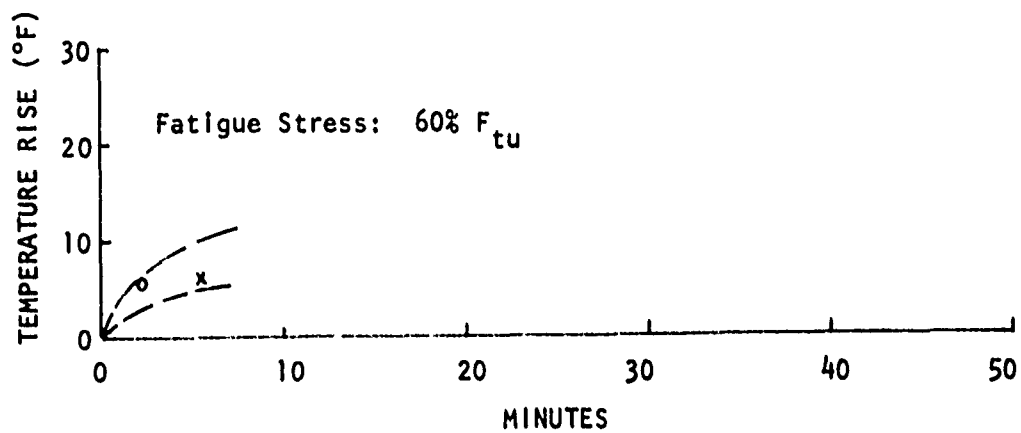
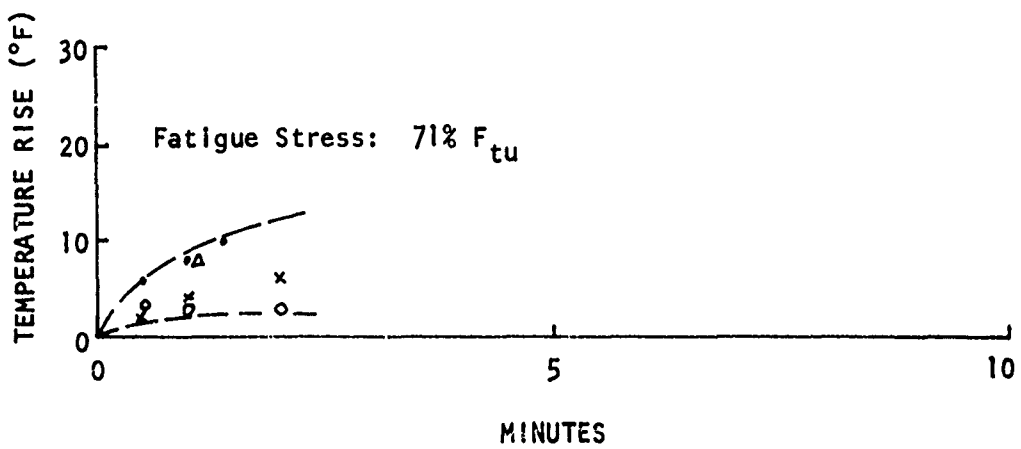


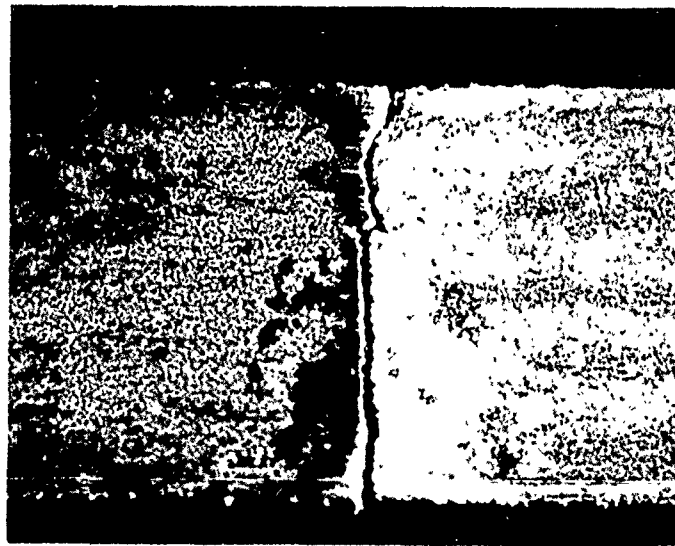
FIGURE 36. TEMPERATURE RISE ON  $\pm 45^{\circ}$  SPECIMEN SURFACES WHEN FATIGUE TESTED IN AN  $170^{\circ}\text{F}/95\%$  R.H. ENVIRONMENT.

- b. Edge effects and the cross sectional area difference between specimens made the applied fatigue stress field different.
- c. The probabilistic nature of microcrack distribution between specimens creates various fatigue failure processes at various locations within the specimens.

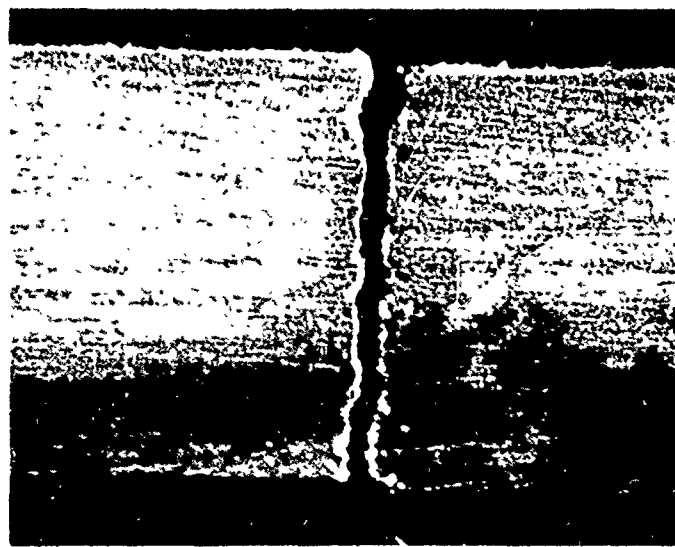
#### 4.2 FATIGUE ANALYSIS

The initiation of the failure process was not observable as the test assembly was enclosed in the metal encased environmental test chamber. The fatigue failure surface of 90° specimens usually yields a clean cut edge appearance such as those shown in Figure 14. The correlation between failure surface and specimen quality can be readily established. Typical failure edges of quality 90° specimens are shown in Figure 37. Porosity and machine defects have an effect on the specimen's low fatigue life as seen by comparing Figures 38 and 39 with test results in 90° specimen fatigue (Tables 7-11). Especially subpanels A9 and A18 were in the neighborhood of the C-scan void area of the original big A-panel of Table 1. Also, by comparing the fatigue tables of 90° specimens, specimens from panel A show reduced fatigue life. Specimens made from subpanels NA suffered a lot of carbide cut defects and rendered only minimum fatigue life. These are indications that the fatigue behavior of 90° specimens is highly sensitive to its fabricated quality.

The surface appearance of  $\pm 45^\circ$  specimens that failed in fatigue, shown in Figure 18, were similar to those of the static failure specimens. The static failure process for  $\pm 45^\circ$  specimens seem to be initiated from the edge area with the peeling of surface layers along a  $45^\circ$  direction. Final failure ran along the worst peeled area. The fatigue failure process is believed to start by microcrack growth throughout the specimen including the edge area. Final rupture occurred after the crack grew to an unstable size. The similarity of failure appearance between static and fatigue  $\pm 45^\circ$  specimens is to be noted. The  $\pm 45^\circ$  panels of Table 1 did not show either the C-scan voids or visual type porosity (under 25X microscope inspection). The fatigue life of  $\pm 45^\circ$  specimens showed significantly less scatter than that of the 90° specimens.

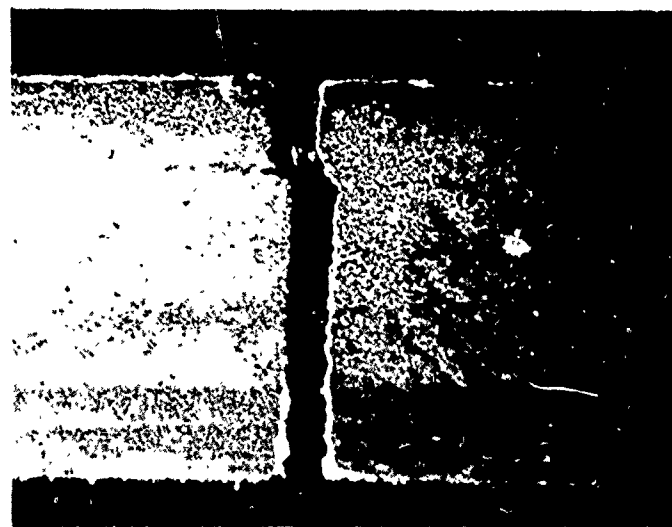


a. FAILURE OF SPECIMEN 90-A16-5 TESTED AT  
75°F/50% R.H. (16X)



b. FAILURE OF SPECIMEN 90-A15-2 TESTED AT  
170°F/50% R.H.

FIGURE 37. FATIGUE FAILURE FROM QUALITY 90°-SPECIMEN.



a. POROSITY THAT INITIATED GAGE FAILURE OF  
SPECIMEN 90-A9-1 TESTED AT 170°F/50% R.H.  
(16X)



b. POROSITY THAT INITIATED EDGE FAILURE OF  
SPECIMEN 90-A11-4 TESTED AT 132°F/95%  
R.H. (16X)

FIGURE 38. POROSITY THAT INVOLVED THE FATIGUE  
FAILURE OF 90°- SPECIMEN.

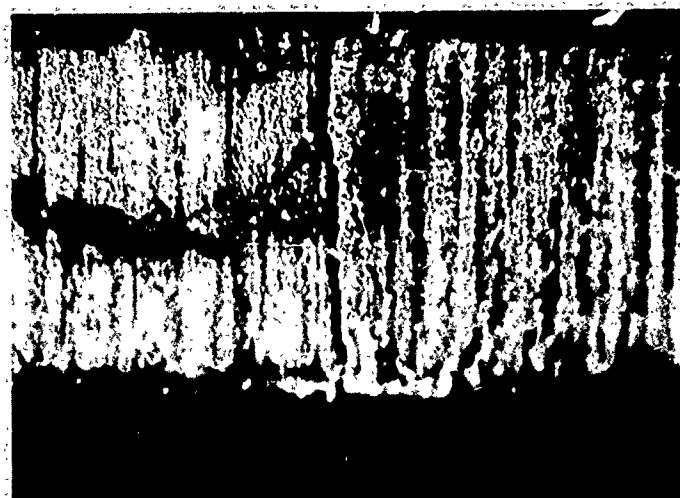


a. DELAMINATION THAT INITIATED EDGE FAILURE OF SPECIMEN 90-A15-4 TESTED AT 170°F/ 50% R.H. (16X).

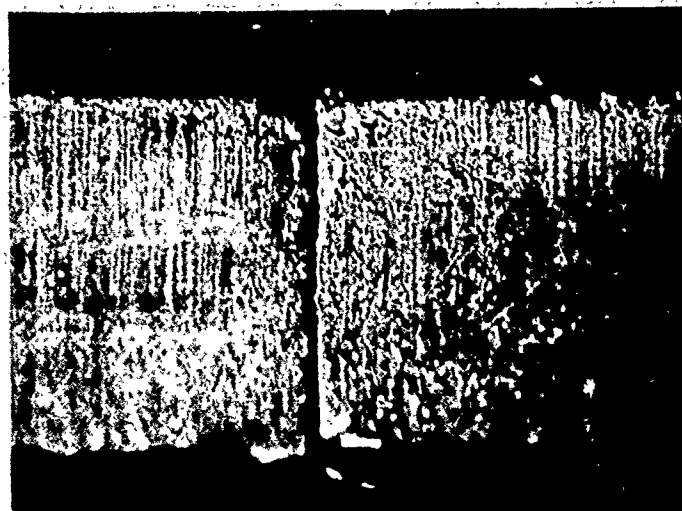


b. DELAMINATION THAT INITIATED EDGE FAILURE OF SPECIMEN 90-A12-6 TESTED AT 132°F/ 95% R.H. (16X).

FIGURE 39. MACHINE DEFECTS THAT INVOLVED THE FATIGUE FAILURE OF 90°-SPECIMEN.



c. EDGE GROVES THAT REDUCED THE FATIGUE LIFE  
OF SPECIMEN 90-NA5-3 TESTED AT 75°F/50%  
R.H. (16X)



d. EDGE GROVES THAT REDUCED THE FATIGUE LIFE  
OF SPECIMEN 90-NA7-3 TESTED AT 75°F/50% R.H.

FIGURE 39 (Continued). MACHINE DEFECTS THAT INVOLVED THE  
FATIGUE FAILURE OF 90°- SPECIMEN.

Since the effect of temperature and humidity on the mechanical properties of Gr/Ep can not be ignored<sup>1</sup>, a fatigue theory, proposed by Schapery<sup>6</sup>, that incorporates the viscoelastic effect will be adopted here to study the fatigue crack growth response of the composite. In its simplest form, this fatigue theory involves the application of the power law for opening-mode crack growth,

$$\frac{da}{dN} = c(\Delta K_I)^q, \quad (6)$$

to a so-called dominant flaw or crack. Here,  $N$  is the number of cycles,  $a$  is the crack size and  $q$  is a positive constant. The coefficient  $c$  can be expected to depend on frequency, temperature, humidity, R-value and probably other parameters, such as mean strain. The amplitude of stress intensity factor,  $\Delta K_I$ , is related to the amplitude of stress level  $\Delta\sigma$  by

$$\Delta K_I = k \sqrt{a} \Delta\sigma \quad (7)$$

where  $k$  is a crack geometry parameter.

We now consider a set of specimens which are identical except for their distribution of initial dominant flaws. Allowing for variation of the  $c$  and  $k$  values from specimen to specimen, the dominant crack in the  $i$ th specimen will have

$$\begin{aligned} c_i &= c_{oi} c \\ k_i &= k_{oi} k \end{aligned} \quad (8)$$

where subscripts "o" and "i" indicate quantities for the initial value and for the  $i$ th specimen respectively. If the specimen fails at  $N = N_{fi}$  as defined by  $a \rightarrow \infty$ , we predict, from equations (6), (7), and (8),

$$\int_0^{N_{fi}} c k^q (\Delta\sigma)^q dN = e^{F_i} \quad (9)$$

By definition,

$$e^{F_i} = (p s_{oi}^p c_{oi} k_{oi}^q)^{-1}, \quad p \equiv \frac{q}{2} - 1 \quad (10)$$

It is seen that the effect of separate statistical distributions of  $a_0$ ,  $c_0$ , and  $k_0$  on failure is through a single statistical distribution parameter,  $F$  which is

$$F = \log \left[ \int_0^N C^k K^q (\Delta \sigma)^q \frac{dN}{a_{TH}} \right], \quad C = C^0 / a_{TH} \quad (11)$$

The temperature and humidity effects are introduced through the time-shift factor  $a_{TH}$ . If the values  $c$  and  $k$  are assumed constant during the constant amplitude fatigue tests, equation (11) becomes

$$\log N + q \log \Delta \sigma = F + \log a_{TH} \quad (12)$$

At each temperature and humidity, the quantity,  $F + \log a_{TH}$  is a statistical quantity. Equation (12) is a good starting point for fatigue data analysis. By looking for the proper  $q$  value that will minimize the square error of quantities  $F_i + \log a_{TH}$  from the statistical mean value  $F + \log a_{TH}$ , equation (12) can be analyzed by linear regression techniques. Thus, the fatigue data in Tables 7 through 16 were analyzed by equation (12) and results are listed in Table 20. The sequence of environmental severity is defined by the corresponding  $\log a_{TH}$  value. The value of the quantities  $\log N$  and  $\log a_{TH}$  are in the order of 1 ~ 5 and that of  $q \log \Delta \sigma$  and  $F$  are in the order of 20 ~ 50. It is obvious that the balance of equation (7) is dominated by the exponent  $q$  and  $\log \Delta \sigma$ . The exponent  $q$ , the unknown quantity, can be determined from the slope of the  $\log N$  vs.  $\log \Delta \sigma$  curve.

TABLE 20. TEST/ANALYSIS CORRELATION STUDY

SPECIMENS	ENVIRONMENT	75/50	132/50	170/50	132/95	170/95
	(°F & % R.H.)	LOG $a_{TH}$	0	-1.1	-2.7	-3.2
	SAMPLE SIZE	14	15	10	14	15
90°	EXPOENT: q	13.20	7.87	3.67	11.70	17.37
	F + LOG $a_{TH}$	48.81	30.79	16.42	43.16	64.79
	SAMPLE SIZE	20	16	16	19	11
±45°	EXPOENT: q	9.83	9.32	11.38	9.79	11.43
	F + LOG $a_{TH}$	5.41	43.41	51.41	44.66	51.12

## 5.0 DISCUSSIONS AND CONCLUSIONS

The basic mechanical properties of AS/3501-6 Gr/Ep composite under combined temperature and humidity environments has been characterized in Reference 1 based on the creep-recovery tests and viscoelastic theory. Under the combined effects of temperature and humidity, short term results from Reference 1 can be used to predict the long term behavior of AS/3501-6. Their validity to long term behavior prediction has been verified by conducting a creep-recovery test with four days per cycle.

The main objective of this Phase II program was to investigate fatigue response of the basic laminates  $(90^\circ)_{20}$  and  $(\pm 45^\circ)_{25}$  and relate it to realistic laminate prediction through viscoelastic analysis. In order to minimize the variables that might effect the fatigue result, the specimen quality and its condition before testing were of vital importance to the final data analysis. Microcracks might be created during the moisture soaking process. But by conditioning the specimens in a 170°F environment as described in Section 2.1, rather than at a higher temperature, no apparent flaws were produced. Defects that might be created by improper machining of the specimen were eliminated by using a new specimen fabrication procedure. Porosities in the specimen were also studied under the microscope and the results were related to the fatigue test data in the fatigue tables.

Fatigue data has been generated for laminates  $(90^\circ)_{20}$  and  $(\pm 45^\circ)_{25}$  at various environments and stress levels. In the process of fatigue testing, a significant temperature rise in the  $\pm 45^\circ$  specimens was observed. Temperature profile tests were subsequently conducted to investigate the transient temperature state within the specimen and the homogeneity of the temperature field. The test data together with the analysis method indicate that the temperature distribution in the fatigue specimens can be considered uniform through the specimen. The continuous rate change of temperature rise on most of the specimen indicates that thermal equilibrium between specimen and environment was not reached during fatigue testing.

Hysteresis tests were conducted at various environments and stress levels to study the energy dissipation associated with each fatigue load-unload cycle. Hysteresis data for the 90° specimen agrees with the temperature prediction of negligible increase. The amount of energy loss in  $\pm 45^\circ$  specimens increased as the stress level and/or temperature level became severe. The dynamic modulus increased in magnitude after one hour of fatigue testing.

From preliminary analysis of the fatigue data, it seems that heating may have a strong bearing on composite's failure mechanism. This fact seems to fit in explaining the temperature rise phenomenon of 90° and  $\pm 45^\circ$  specimens. For 90° specimens, there was always a dominant flaw among a distribution of cracks and voids. This dominant flaw suffered continuous crack tip heat build-up due to the fatigue cycling. This heat build-up was confined locally to the low thermal conductivity of polymer. On the other hand, the  $\pm 45^\circ$  specimen was under cyclic in-plane and interlaminar shearing load during the uniaxial fatigue testing. The cross-ply layup of  $\pm 45^\circ$  specimen tends to constrain any single dominant flaw to grow to unstable state. As a result of this constraining action, less dominant flaws gradually grew to become large flaws one by one. Final fatigue failure happened from the coalescence of those large flaws. As the population of large flaws grew, more local heating area were exposed to the surface area. This explains the temperature rise phenomenon detected by temperature sensor on  $\pm 45^\circ$  specimen.

Also, from preliminary fatigue analysis, the parameter  $q$  of equation (6) is probably the dominant factor in introducing the effect of temperature and humidity on fatigue behavior of Gr/Ep composite, together with the time shift factor  $a_{TH}$ . The proper fatigue analysis technique hinges on a clear understanding of  $q$ . The parameter  $c$  of equation (6) will also be investigated for its possible role in our crack propagation model.

## 6.0 REFERENCES

1. Renton, W. J. and Ho, T. L., "The Effect of Environment on the Mechanical Behavior of AS/3501-6 Graphite/Epoxy Material", Final PHase I Report, NASC Contract No. N00019-77-C-0369, June 1978.
2. Shen, Chi-hung and Springer, G. S., "Moisture Absorption and Desorption of Composite Materials", J. Composite Materials, Vol. 10, 1976.
3. Schapery, R. A., "Effect of Cyclic Loading on the Temperature in Viscoelastic Media with Variable Properties", AIAA, Vol. 2, May 1964.
4. Dally, J. W. and Brontman, L. J., "Frequency Effect on the Fatigue of Glass Reinforced Plastics", J. Composite Materials, Vol. 1, 1967.
5. Schneider, P. J., "Conduction Heat Transfer", Addison-Wesley, 1955.
6. Schapery, R. A., "Deformation and Failure Analysis of Viscoelastic Composite Materials", Proceedings of ASME National Meeting, Special Session on Inelastic Behavior of Composite Materials, AMD Vol. 13, December 1975.

DISTRIBUTION LIST

	<u>No. of Copies</u>
Naval Air Systems Command Attn: Code AIR-5163D3 Washington, DC 20361	8
Office of Naval Research (Code 472) Washington, DC 20350	1
Office of Naval Research, Boston 495 Summer St. Boston, MA 02210 ATTN: Dr. L. H. Peebles	1
Naval Research Laboratory Codes 6306 and 6120 Washington, DC 20350	2
Naval Surface Weapons Center Code R-31 White Oak, Silver Spring, MD 20910	1
Naval Air Propulsion Test Center ATTN: J. Glatz Trenton, NJ 08628	1
Commander U. S. Naval Weapons Center China Lake, CA 92555	1
Naval Ship R&D Center ATTN: Mr. M. Krenzke, Code 727 Washington, DC	1
Naval Sea Systems Command Navy Dept. Codes 05R and 05D23 Washington, DC 20360	2
Commander Naval Air Development Center ATTN: Aero Materials Lab Aero Structures Div Radomes Section Warminster, PA 18974	3

DISTRIBUTION LIST (Cont'd)

No. of Copies

Air Force Materials Laboratory ATTN: Codes LC (1 copy) LN (" ") LTF (" ") LAE (" ") Wright-Patterson AFB, OH 45433	4
Air Force Flight Dynamics Laboratory ATTN: Code FDTC Wright-Patterson AFB, OH 45433	1
U. S. Applied Technology Laboratory U. S. Army Development Laboratories (AVRADCOM) ATTN: DAVDL-ATL-ATS Fort Eustis, VA 23604	1
Director Plastics Technical Evaluation Center Picatinny Arsenal Dover, NJ 07801	1
Department of the Army Army Materials & Mechanics Research Center Watertown, MA 02172	1
NASA Langley Research Center Hampton, VA	1
NASA Headquarters Code RV-2 (Mr. N. Mayer) 600 Independence Ave., SW Washington, DC 20546	1
AVCO Corporation Applied Technology Division Lowell, MA 01851	1
Bell Aerospace Co. ATTN: Mr. F. M. Anthony Buffalo, NY 14240	1
The Boeing Company Aerospace Division P. O. Box 3707 Seattle, WA 98124	1
Boeing-Vertol Co. P. O. Box 16858 ATTN: Dept. 1951 Philadelphia, PA 19142	1

DISTRIBUTION LIST (Cont'd)

No. of Copies

Brunswick Corporation  
Technical Products Division  
325 Brunswick Lane  
Marion, VA 24354

1

Celanese Research Company  
Box 1000  
ATTN: Mr. R. J. Leal  
Summit, NJ 07901

1

Defense Ceramic Information Center  
Battelle Memorial Institute  
505 King Ave  
Columbus, OH 43201

1

E. I. DuPont de Nemours & Co.  
Textile Fibers Dept.  
Wilmington, DE 19898

1

Ewald Associates, Inc.  
105 Skyline Drive  
Morristown, NJ 07960

1

Fiber Materials, Inc.  
ATTN: Mr. J. Herrick  
Biddeford Industrial Park  
Biddeford, ME

1

General Dynamics  
Convair Aerospace Division  
ATTN: Tech Library  
P. O. Box 748  
Fort Worth, TX 76101

1

General Dynamics  
Convair Division  
ATTN: Mr. W. Scheck; Dept. 572-10  
P. O. Box 1128  
San Diego, CA 92138

1

General Electric  
R&D Center  
ATTN: Mr. W. Hillig  
Box 8  
Schnectady, NY 12301

1

General Electric Company  
Valley Forge Space Center  
Philadelphia, PA 19101

1

DISTRIBUTION LIST (Cont'd)

No. of Copies

B. F. Goodrich Aerospace & Defense Products 500 South Main St Akron, OH 44318	1
Graftex Division EXXON Industries 2917 Highwoods Blvd. Raleigh, NC 27604	1
Great Lakes Research Corporation P. O. Box 1031 Elizabethton, TN	1
Grumman Aerospace Corp ATTN: Mr. G. Lubin Bathpage, LI, NY 11714	1
Hercules Incorporated ATTN: Mr. E. G. Crossland Magua, UT 84044	1
HITCO 1600 W. 135th St Gardena, VA 90406	1
Illinois Institute of Technology Research Center ATTN: Dr. K. Hofer 10 West 35th St. Chicago, IL 60616	1
Lockheed California Co. ATTN: Mr. J. H. Wooley Box 551 Burbank, CA 91520	1
Lockheed-Georgia Co. ATTN: Mr. L. E. Meade Marietta, GA 30063	1
Lockheed Missiles & Space Co. ATTN: Mr. H. H. Armstrong, Dept. 62-60 Sunnyvale, CA 94088	1
Material Sciences Corporation 1777 Walton Road Blue Bell, PA 19422	1

DISTRIBUTION LIST (Cont'd)

	<u>No. of Copies</u>
McDonnell Douglas Corp. McDonnell Aircraft Co. ATTN: Mr. J. Juergens P. O. Box 516 St. Louis, MO 63166	1
McDonnell-Douglas Corp. Douglas Aircraft Co. ATTN: Mr. R. J. Palmer 3855 Lakewood Blvd. Long Beach, CA 90801	1
Monsanto Research Corp. 1515 Nicholas Road Dayton, OH 45407	1
North American Aviation Columbus Division 4300 E. Fifth Ave Columbus, OH 43216	1
Northrop Corp. 3901 W. Broadway ATTN: Mr. G. Grimes, Mail Code 3852-82 Hawthorne, CA 90250	1
Philco-Ford Corp. Aeronutronic Division Ford Road Newport Beach, CA 92663	1
Rockwell International Corp. ATTN: Mr. C. R. Rousseau 12214 Lakewood Blvd Downey, CA 90241	1
Stanford Research Institute ATTN: Mr. M. Maximovich 333 Ravenswood Ave, Bldg 102B Marlo Park, CA 94025	1
TRW, Inc. Systems Group One Space Park, Bldg. 01; Rm 2171 Redondo Beach, CA 90278	1
TRW, Inc. 23555 Euclid Ave Cleveland, OH 44117	1

DISTRIBUTION LIST (Cont'd)

	<u>No. of Copies</u>
Union Carbide Corporation Chemicals & Plastics One River Road Bound Brook, NJ	1
Union Carbide Corporation Carbon Products Division P. O. Box 6116 Cleveland, OH 44101	1
United Aircraft Corporation United Aircraft Research Laboratories E. Hartford, CT 06108	1
United Aircraft Corporation Pratt & Whitney Aircraft Division East Hartford, CT 06108	1
United Aircraft Corporation Hamilton-Standard Division ATTN: Mr. T. Zajac Windsor Locks, CT	1
United Aircraft Corporation Sikorsky Aircraft Division ATTN: Mr. J. Ray Stratford, CT 06602	1
University of California Lawrence Livermore Laboratory ATTN: Mr. T. T. Chiao P. O. Box 808 Livermore, CA 94550	1
University of Maryland ATTN: Dr. W. J. Bailey College Park, MD 20742	1
University of Wyoming Mechanical Engineering Dept. ATTN: Dr. D. F. Adams Laramee, WY 82071	1
Westinghouse R&D Center ATTN: Mr. Z. Sanjana 1310 Beulah Road Churchill Boro Pittsburgh, PA 15235	1